Universiteit Utrecht

Archeointensities from the Hertenrits Culture, Suriname

MSc Thesis

May, 2015

Renoeka Wanita Ramcharan

Utrecht University

Abstract

Global geomagnetic field models (e.g. CALS10K, SHA.DIF.14K, pfm9k.1) are predominantly based on data from the Northern hemisphere, while also observations of the field become increasingly sparse going further back in time. Therefore, more data from especially the Southern hemisphere is required to improve our understanding of the geomagnetic field. In this study we aimed to obtain absolute archeointensities of the geomagnetic field in Suriname on unoriented archeological potsherds from six different levels of the Wageningen-1 mound, Hertenrits Culture, dated between 1145 ± 25 and 1310 ± 30 BP (655 to 975 AD). On representative shards from each level rock magnetic analyses and thermal demagnetization experiments have been carried out. Archeointensity analyses have been performed using the IZZI-Thellier method (Tauxe and Staudigel, 2004) on samples from all six levels, using the 2G DC SQUID system at Fort Hoofddijk (Utrecht University) and by the Microwave-Thellier method on subsamples that had a relatively high magnetic moment (levels 4 – 6) and were stable to microwave demagnetization, using the 14 GHz system at University of Liverpool. Laboratory alteration was monitored by pTRM checks and pTRM Tail checks (Riisager and Riisager, 2001). Average archeointensities between 10.52 ± 0.75 μT and 16.18 ± 2.16 μT were obtained using the conventional Thellier method; these values are three to four times lower than expected from geomagnetic field models. From these field models, i.e. SHA.DIF.14K (Pavón-Carrasco et al., 2014) and pfm9k.1 (Nilsson et al., 2014), archeointensities ranging from 37.01 ± 0.89 to 45.79 ± 0.93 and 37.6 ± 3.68 to 40.7 ± 3.21 respectively, are predicted. Besides by chemical alteration (e.g. Coe, 1967b) or the presence of a multidomain component (McClelland et al., 1996), the archeointensity results may have been biased by cooling rate effects (Dodson and McClelland-Brown, 1980; McClelland, 1984) and or by remanence anisotropy (Selkin et al., 2000). The latter have not been tested in this study. Only three out of 27 Microwave-Thellier measurements passed the set of criteria, yielding an average of 40.4 ± 3.7 μT (for 715 to 975 AD); these values are consistent with values expected from the geomagnetic models, but they seem fortuitous. To support our low, but high-quality IZZI-Thellier data and enhance the reliability of the geomagnetic models, definitely more paleomagnetic research is required over a larger time period and other regions around the equator and especially on the Southern hemisphere, preferably incorporating full vector analysis.

Acknowledgement

First of all, I would like to thank my beloved parents, who have been there for me at every step of my life journey; without their love, encouragement and (financial) support I would never be writing this thesis. Secondly, I am thankful to my supervisors Prof. Dr. C. G. Langereis and Dr. Lennart de Groot of Utrecht University for enabling me to execute this research in the first place and Dr. Andy Biggin of University of Liverpool for having me over at Liverpool; I also thank them for their unconditional guidance, valuable insights, advices and time during this research, as well as for arranging any practical matters related to it.

Further I would like to thank the staff and personnel of the *Stichting Surinaams Museum* for providing the archeological pottery shards from their collection.

I take this opportunity to acknowledge also all my previous lecturers I had the pleasure to learn from, as well as the staff and personnel of Utrecht University who have helped me in one way or another during my study at Utrecht University; finally I thank my sisters, brother and all my other family members, friends and fellow students for their valuable support through this task.

The Hague, 2015

Table of Contents

Abstract 1

Acknowledgement 2

1 Introduction 4
2 Background 6
2.1 Theory 6
2.2 Previous research 12
2.3 Research area 15
3 Material and Methods 20
3.1 Material 'sampling' 20
3.2 Supporting Rock magnetic analyses 21
3.2.1 Thermomagnetic runs 22
3.2.2 Hysteresis parameters and back-field curves 22
3.2.3 Thermal demagnetization 23
3.3 Archeointensity Analysis 24
3.3.1 Microwave-Thellier excitation 24
3.3.2 IZZI-Thellier method 26
4 Results 28
4.1 Rock Magnetism 28
4.2 Archeointensity 37
5 Discussion 43
6 Conclusion 49

References 51

Appendices 57

1 Introduction

To determine the behavior of the geomagnetic field, the acquisition of well dated and widely distributed magnetic measurements at the Earth's surface is required (Genevey and Gallet, 2002). Prior to the period when direct geomagnetic measurements were possible (around 1600 AD), the secular variation in the geomagnetic field can be explored from the analysis of the remanent magnetization of man-made materials and rocks (Daly and Le Goff, 1996). After Émile and Odette Thellier produced the first reliable determinations of paleointensities back in 1938, following an experimental protocol used earlier by Johann Koenigsberger (Dunlop, 2011), a great number of modifications and additions have been suggested to the basic experimental protocol due an increased understanding of the potential problems facing paleointensity determinations (Biggin et al., 2007). Consequently, many geomagnetic paleointensity data have been (and are being) produced. Using these data sets, several geomagnetic field models have been developed (e.g. Figure 1, Pavón-Carrasco et al., 2014). However, the global geomagnetic field models are predominantly based on data from the Northern hemisphere, and data become sparse going further back in time. Although some studies have been done in Antarctica (e.g. Lawrence et al., 2009; Brachfeld et al., 2000) and in Argentina (e.g. Creer et al., 1983, Gogorza et al., 2002; 2004; 2006), not much significant research on this topic has been carried out around the equator and on the Southern hemisphere. To improve our understanding of the geomagnetic field more data from especially the Southern hemisphere is required to update the geomagnetic models (e.g. CALS10K (Korte et al., 2011); SHA.DIF.14K (Pavón-Carrasco et al., 2014); pfm9k.1 (Nilsson et al., 2014)). If the models can be improved we might be able to better understand observed rapid changes in the geomagnetic field (e.g. magnetic jerks) and it will also help archaeologists to date in-situ archaeological artefacts by correlating observed magnetic directions and – intensities to an improved paleosecular variation record.

To follow up on the few studies that already have been performed, in this study absolute values of archeointensities will be measured on samples from Suriname, which is located on the Northeastern coast of South-America, between 2° - 6° N and 54° - 58° W. The research will focus on unoriented, undecorated archaeological pottery fragments from Wageningen-1, a mound belonging to the Hertenrits Culture, Arauquinoid Tradition, in the western district Nickerie. The mound has been excavated by archeologist Dr. Aad H. Versteeg in 1978 and the

pottery shards have been collected in the summer of 2014 from the *Stichting Surinaams Museum*. Although the temperatures to which they have been baked are unknown, the Wageningen-1 mound is the best dated archaeological site of Suriname so far, with four ^{14}C-datings, dating the levels of 0.75 – 3 meter below the surface between respectively 975 and 655 AD (Versteeg, 2003, p. 269-270). As opposed to the other Traditions found in Suriname, the Indians belonging to the Arauquinoid Tradition raised mound sites and agricultural fields nearby, which made permanent farming possible in Western Suriname.

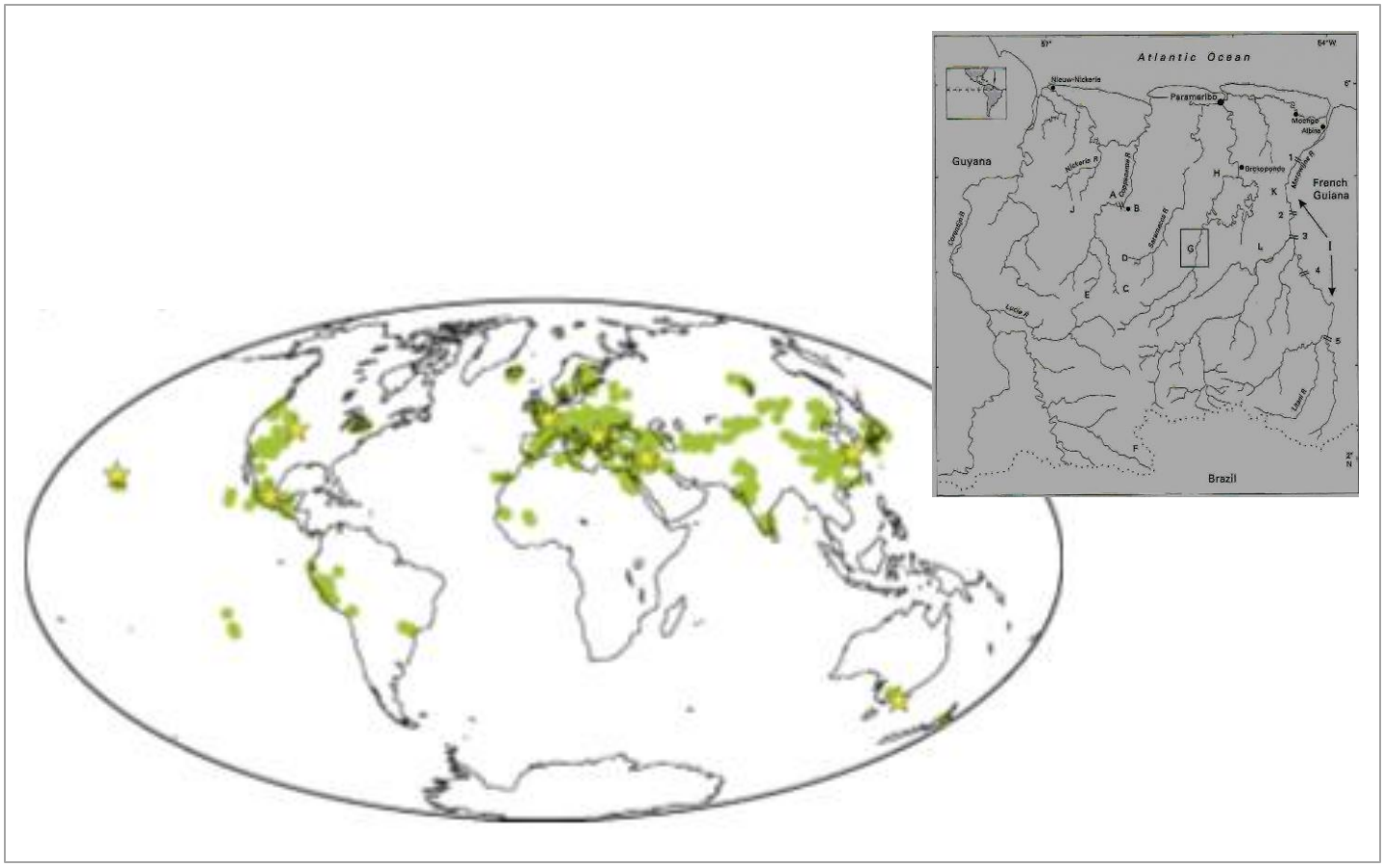

Fig. 1 Field model SHA.DIF.14K (Pavón-Carrasco et al., 2014), showing the spatial distribution of the input data, including the research country Suriname (marked by an orange star on the model and given in the figure on the right as well). Yellow stars in the figure show the selected locations for the comparison between the model and input data.

2 Background

This chapter aims to provide some background information, which is essential in understanding the current research and its importance. First, the physics behind paleointensity determinations will be described (2.1), followed by relevant previous studies (2.2) that have been carried out on especially the Southern hemisphere and finally the research area (2.3) will be treated.

2.1 Theory

To be able to recover the intensity of the Earth's magnetic field in ancient times, the ratio between the natural remanent magnetization (NRM) produced by cooling in the ancient field and the thermoremanent magnetization (TRM) after cooling in the present field, should be the same as the ratio of the field themselves: $\boldsymbol{H_{anc}/H_{now} = NRM/TRM}$. (eq. 1)

Following this formula a baked clay that looses a certain amount of its NRM during heating will acquire the same amount of magnetization during cooling if the field *H* in the furnace is equal to the field that imparted the NRM. However, before this equation can be valid, a number of conditions must be first met:

1. TRM intensity must be proportional to field strength, which is usually true for weak fields like the Earth's.
2. At each stage of heating, newly acquired TRM must completely replace the corresponding part of the NRM, and not simply be added to it.
3. The NRM and the minerals carrying it must remain unaltered since the time of the original firing and in all subsequent re-firings.

Unfortunately, just a small number of natural materials are ideal recorders of the Earth's magnetic field. They contain ultrafine particles of magnetite (and sometimes hematite) in which all atoms cooperate by lining up their magnetic moments to form a single magnetite domain. These single-domain (SD) grains respond to thermal energy and at high temperature readily turn their moments like compass needles into the local field direction. As each grain passes through its individual blocking temperature T_B during cooling, the compass needle can no longer turn, even if the magnetic field would change later. A memory of the field that was acting at T_B is thus

preserved as TRM. On the other hand, larger grains, containing multiple domains (further referred as multidomain or MD) also gain TRM in cooling, but are less stable. MD grains have a wide span of unblocking temperatures (and not a single T_B as with SD grains); consequently, the compass needle of a particular MD grain will be free to rotate over a wider range during heating (Dunlop, 2011).

In 1938 Émily Thellier established his laws of additivity, reciprocity and independence, which are only obeyed by SD grains (e.g. bricks and other baked clays) and produced the first reliable paleointensity determination, using an experimental protocol set by Johann Koenigsberger (Dunlop, 2011), together with Odette Thellier. These laws deal with partial TRMs, produced by cooling a sample in a field over only part of the temperature range from the Curie point T_c to room temperature T_0. The reciprocity law states that blocking and unblocking are reciprocal processes: pTRM that is frozen in at T_B during cooling is unfrozen at exactly the same T_B during reheating. The independence law states that two or more pTRMs are independent of one another if they have mutually exclusive ranges of T_B (ranges of T_B occur because pTRMs comprise the moments of SD grains with many different sizes and shapes). From the independence law, the additivity law follows: pTRMs with mutually exclusive ranges of T_B add (vectorially, if they were produced by fields having different directions). The Thellier and related methods which link together NRM loss and pTRM gain in arbitralily narrow intervals of T are only useful if the magnetic grains responsible can be separated into groups, each of which magnetizes/demagnetizes over one and only one T interval and is unaffected by the magnetization/demagnetization of all the other groups. Opposed to SD grains, this is not the case for MD grains: their pTRMs, even if produced over non-overlapping T intervals, decay over intervals that overlap considerably and may extend to T_c.

These laws and the idea behind blocking/unblocking can be better explained by Néel's theory of single domain pTRM, quantified in 1949. He assumed that ultrafine grains contain a single magnetic domain which can change only by rotating its moment $m= VM_s$, where V is the volume and M_s the spontaneous magnetization of the SD grain. At normal temperatures, the energy barrier between + and – states (m respectively parallel or antiparallel to H) is large and rotation only occurs if $H > H_c$ (the microscopic coercive force). As T increases, the barrier shrinks; eventually it becomes small enough (at T_B) to be crossed with aid of random thermal energy kT.

It was Néel who predicted the relaxation time τ for thermal activation over the energy barrier $\Delta E = 1/2\mu_0 V M_s H_c$. For weak field, $\mu_0 H \leq 100$ μT:

$\tau^{-1} = 2f_0 \exp(-\Delta E/kT) = 2f_0 \exp(1/2\mu_0 V M_s H_c/kT)$ (Néel, 1949). (eq. 2)

Current estimates for the frequency factor f_0 are 10^9-10^{10} s $^{-1}$. As we can see from the latter equation, relaxation time depends exponentially on grain properties (size, V and shape or other anisotropy, through H_c) and on temperature T (directly, but also via $M_s(T)$, which drops rapidly near T_c). For any specific set of identical grains (V, H_c), τ changes with cooling from very small (unblocked or thermal equilibrium state) to enormous (blocked state, transitions impossible). As τ passes quite abruptly through its blocking temperature, locking in TRM, each grain has a 'sharp' value of T_B, which gives individual pTRMs their non-overlapping independent character. Blocking and unblocking can be best understood by using a Néel's diagram of V vs H_c (Figure 2). Rearranging equation 2 under blocking/unblocking conditions results in

$VH_{c0} = 2kT \log(2f_0 t)/(\mu_0 M_{s0} \beta^2(T))$, (eq. 3)

where H_{c0} and M_{s0} are room temperature values and $\beta(T)$ is the normalized T dependence of M_s and H_c (shape anisotropy assumed, as for magnetite). Equation 3 (a rectangular hyperbola), represents the blocking/unblocking curve, joining all SD sets with a common value of T_B/T_{UB}.

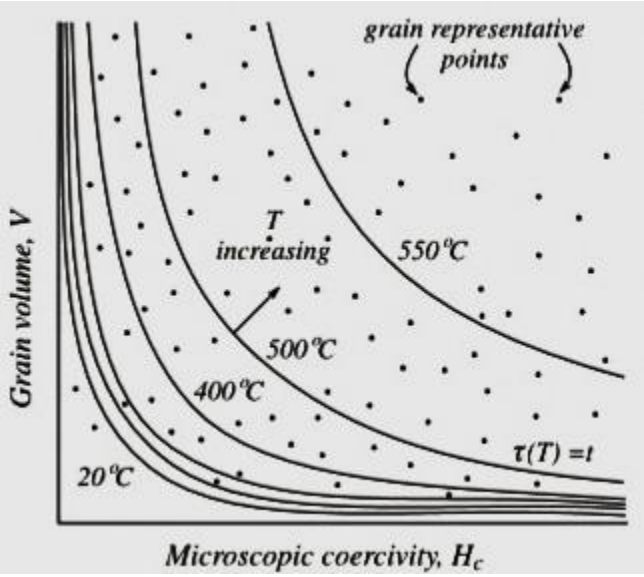

Fig. 2 Néel's diagram of grain volume V vs microscopic coercivity H_c for τ=t, a typical experimental time (From Dunlop, 2011).

The final key to paleointensity determination by the Thellier method and most others is a pTRM intensity that is proportional to H (Dunlop, 2011). This property was explained by Néel (1949) by stating that in an unblocked state, just above T_B, a SD grain has a magnetization that is in thermal equilibrium with $\boldsymbol{H} = H\boldsymbol{n}$ ($\boldsymbol{n}$ being a unit vector). As it goes through T_B, the pTRM moment that is locked in is given by: $\boldsymbol{m}(T_B) = VM_s(T_B)tanh(VM_s(T_B)H/kT_B)\boldsymbol{n} \approx V^2M_s^2(T_B)/kT_B)\boldsymbol{H}$. This approximation is valid for H ~ Earth's field and small V, appropriate for most SD grains of magnetite.

MD behavior can be recognized in paleointensity results by several properties:

1. Reproducible (not caused by alteration) non-linearity of the Arai plot. With increasing grain size, the Arai plot sags more and more below the ideal SD line (Levi, 1977; Koenigsberger, 1938).
2. High-temperature thermal demagnetization tails: residual undemagnetized pTRM (T_i, T_0, H) after zero-field heating to T_i (e.g. Biggin and Perrin, 2007). The pTRM tail check (Riisager and Riisager, 2001) adds a third, zero-field, heating-cooling step to T_i to the Coe version of the Thellier method. In the notation of Yu et al. (2004), the ZI (zero-field, in-field) Coe sequence becomes a triple step-heating, ZIZ.
3. A third MD property is dependence of pTRM on the order of in-field and zero-field steps. Biggin and Böhnel (2003) found improved linearity of the Arai plot by reversing the Coe method, performing the in-field heating-cooling before the zero-field step (ZI→ IZ).

The technique of Aitken et al. (1988) is essentially a reversed version of Coe's method (Coe, 1967a). In Aitken experiments, the remagnetization treatments are performed prior to the demagnetization treatments at every temperature step and the pTRM tail checks are omitted. Tauxe and Staudigel (2004) and Yu et al. (2004) have alternated Coe and Aitken protocols in successive steps – the IZZI method. This is also the method employed in the current study.

4. Zigzagging of the Arai plot is also an indicator of MD effects, specifically of 'low-temperature tails' in which pTRM demagnetizes below (rather than above) T_B.

High temperature thermal demagnetization tails and sagging Arai plot data may seem mutually incompatible. Each T_B has a spectrum of corresponding unblocking temperatures T_{UB}; while SD

grains demagnetize in a narrow range straddling T_B, following the reciprocity law quite closely, MD grains demagnetize over extremely broad ranges, starting not far above room temperature T_0 and extending most of the way to T_c. Unblocking below T_B accounts for sagging of the Arai plot, while unblocking above T_B explains high temperature pTRM tails.

To decrease MD effects, one thus need to remove as much MD NRM as possible before beginning the paleointensity experiment (Dunlop, 2011). Pre-cleaning samples using alternating field (AF) or low-temperature demagnetization (LTD) before beginning stepwise demagnetization preferentially erases MD remanence (Schmidt, 1993). These treatments are laborious to apply in paleointensity work, as the treatment must be repeated for each new pTRM, which is very time consuming for LTD. However, Biggin et al. (2007) found AF treatment prior to each measurement worthwile, but Dunlop et al. (2005) saw only marginal improvements from AF cleaning at each step and no improvement after using LTD.

The relative orientation of NRM and pTRM not only affects the tail checks (Yu and Dunlop, 2003), but the entire outcome of the Thellier experiment (Xu and Dunlop, 2004). Data deviate less from ideal SD behavior if H is approximately perpendicular to the NRM. This has also been theorized and demonstrated experimentally by Biggin (2006) and Biggin et al. (2007).

Another way of discriminating against MD carriers is to use separated silicate crystals containing single-domain or nearly SD magnetic inclusions (usually magnetite). They have the added advantage of encasing the magnetic material in a non-reactive silicate host, preventing alteration during the Thellier experiment (Dunlop, 2011).

Day et al. (1977) stated that the transition from single-domain to truly multidomain behavior is not abrupt; rather, there is a transition region. To discriminate domain states (SD, pseudo-single-domain PSD and MD), they proposed a graph of the ratio of saturation remanence to saturation magnetization, M_{rs}/M_s, against the ratio of remanent coercive force to ordinary coercive force, H_{cr}/H_c. Following Day et al. (1977), the M_{rs}/M_s vs H_{cr}/H_c graph is generally divided into SD, PSD and MD regions, using SD and 'true' MD values of the parameters to define the limits of the PSD region (Dunlop, 2002). Day et al. (1977) used $M_{rs}/M_s = 0.5$ and $H_{cr}/H_c = 1.5$ as SD limits for titanomagnetites of all compositions.

Analog to the Thellier method, Walton (1991) and Walton et al. (1993, 1996) invented a new paleointensity method which uses microwave absorption at near-resonance frequencies to selectively demagnetize magnetic mineral grains only, while the remainder of the rock or archeological sample remains cool, reducing the potential for alteration of the magnetic grains. The microwave energy that is absorbed generates magnons (quantized spin waves) which directly excite the coupled ferromagnetic spins in SD and MD particles. The generation of spin waves within the magnetic grain enables the individual domain magnetizations to reverse, and the whole sample to demagnetize in a zero field (Walton et al., 1996) or to realign with an ambient fixed field to produce a thermoremanent magnetization (TRM). In conventional thermal demagnetization and pTRM production, the mechanism of heating is the production of phonons (quantized lattice vibrations). As magnetic grains and matrix are heated to temperatures of 500 °C or above, more than enough opportunities are created for alteration, e.g. oxidation or oxyexsolution of (titano)magnetite grains and production of chemical and thermochemical remanences (Calvo et al., 2002; Draeger et al., 2006). Alteration is still the major cause of failed paleointensity experiments (e.g. Coe, 1967b) and proposed correction techniques using pTRM checks are problematic (McClelland and Briden, 1996).

Although microwave methods illuminate sample alteration, they do not eliminate curved Arai plots caused by MD grains (Biggin et al., 2007). Dekkers and Böhnel (2006) have proposed a new approach, which is based on the proportionality between pTRM and field common to MD and SD grains: the multispecimen parallel differential pTRM technique. In this technique, multiple specimens are heated and cooled only once, each to the same temperature, but in a different field. The paleointensity is then considered to be the field H which leaves the total remanence unchanged after this pTRM remagnetization: H is the axis-crossing point of a linear fit to all the Δ (pTRM + TRM – initial TRM) specimen data. Although this approach eliminates magnetic history effects, principally permits the use of MD grains and reduces alteration by once-only heating to intermediate temperatures, only a small part of the TRM is used and there are no built-in checks for alteration or multiple components of NRM incorporated. It is also very difficult to find material with identical mineralogy and rock magnetic properties.

2.2 Previous Research

As we saw in the introduction, the overall distribution in the SHA.DIF.14K model by Pavón-Carrasco et al. (2014) is dominated by Northern hemisphere data. The few studies that have been performed around the equator, i.e. in Cameroun (Thouveny and Williamson, 1988), Uganda (Mothersill, 1996) and in Kenya (Barton and Torgersen, 1988), concern directional studies on sediments. Intensity records from the Southern hemisphere used for previous geomagnetic modelling were mainly limited to calibrated relative intensity records of sediments from Argentina (Gogorza et al., 2004, 2006), North Queensland, Australia (Constable and McElhinny, 1985), Antarctic Peninsula (Brachfeld et al., 2000) and West Amundsen Sea (Hillenbrand et al., 2009). Other data of the Southern hemisphere concern also directional data, obtained from sedimentological analyses (e.g. see Creer et al., 1983; Gogorza et al., 2002; Irurzun et al., 2006 (Argentina); Turner and Lillis, 1994 (New Zealand); Barton and McElhinny, 1981 (Western Victoria, Australia)). Some of the studies performed on the Southern hemisphere are described below.

Lawrence et al. (2009) provided new paleointensity and paleodirectional data from samples taken during two field seasons (70 sites from 2003–2004 season and 30 sites from 2006–2007 season) in the Erebus Volcanic Province (EVP), Antarctica, as well as 21 new age determinations by the $^{40}Ar/^{39}Ar$ incremental heating method. At each field site, minimal 10 standard 2.5 cm diameter samples were drilled using a gasoline powered drill with a mixture of water and glycol for the drilling fluid. The samples were oriented using at least two of three methods: magnetic compass, sun compass, and/or a differential Global Positioning System (GPS) orientation technique. They combined their data with previously published paleomagnetic and geochronological results of this area, which resulted in 133 sites, of which 91 have radioisotopic dates, ranging from 0.03 to 13.42 Ma. Modified Thellier-Thellier paleointensity estimates are reported for 47 sites, of which 37 have dates. A mean EVP paleointensity of 31.5 ± 2.4 μT was obtained, derived from 41 high-quality sites. 125 High-quality EVP directional data selected from the merged data set resulted in a mean direction with an inclination anomaly of ~3° and a dispersion of 23.9 ± 2.1° (with virtual geomagnetic pole (VGP) latitude cut off at 45°). They concluded that high VGP dispersion and low-intensity values support the global observation of anticorrelation between directional variability and field strength.

Creer et al. (1983) produced the first palaeomagnetic secular variation results (0 – 14000 years BP) for South America, using the bottom sediments from three lakes in the region of 41° S 71.5° W in Rio Negro Province (Western Argentina): Laguna el Trebol, Brazo de Campanario and Lago Morenito. These small lakes were chosen in order to avoid the effects of turbidity currents and other sources of potential post-depositional disturbance of the sediment; in total, 88 samples were subjected to sedimentological analysis. The intensity of natural remanent magnetization (NRM) was measured in the Buenos Aires and Edinburgh palaeomagnetic laboratories using Digico magnetometers; in Buenos Aires another fluxgate slow speed spinner magnetometer was used as well. Based on the magnetic susceptibility and intensity of remanent magnetization, different lithological units were defined at the within-lake level. Inter-lake correlation was derived from the inclination and declination patterns and from a set of radiocarbon age determinations. Records of about 6000 ^{14}C years BP were obtained for Laguna el Trebol and Brazo de Campanario, while Lago Morenito provided a record extending back to about 14000 ^{14}C years BP. All the individual measurements were transformed to a time-scale prior to stacking to produce type-curves. Although records exhibit variations with similar overall characteristics as those previously obtained for Europe and North-America, no correlation with the Northern hemisphere patterns was found. From spectral analysis of declination/inclination pairs and VGP paths, clockwise as well as anticlockwise precession of the geomagnetic vector was found.

A similar research was carried out by Gogorza et al. (2000) on four cores from the bottom sediments of Lake Moreno (Southern Argentina) and integrated with data obtained by Creer et al. (1983). Secular variation of the geomagnetic field (0 – 12 kyr) was studied using spectral analysis and precession analysis of the magnetic vector. The spectrum obtained from spectral analysis showed major peaks at periodicities of about 1500, 2400, 3300 and 6200 year for inclination data and major peaks at periodicities of about 1200, 2300, and 3500 year for declination data. From analysis of the VGP path plots, both clockwise and counterclockwise precession of the geomagnetic vector was evident. In a later study, Gogorza et al. (2002) investigated palaeosecular variations 0 – 19 kyr as recorded by sediments from Escondido Lake (Southwestern Argentina) and Irurzun et al. (2006) were able to construct a palaeosecular variation record for the past 24000 years from bottom sediments from lake El Trébol (Patagonia, Argentina), using radiocarbon age estimates and previous studies.

Four cores from Lake Escondido, South Argentina and four cores from Lake El Trébol, Patagonia, Argentina (Gogorza et al., 2004) have been used to estimate relative changes in geomagnetic field intensity over respectively the last 16000 years BP and 21000 years BP. Rock magnetic studies indicated that the main magnetic mineral was pseudo-single domain magnetite in a range of grain sizes and concentrations suitable for paleointensity studies. The remanent magnetization at 20 mT (NRM_{20mT}) was normalized using the anhysteric remanent magnetization at 20 mT (ARM_{20mT}), the saturation of the isothermal remanent magnetization at 20 mT ($SIRM_{20mT}$) and the low field magnetic susceptibility (*k*). Coherence function analysis indicated that the normalized records were not significantly affected by environmental influences. The paleointensity (NRM_{20mT}/ARM_{20mT}) versus age curve of the two lakes were in good agreement. For the Lake Escondido sediments, ARM_{100mT} was the best normalizer; the record of relative paleointensity (NRM_{20mT}/ARM_{100mT}) showed peaks and troughs whose amplitudes were similar to those in the St. Lawrence Estuary, Lake Baikal and Lake Pepin (Gogorza et al., 2004).

Constable and McElhinny (1985) have obtained secular variation records from cores from Lakes Barrine and Eacham, two volcanic crater lakes situated on the Atherton Tableland of North Queensland, Australia. Results from several cores were stratigraphically correlated, stacked and smoothed. The chronology provided by radiocarbon dating indicated that the Lake Eacham sequence spans the last 5700 calendar years and the Lake Barrine ~1600 to 16200 years BP, although the timescale for the latter was less well constrained. From VGP paths, two periods of anticlockwise motion between ~5710 and 3980 BP and 10500 and 8800 BP were observed. They found that these periods correspond to periods of anticlockwise motion in South-eastern Australian records (i.e. Barton & McElhinny, 1981) and Argentine records (i.e. Creer et al., 1983).

Brachfeld et al. (2000) have tried to examine past geomagnetic field behavior at high Southern latitudes from thick Holocene sedimentary sections (> 45 m). These were cored in the Palmer Deep, a half-graben on the Western margin of the Antarctic Peninsula, during cruise 95-10 of the *R.V. Polar Duke*, cruise 98-02 of the *R.V. Lawrence M. Gould*, and during Ocean Drilling Program (ODP) Leg 178. The sediments displayed a stable, single-component remanent magnetization after removal of a low-coercivity drilling overprint. Two short cores that

recovered the uppermost 2.6 m of sediment had inclinations that fluctuated at that time (-57°) measured at Faraday Station and several features with wavelengths of 10 to 20 cm appeared to be correlative. Inclinations measured on u-channels taken from the pristine center of a split core were preferred over shipboard measurements. The upper ~25 m represented continuous sedimentation over the past 9000 year, with an average sedimentation rate exceeding 250 cm/kyr (0.25 cm/yr). Given that remanence measurements on u-channels average over an interval < 7 cm long, they obtained independent measurements of the paleogeomagnetic field that average over only ~30 yr. This high- resolution record was characterized by an inclination that fluctuated within ± 15° of the current GAD inclination.

Relative intensity variations derived from sediment records have to be calibrated to absolute values before including them in the modelling. For the CALS10K model each record was initially scaled by an independent constant factor, based on a robust estimate of the ratio of the data to CALS3k.3 intensity predictions at the same location. A first model was created and the relative intensity records were iteratively re-calibrated by comparing the scaled data to the new model at each iteration until convergence was reached (Korte et al., 2011). (See Donadini et al. (2009); Korte and Constable (2011) for more details). The new geomagnetic field model SHA.DIF.14K is based on archaeomagnetic and lava flow data from the upgraded database GEOMAGIA50v2, avoiding the use of lake sediment data (Pavón-Carrasco et al., 2014).

2.3 Research area

Suriname forms part of the area known as the 'Guianas'; the larger part of the Guianas consists of a massif of mainly Proterozoic rocks (so-called Guiana Shield). The massif has comparable geological characteristics in the entire Guianas and extends for the greater part from the Orinoco River and the Atlantic Ocean in the North to the Amazon River in the South (Wong et al., 1998, p. 1). The Precambrian Shield is made up essentially of clearly outlined belts of metamorphic rocks interspersed with granitic and acid volcanic rocks, and intersected by gabbro bodies and dolerite dikes. Suriname has a humid tropical climate, with relatively high average temperatures of ~27 °C. Covering an area of ~164.000 km^2, four landscape types can be distinguished from South to North: respectively the Precambrian Shield, the Cover Landscape, the Old Coastal Plain

and the Young Coastal Plain (Versteeg, 2003, p. 26). While the southern part of Suriname is mainly covered by forest and small hills, the northern part is covered mainly by sediments of the Guiana Basin deposited from the Late Cretaceous onwards (however, no Cretaceous rocks crop out) and erosion products of the Amazon Basin, which were transported westward from the mouth of the Amazon River by the North Equatorial Current. These deposits reflect the provenance of the sediments (both the hinterland and the Amazon River), sea-level fluctuations, climatic changes, etc. (Wong et al., 1998, p.1; Versteeg, 2003, p. 31).

The pre-Columbian cultures that developed in the Guianas and on the banks of the Amazon and Orinoco River have been classified according to the pottery they have left behind. It was remarkable that certain aspects of pottery in the North of South America, often special types of decoration, remained unchanged over long periods of time and over large distances. The particular type of decoration or the kind of pottery vessel with a certain type of decoration was interpreted as being important to the group and its identity, else it would not have remained unchanged over such great distances in place and time (Versteeg, 2003, p. 78). Such a continuity over long distances and periods of time is called a Tradition. Within a Tradition, one can distinguish Cultures. In Suriname three Traditions are found so far: the Saladoid, the Barrancoid and the Arauquinoid Tradition; their names are derived from names of localities in Venezuela (respectively Saladero, Barrancas and Arauquin), where the archaeological material was first found 50-70 years ago. Many sites in Suriname belong to the third Tradition, within which we distinguish three distinct Cultures: the Hertenrits Culture in Western Suriname, the Kwatta Culture in Central Suriname and the Barbakoeba Culture in Eastern Suriname. Barbakoeba sites are also found in French Guiana, and further to the East there is also the Thémire Culture, which belongs partly to the Arauquinoid Tradition (Versteeg, 2003, p. 79).

The pottery shards used in the current study come from the Wageningen-1 mound (SUR-210), which forms part of the Hertenrits Culture, together with Wageningen-3 (SUR-212), Hertenrits (SUR-19), Wageningen-2 (SUR-211), Burnside mound (SUR-306), Nickerie-2 (SUR-365) and Prins Bernhard Polder (SUR-361). See Figure 3 below; the numbers given are the archaeological site names, as indicated above in parentheses. The first four mounds are located more or less in a straight line and found near clusters of raised fields. The archaeological material found at these sites and the available ^{14}C dates suggest that all these sites were inhabited around 700 AD. In

view of material findings, location, size and date of the Hertenrits mound, the Hertenrits mound was likely the social and political centre of this group of sites (Versteeg, 2003, p. 110). The clay, temper and firing conditions of Hertenrits and Wageningen-1 mound are comparable to those of the Buckleburg-1 mound (SUR-213), although the patterns of decoration differ completely. In the upper layers of the Buckleburg mound, pottery temper is only made up of crushed pottery, whereas in the oldest, lower layers it contains percentages of atypical materials such as quartz, charcoal/cariapé, shell and mica. The soft clay was flattened on a mat and the griddle was formed on it before it was baked (Versteeg, 2003, p. 104, 106).

Based on the pottery and the ^{14}C datings, a distinction can be made between Early Hertenrits and Late Hertenrits pottery in the Hertenrits Culture. Early Hertenrits pottery is found in the lower habitation levels of the Hertenrits mound and throughout all habitation layers of the Wageningen-1 mound; it is characterized by simple decoration patterns and a few animal-shaped adornos. Late Hertenrits is found in the topmost habitation level of the Hertenrits mound and at Prins Bernhard Polder and characterized by a wide range of shapes and decoration patterns (Versteeg, 2003, p. 113). Early Hertenrits is dated to ca. 700-1000 AD, while Late Hertenrits is dated to ca. 1000-1250 AD. The occupation of the Wageningen-1 mound is believed to have stopped before the beginning of the Late Hertenrits phase. There is no clear date for the end of the Hertenrits Culture. Although indications for the presence of this Culture continue up to 1250 AD, there are not many dates for sites with a Late Hertenrits component. Colonial artefacts have never been found in any of the sites; if the Hertenrits sites were still inhabited by 1499, they were probably abandoned soon after. It is also possible that these villages had been abandoned earlier, around 1250 AD (Versteeg, 2003, p. 116-119).

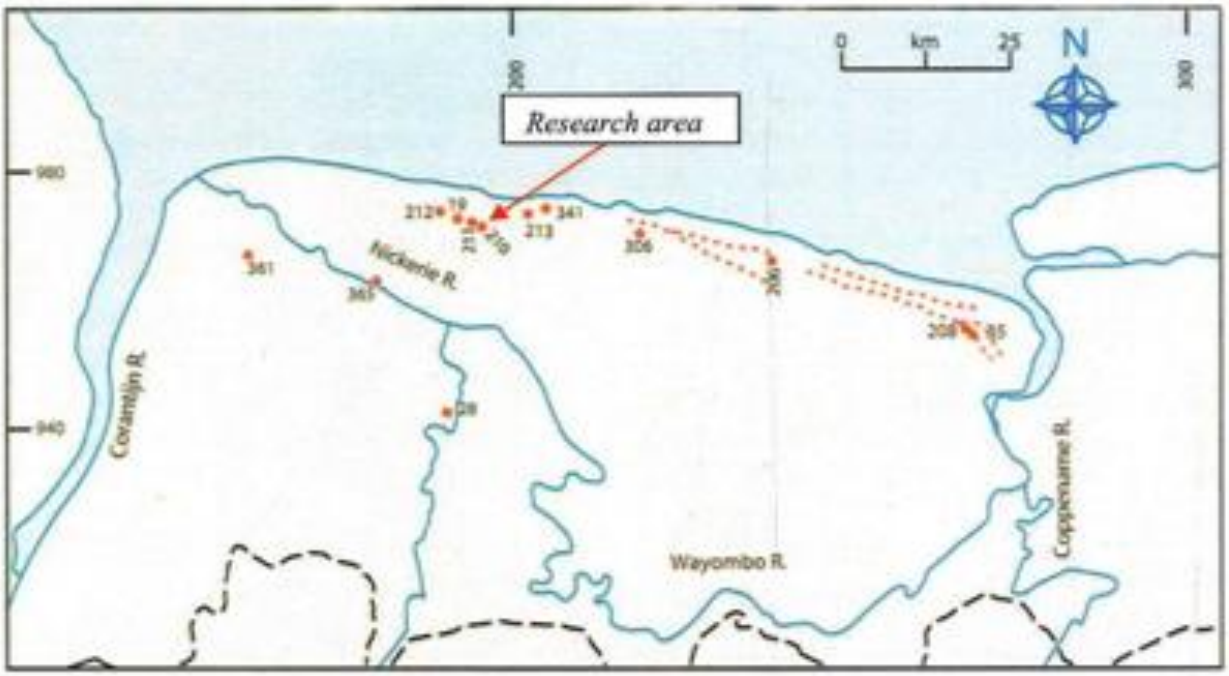

Fig. 3 The most northwestern part of Suriname, with the most important archaeological sites indicated; the samples used for this study are from archaeological site SUR-210 (Wageningen-1 mound). Interrupted red lines indicate sandridges or cheniers; dashed black lines indicate the border of the coastal plain and the interior (Figure from Versteeg, 2003, p. 97).

The Wageningen-1 mound was excavated by archaeologist Dr. Aad H. Versteeg in 1978, as part of a joint project of the *Vrije Universiteit*, Amsterdam and the *Stichting Surinaams Museum*. About half of the pottery of Wageningen-1 mound is more or less light grey at the surface, while the other half is orange-grey to orange. The surface is usually well-polished and the cross-section is mostly grey (Versteeg, 2003, p. 114).

Dated layers of peat and pollen analysis show that between 300 and 1000 AD freshwater conditions prevailed in the coastal plain of Western Suriname, where there are few cheniers; this is the area west of the Burnside mound (SUR-306) (Versteeg, 2003, p. 97). A group of Indians must have reacted to the changing conditions by raising a mound of clay, with relatively small, square, agricultural plots nearby, consisting of clay bodies surrounded by trenches. This water management system made permanent farming possible. Fertility of these raised fields could be sustained by spreading the organic sediment from the ditches onto the fields (Versteeg, 2003, p. 38, 98).

The Indians thus constructed their agricultural fields, as well as their villages: clay mounds with a 100-150 m diameter were thrown up as dry locations for settlement. The mounds were not constructed in one major operation, but in phases. Archaeologically, these phases are represented by alternating light and dark layers in the mound. In Suriname the subsoil of all investigated mounds contains a thick layer of peat. On top of this there are large numbers of grey clay layers about 10-20 cm thick. Artefacts are found concentrated in the darker layers. The grey layers clearly reflect mound construction, while the dark ones reflect periods of human occupation (Versteeg, 2003, p. 100-103). In Figure 4 a picture of the stratigraphy of Wageningen-1 mound is given.

Fig. 4 Stratigraphy of Wageningen-1 mound. The mound was raised by the Indians by applying the clay by hand. Alternating light and dark layers represent different phases of construction. Depth of the pit is ca. 2.80 m (From Versteeg, 2003; p. 112).

3 Material and Methods

3.1 Material 'sampling'

The *Stichting Surinaams Museum* provided 25 undecorated archaeological pottery shards from their collection. These were collected during the summer holidays of 2014. The shards come from depths of 0.75 – 3 m of the Wageningen-1 mound (SUR-210), dated between 1145 ± 25 and 1310 ± 30 BP; the mound was excavated by archaeologist Dr. Aad H. Versteeg in 1978. For the dating, a 1σ calibration-result was read from the CAL20 computer program in the first instance and subsequently the lowest and highest reading were rounded-off to the next decade (Versteeg, 2003, p. 267), resulting in dates between 670 and 960 AD (see Table 1). In this study, the ^{14}C dates were re-calibrated with the OxCal 4.2 program (Ramsey, 2009), using the IntCal13 curve (Reimer et al., 2013). After re-calibration, the dates of the samples are found to be between 656 and 974 AD (Table 1). Below an overview is given of the datings of material from the Wageningen-1 mound, with the corresponding depths (Table 1, left). Table 1 (right) presents the sample names as used throughout this study and corresponding depths of the potsherds. The levels are named according to the order in which the shards were received, and thus do not indicate an increase/decrease in depth. As the shards from level 5 and 6 could be distinguished in two main types, a distinction was made into an A- and a B-level. When the depths of the material used for this study are compared with the actual datings plotted against the corresponding depths (Figure 5), we notice an almost linear trend, thus we may interpolate the ages of the shards used.

Table 1 Ages and depths of Surinamese potsherds used in this study

		CAL20	OxCal 4.2
Depth (cm)	*Age (14C yrs BP)*	*Age (calAD)*	*Age (calAD)*
295	1310 ± 30	715 ± 45	712.5 ± 56.5
225	1245 ± 25	790 ± 70	775.5 ± 93.5
200	1230 ± 25	775 ± 5	785.5 ± 95.5
155	1240 ± 30	795 ± 75	780 ± 96
125	1210 ± 25	830 ± 40	803 ± 86
75	1145 ± 25	925 ± 35	875.5 ± 98.5

Sample (SUR-)	*Depth (cm)*
1	307
2	164
3	292
4	145
5A	75
5B	75
6A	98
6B	98

Left: Ages of shards from Wageningen-1 mound, with corresponding depths; Right: Sample names as used throughout this study, with related depths.

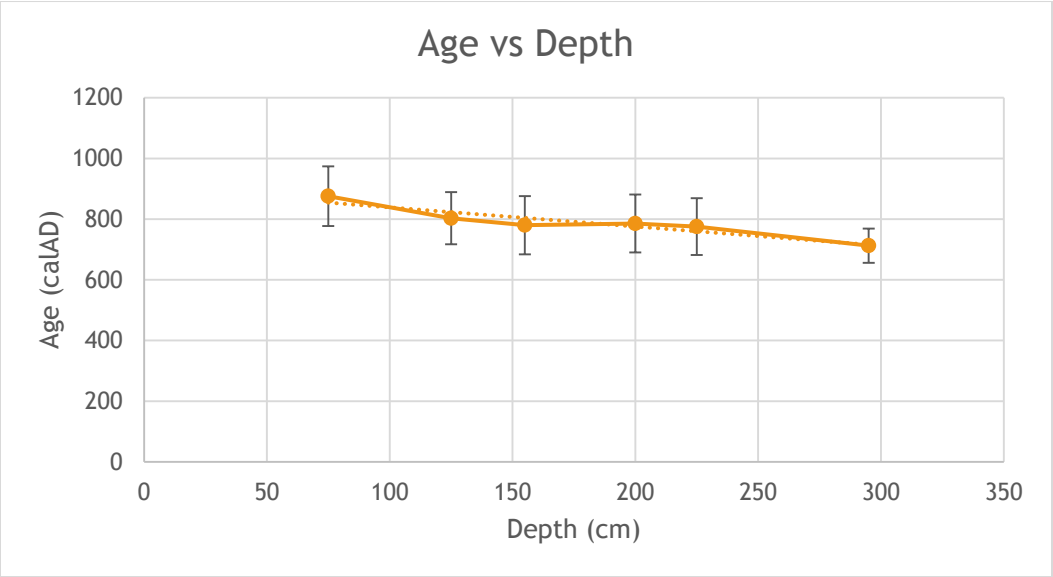

Fig. 5 Graph of the calibrated ages of the dated material from the Wageningen-1 mound against the associated depths; dashed line shows a linear trend, from which we can interpolate the ages of the potsherds used in this study.

First, rock magnetic experiments have been carried out at Paleomagnetic Laboratory Fort Hoofddijk (Utrecht University). Afterwards, specimens of each level have been thermally demagnetized. Finally, archeointensities have been measured, using respectively the Microwave-Thellier method (University of Liverpool) and the IZZI-Thellier method (Utrecht University). After measuring the intensities, the results were interpreted and compared with the global geomagnetic models SHA.DIF.14K and pfm9k.1. Potential anisotropy and cooling rate effects have not been tested.

3.2 Supporting Rock magnetic analyses

Several rock magnetic experiments have been carried out to characterize the magnetic properties and identify the carrier(s) of the magnetization of the archaeological pottery shards from each level. Each of these is described below.

3.2.1 Thermomagnetic runs

Both high-field and low-field thermomagnetic experiments have been completed on one representative shard per level. High-field thermomagnetic runs (magnetization versus temperature) were measured in air by the modified horizontal translation Curie balance at Fort Hoofddijk, which has a sensitivity of approximately 2×10^{-9} Am^2. After careful weighing, approximately 40-70 mg of powdered samples from each level were put into a quartz glass sample holder and held in place by quartz wool; the applied minimal field ranged between 100 and 260 mT, B_{max} was set on 300 mT. Low-field thermomagnetic experiments (susceptibility versus temperature) were also performed on the same shards using the KLY3-CS susceptibility bridge at Fort Hoofddijk. Opposed to the Curie balance, granular material of 100-210 mg were used. In Table 2 the mass of the specimen used for each method (high-field and low-field) is given.

Table 2 Mass of material used for each method

Sample (SUR-)	m Curie balance (mg)	m Kappa-bridge (mg)
1	63.02	101.4
2	38.02	210.2
3	47.78	214.45
4	54.04	205.16
5A	71.5	180.08
5B	61.45	206.58
6A	54.83	207.3
6B	51.74	203.79

3.2.2 Hysteresis parameters and back-field curves

In addition to the high-field and low-field thermomagnetic experiments, hysteresis parameters and back-field curves were measured for each level at room temperature, using the newly acquired Vibrating Sample Magnetometer (Hugo Kruytgebouw, Utrecht University). This magnetometer has a noise of ~0.8×10^{-9} Am^2 (at 10 mm). For the hysteresis loops, a maximum field of 16000 Oe (1.6 T) was applied. Samples ranging from 3-5 mm were attached to the glass

sample holder using teflon tape. Hysteresis loops were measured to determine the saturation magnetization (M_s), the saturation remanent magnetization (M_r) and coercive force (H_c). These parameters were determined after correcting for the paramagnetic contribution of the sample. The remanent coercivity (H_{cr}) was determined by measuring back-field curves from the same specimen.

3.2.3 Thermal demagnetization

Thermal demagnetization has been performed on two to three samples per level (in total 16 samples); for these experiments only, the subdivision of levels 5 and 6 was not wielded. The potsherds were first cut into small cubic samples of approximately ~1 cm cube, with their thickness depending on the thickness of the pottery; to enable measuring on the spinner, they were cast into standard size cylindrical samples (diameter of ± 2.5 cm and $h < 2$ cm) using ceramic paste in the shielded room. As the ceramic paste can be slightly magnetic, its magnetization was first analyzed to determine whether usage of the paste was admissible (using an 'empty' dummy specimen). The maximum contribution of the paste was found to be generally below 2% of the signal of the samples, at maximum 5%. The specimens have been heated using the TD48-SC thermal demagnetizer at successive temperature steps of 50, till 450 °C and afterwards with temperature intervals of 20, till 570 °C. The last heating step was from 570 to 580 °C. It must be emphasized that the samples were taken unoriented; paleomagnetic directions can therefore not be derived from these demagnetizations, but the nature of the demagnetization behavior and the presence of overprints can be reliably assessed.

All measurements on remanent magnetization have been carried out using a manual AGICO JR6 dual speed spinner magnetometer, which is controlled by Microsoft Windows software Rema6W. The measuring principle is based on the law of electromagnetic induction. A specimen of defined size and shape rotating at a constant speed in a vicinity of a nearby detector induces an AC voltage signal. The amplitude and phase of the induced signal depend on the magnitude and direction of the vector of magnetic remanence of the specimen. The JR-6 series dual speed spinner magnetometer is based on the "classical" design where a specimen rotates about a single axis inside a pair of the Helmholtz coils (Agico, 2004). In such an arrangement only the components of magnetic remanence vector in the plane perpendicular to the axis of rotation are

measured; the component of the vector parallel to the rotation axis induces no signal. To measure the full vector of magnetic remanence, the specimen must be at least once manually re-positioned, thus two measuring positions are needed at the minimum. The JR-6 series spinner magnetometer features two speeds of rotation: the high speed (87.7 revolutions per second), and the low speed (16.7 rps). The low speed of rotation increases the possibility of measuring fragile specimens, soft specimens, and specimens with considerable deviations in size and shape. The measuring range is from about 2.4×10^{-6} Am^{-1} up to 12.500 Am^{-1} (Chadima et al., 2011).

All 16 samples have been successively measured in four positions to reduce measurement errors due to the inaccurate shape of specimen, instrument noise, and to eliminate any residual non-compensated components of remanence vector of the holder. The acquisition time was set on normal and a low speed of rotation was chosen. Acquired data were automatically sorted according to the specimen names, and further processed using Remasoft.

3.3 Archeointensity Analysis

To measure the archeointensity from the pottery shards, two methods were used: (1) Microwave-Thellier method and (2) the conventional IZZI-Thellier method; these will be described in more detail in the next sections.

3.3.1 Microwave-Thellier excitation

Archeointensity measurements using the Microwave-Thellier method, incorporating pTRM and pTRM Tail checks (Riisager and Riisager, 2001) have been performed on 50 specimens from shards of levels 4-6, using the 14 GHz microwave system at University of Liverpool (i.e. *'Tristan'*). This system incorporates a resonant microwave cavity and a cryogenic magnetometer, is fully automated, and permits the applied microwave power, magnetic field strength and direction to be defined by the operator. Once the sample is prepared and inserted into the system, the orientation remains fixed, thus any change in the direction of magnetization can easily be recognized. First, specimen with a 5-mm-diameter core typically 3 to 6 mm long were drilled from all shards of levels 4-6, and smoothed (for a flat surface). Then, 1 specimen per shard was subjected to microwave demagnetization, to check its stability. Those shards that were

found to be stable to microwave demagnetization, were used for archeointensity measurements. Shards from levels 1-3 could not be analyzed on the microwave, as these exhibit relatively weak magnetic moments. For microwave demagnetization the sample is placed in the centre of the resonant cavity. When microwave power is applied, the microwave field couples with the magnetic system in the sample, producing magnons (spin waves). As the power is increased the number of magnons increases, increasing the energy of the magnetic system and demagnetizing the sample (Biggin et al., 2007). As the application of a single alternating field demagnetization (AFD) treatment prior to a measurement has been found to improve the linearity of Arai plots in a standard Thellier experiment (Biggin et al., 2007), microwave demagnetization treatments have been employed prior to each intensity measurement for experiments on the microwave. Microwave power was applied 5 s and increased incrementally from 5 to 40 W, until the sample had been completely remagnetized and the magnetization was in the direction of the applied field. If this was not obtained at 40 W, the time was then increased gradually. For each power step, the pre-measurement demagnetization treatment (Z-step) was carried out, then the sample was 'heated' in a known laboratory magnetic field of 30 μT (I-step), followed by again 'heating-cooling' in zero field (pTRM Tail check); finally the pTRM check step was performed for every two power steps.

Parameters and Criteria for archeointensity determination (Microwave-Thellier)

The microwave data were analyzed using the ExThellier_CSV software. The values of the ancient field were obtained from the slopes, determined by least squares analysis, of linear segments in 'NRM lost' versus 'TRM gained' ('Arai') diagrams (Nagata et al., 1963). A number of parameters were produced from the paleointensity results. When analyzing the results, the points on the Arai plot which were chosen to produce the determination, were selected objectively, using criteria normal to ancient paleointensity studies: a primary directional component coupled with the most linear portion on the Arai plot and the best pTRM check results. To obtain acceptable results, the measurements were filtered through a set of selection criteria. For the microwave experiments in which both pTRM checks and pTRM tail checks (Riisager and Riisager, 2001) were employed, the criteria were: MAD $\leq 15°$, $\alpha \leq 15°$, $N \geq 4$, $f \geq 0.15$, $q \geq 1$, $\beta \leq 0.10$, DRAT $\leq 10\%$, DRAT(Tail) $\leq 10\%$. MAD is the maximum angular deviation, α the angle between the origin-anchored and centre-of-mass-anchored vectors on the

Zijderveld plot (Zijderveld, 1967), N the number of points used to produce the determination, *f* defines the fraction of the sample's NRM which is used to produce the determination, *q* the quality factor, given as $q = f*g/\beta$ where the *g* (gap) value is a measure of the regularity of the spacing of the points along the best-fit line (Coe et al., 1978). The β value is the standard error of the slope of the best fitting straight line on the Arai plot divided by the value of the slope itself. The DRAT parameter is the Max |ΔpTRMcheck| divided by the *f* value (Selkin and Tauxe, 2000). Max |ΔpTRMcheck| refers to the maximum absolute amount of discrepancy between a pTRM check and an original measurement of pTRM that falls within the selected temperature range of the experiment, expressed generally as a percentage of the initial NRM measurement for that sample. DRAT(Tail) is calculated in the same way as DRAT but using the maximum discrepancy measured by the tail checks (Riisager and Riisager, 2001).

In microwave demagnetization/remagnetization, magnons are directly excited with the use of high-frequency microwaves, thus eliminating the need to heat the bulk sample. Some heating of the bulk sample does occur due to the generation of phonons in the relaxation process, but to a much lower extent than in conventional heating. Each microwave application lasts only for a few seconds, as opposed to heating/cooling times of the order of an hour. Since alteration is both time- and temperature-dependent (Walton 1988), microwave demagnetization/remagnetization offers a distinct advantage over conventional demagnetization/remagnetization, especially in the context of paleointensity determinations (Hill & Shaw, 1999). As well as reducing experimental time, this method eliminates the need for accurate power and microwave absorption reproducibility. However, this method is only applicable if the samples are magnetically isotropic (Shaw et al., 1996).

3.3.2 IZZI-Thellier method

The aim was to measure 7-8 samples per level using the IZZI-Thellier method. Besides all the shards that had been measured on the microwave, one to two representative shards of the remaining levels (1-3) were also first cut into small cubic samples of approximately 1 cm cube, with its thickness depending on the thickness of the pottery. They were prepared in the same way as the samples for the thermal demagnetization experiments, i.e. casted in ceramic paste in the shielded room to facilitate easy measuring on the cryogenic magnetometer. (The magnetic allowance of the ceramic glue was already explored prior the thermal demagnetization). For

practical reasons only 42 out of the 53 samples could be prepared for measurements. Apart from these 42 samples, 10 more volcanic samples from two lava flows (T-3 and T-18) from the Azores were measured. Paleointensity measurements were performed in air, using the IZZI-Thellier method (Tauxe and Staudigel, 2004) on the 2G DC SQUID magnetometer (Fort Hoofddijk). The temperature steps used increased progressively from 50 °C to 400 °C in steps of 50 °C and from 400 °C to 560 °C in steps of 40 °C. The last step measured was 590 °C. The heating-cooling procedure followed was:

1. Heating to T_i and cooling to T_r (room temperature) in a zero field (the demagnetization (Z) step)
2. Heating to T_i and cooling to T_r in a known laboratory magnetic field of 50 μT, applied along the z-axis of the specimens (the remagnetization (I) step)
3. Heating to T_{i+1} and cooling to T_r in a magnetic field of 50 μT, applied along the z-axis of the specimens (the remagnetization (I) step)
4. Heating to T_{i+1} and cooling to T_r (room temperature) in a zero field (the demagnetization (Z) step)

After the next demagnetization step (at T_{i+2}), a 'pTRM check' step was involved in order to detect any chemical alteration in the magnetic mineralogy of the samples during the experiment:

5. Heating to T_{i+1} and cooling to T_r in an applied magnetic field of 50 μT, along the z-axis of the specimens (thus pTRM checks every two thermal steps).

During the 'remagnetization' steps, the samples were positioned in such a way that the laboratory field made an angle between 45° and 90° with the NRM (semi-perpendicular approach).

Parameters and Criteria for archeointensity determination (IZZI-Thellier)

The data obtained from the IZZI-Thellier method were analyzed using the ThellierTool 4.2 software (Leonhardt et al., 2004). Although parameters produced are comparable to the microwave, the values used for the set of criteria differed, as there is no commonly agreed parameter set and criteria range. The slope of the best fit line, the standard deviation of the linear

fit (Std), the fraction of NRM (*f*), gap factor (*g*), quality factor (*q*) (Coe et al., 1978) as well as the weighting factor (*w*) (Prévot et al., 1985) were determined for a chosen segment of the Arai diagram, either automatically or manually, taking into account that the selected temperature segment for intensity analyses matched the temperature range which carried the characteristic remanent magnetization of the sample. Inclination (Inc), Declination (Dec) and maximum angular deviation were also calculated for both anchored-to-the-origin (MAD) and not-anchored (MAD') fits by principle component analysis (PCA) (Kirschvink 1980), as well as the angular difference between anchored and not-anchored solution (α). To monitor the effect of magnetomineralogical changes from pTRM checks, three parameters were determined: d(CK) (Leonhardt et al., 2000) and DRAT (Selkin and Tauxe, 2000) describe deviations of pTRM checks at a given temperature step, while the cumulative check error (dpal) (Leonhardt et al., 2003) is related to the cumulative difference of the individual checks from room temperature up to the maximum temperature used for the best fit line. This parameter estimates the overall alteration, as even small individual differences between checks and pTRM values can sum to significant alteration errors (Leonhardt et al., 2004). All calculations were done using full vector subtraction. A quality class (A/B or C) was assigned to the determination by comparing the results with the given criteria; if the results did not comply with criteria A and B values, then the determination was termed to be of class C. Criteria for class A were: $N \geq 5$, Std ≥ 0.1, $f \geq 0.3$, $q \geq 1$, MAD ≤ 6, MAD' ≤ 999, $\alpha \leq 15$, d(CK) ≤ 5, d(pal) ≤ 5, and Drat ≤ 999, where N is the minimum number of successive measurement steps. For class B, the changed criteria were Std ≥ 0.15, $q \geq 0$, MAD ≤ 15, d(CK) ≤ 7 and d(pal) ≤ 10.

4 Results

First, an overview of the supporting rock magnetic analyses will be given, followed by hysteresis parameters, thermal demagnetization plots and the archeointensity results. A complete overview of all the hysteresis loops and plots obtained from the archeointensity experiments, will be given in respectively Appendix 1 and 2.

4.1 Rock Magnetism

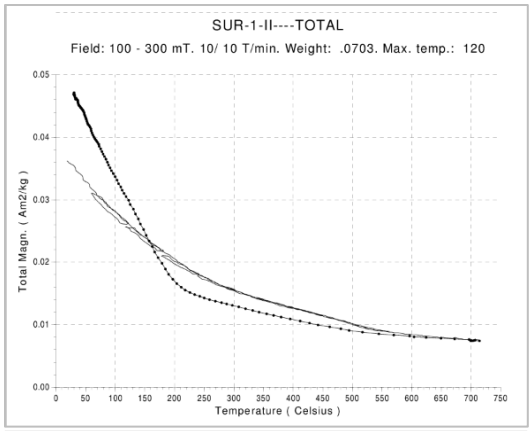

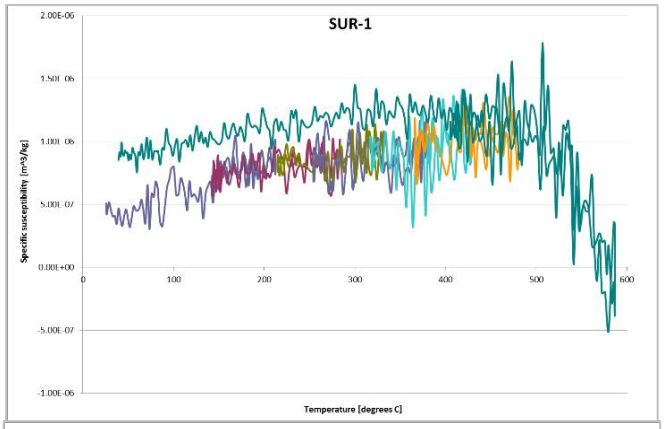

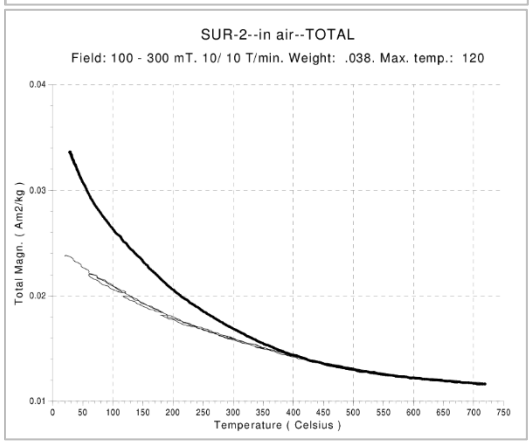

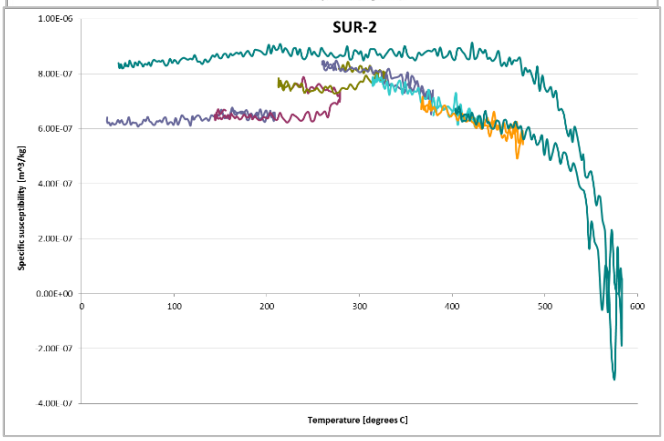

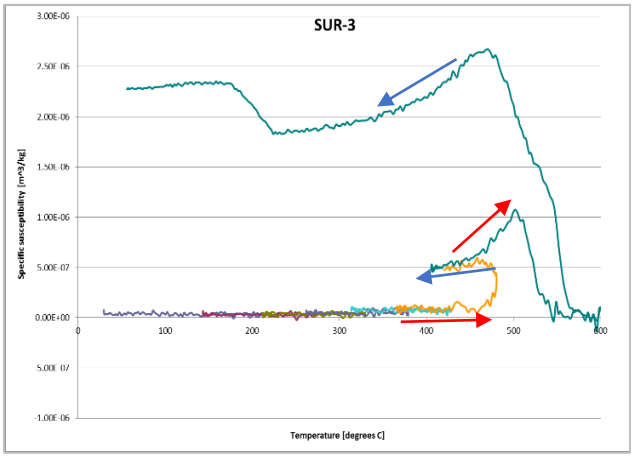

The next figures (Figure 6) are the results of high-field (left) and low-field (right) thermomagnetic runs, acquired for identical shards from each level (respectively 1 to 6B).

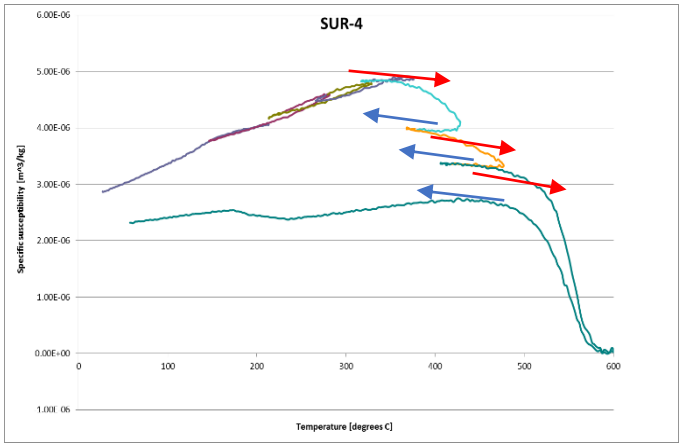
SUR-4
6.00E-06
5.00E-06
4.00E-06
3.00E-06
2.00E-06
1.00E-06
0.00E+00
0
100
200
300
400
500
600
Specific susceptibility [m^3/kg]
Temperature [degrees C]

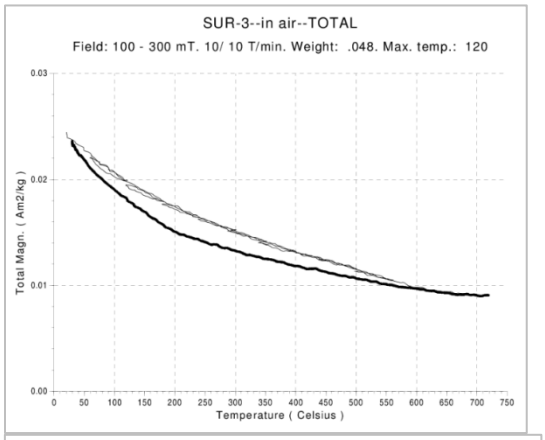
SUR-3--in air--TOTAL
Field: 100 - 300 mT. 10/ 10 T/min. Weight: .048. Max. temp.: 120
Total Magn. (Am2/kg)
Temperature (Celsius)

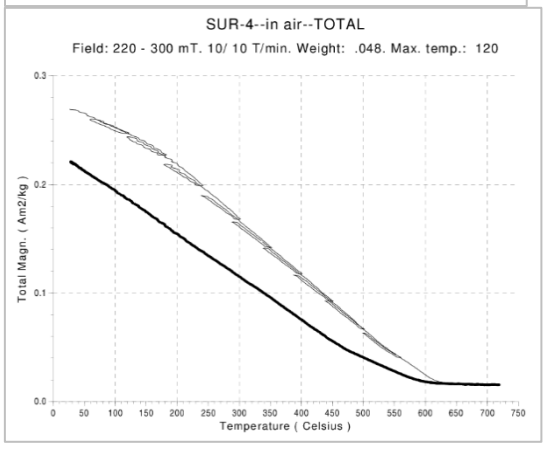
SUR-4--in air--TOTAL
Field: 220 - 300 mT. 10/ 10 T/min. Weight: .048. Max. temp.: 120
Total Magn. (Am2/kg)
Temperature (Celsius)

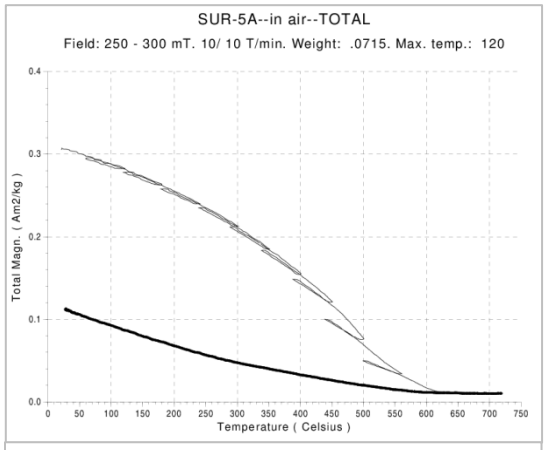
SUR-5A--in air--TOTAL
Field: 250 - 300 mT. 10/ 10 T/min. Weight: .0715. Max. temp.: 120
Total Magn. (Am2/kg)
Temperature (Celsius)

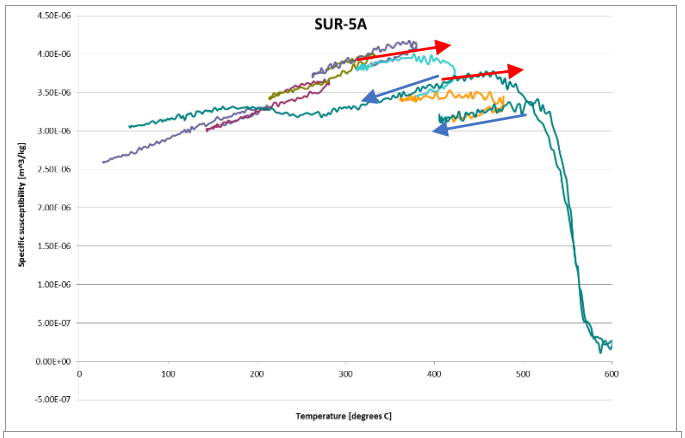
SUR-5A
Specific susceptibility [m^3/kg]
Temperature [degrees C]

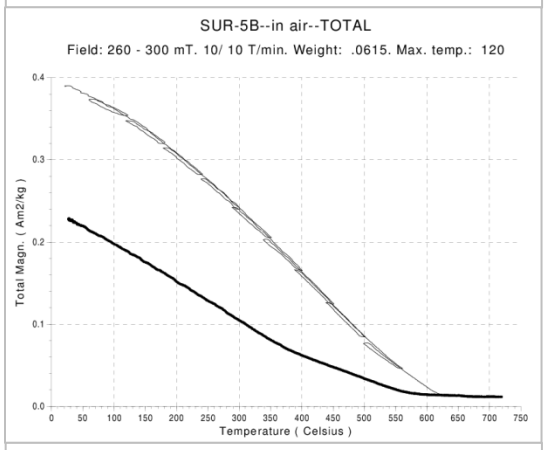
SUR-5B--in air--TOTAL
Field: 260 - 300 mT. 10/ 10 T/min. Weight: .0615. Max. temp.: 120
Total Magn. (Am2/kg)
Temperature (Celsius)

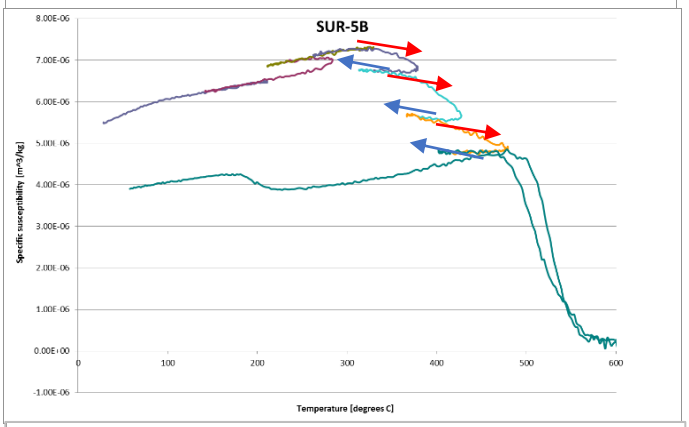
SUR-5B
Specific susceptibility [m^3/kg]
Temperature [degrees C]

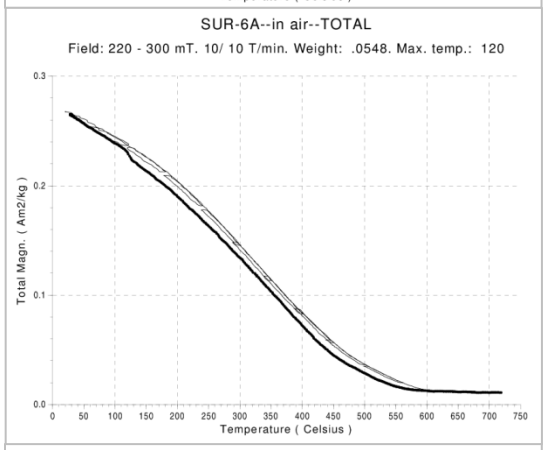
SUR-6A--in air--TOTAL
Field: 220 - 300 mT. 10/ 10 T/min. Weight: .0548. Max. temp.: 120
Total Magn. (Am2/kg)
Temperature (Celsius)

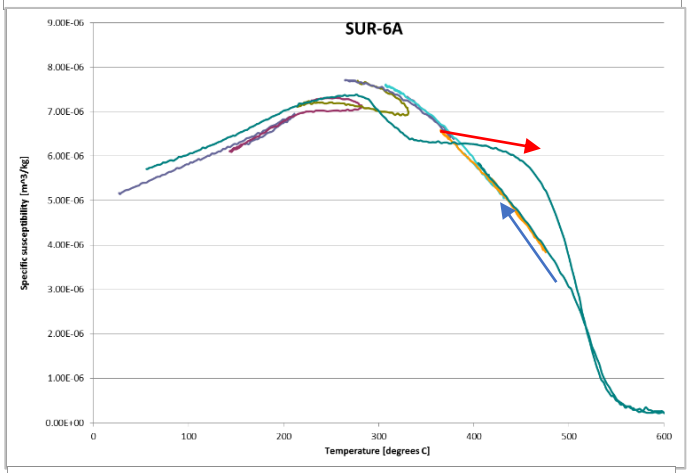
SUR-6A
Specific susceptibility [m^3/kg]
Temperature [degrees C]

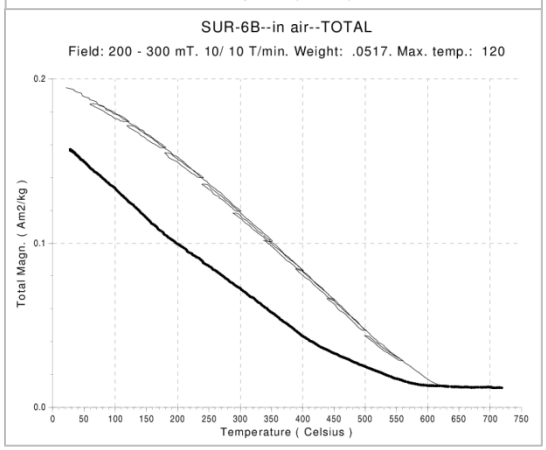
SUR-6B--in air--TOTAL
Field: 200 - 300 mT. 10/ 10 T/min. Weight: .0517. Max. temp.: 120
Total Magn. (Am2/kg)
Temperature (Celsius)

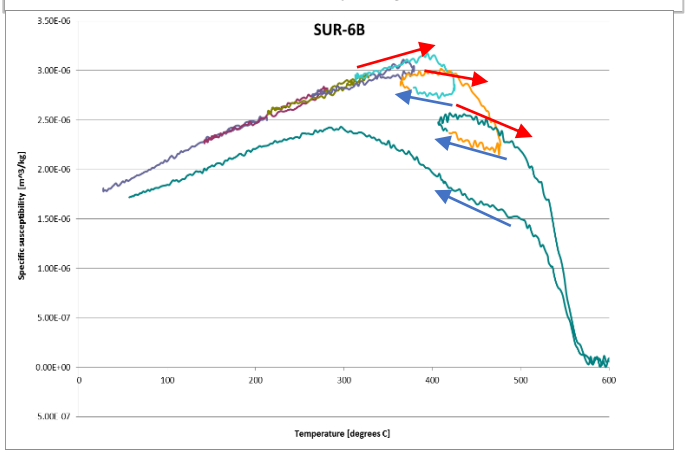
SUR-6B
Specific susceptibility [m^3/kg]
Temperature [degrees C]

Fig. 6 (Above) (Left) High-field (magnetization versus temperature) and (Right) Low-field thermomagnetic runs (susceptibility vs temperature), with several heating-cooling steps. In the high-field thermomagnetic curves, thick lines indicate the heating curves and thin ones cooling. In the low-field thermomagnetic runs heating is indicated by red arrows and blue ones indicate cooling steps. All measurements were performed in air.

The total magnetization is quite low in the selected shards from the first three levels (between 0.02 and 0.04 Am^2/kg) and an order of magnitude higher for levels 4-6 (between 0.2 and 0.4 Am^2/kg). All specimens show a gradual decrease in magnetization up to their respective Curie temperatures (T_c) in the high-field thermomagnetic runs. Levels 1-3 reveal a concave up demagnetization behavior with increasing temperature; samples from levels 4-6 a more linear or concave down trend, with specimen SUR-5A (from level 5A) being most concave down. Although the signal-to-noise ratio in the temperature versus magnetic susceptibility graphs of level 1 and 2 is quite low, a slight increase of susceptibility from room temperature up to 450 °C can be observed, followed by a rapid decrease between 450 and 580 °C. Low-field magnetic susceptibility for the other samples (except from SUR-3) increases sharper from room temperature up to approximately 350, 375, 325, 300 and 400 °C for respectively levels 4, 5A, 5B, 6A and 6B and then decreases rapidly to 580 °C. For level 3 (SUR-3, right), the susceptibility remains almost unchanged until 450 °C, before increasing more rapidly to 580 °C; moreover, there is a remarkable increase between 180 and 230 °C, during the last cooling step. Most samples show irreversible behavior for temperatures exceeding ~400 °C, and all (except the one from SUR-3) decrease in both susceptibility as well as in magnetization with increasing temperature up to approximately 600 °C – implying magnetite as main carrier of the magnetic remanence.

Hysteresis parameters

The parameters acquired after measuring the hysteresis loops and back field curves were compiled and presented in Table 3. Herein, M_s is the saturation magnetization, M_{rs} the saturation

remanent magnetization, H_c the coercive force and H_{cr} the remanent coercivity. See Appendix 1 for an overview of all hysteresis loops and back-field curves.

The hysteresis loops of all the different levels are narrow waisted (Appendix 1), indicating a typical pseudo-domain assemblage (Tauxe et al., 1996). H_c and H_{cr} values range respectively from 3681.97 to 16453.28 A/m and 9767.98 to 40093.12 A/m (Table 3).

Table 3 Hysteresis parameters of the Surinamese pottery specimens

Sample	M_s (Am^2/kg)	M_{rs} (Am^2/kg)	H_c (A/m)	H_{cr} (A/m)	M_{rs}/M_s	H_{cr}/H_c
SUR-1	1.60E-03	2.97E-04	1.28E+04	4.69E+04	0.19	3.66
SUR-2	5.00E-02	8.72E-03	3.68E+03	9.77E+03	0.17	2.65
SUR-3	8.11E-04	1.92E-04	1.65E+04	4.01E+04	0.24	2.44
SUR-4	3.28E-02	7.98E-03	1.19E+04	2.82E+04	0.24	2.36
SUR-5A	2.69E-02	7.20E-03	1.36E+04	2.84E+04	0.27	2.08
SUR-5B	1.63E-02	3.62E-03	7.21E+03	1.76E+04	0.22	2.44
SUR-6A	1.71E-02	3.78E-03	9.89E+03	2.56E+04	0.22	2.59
SUR-6B	1.18E-02	2.92E-03	1.00E+04	2.22E+04	0.25	2.21

To determine the domain state of the samples properly, the ratio of saturation remanence to saturation magnetization (M_{rs}/M_s) is plotted against the ratio of remanent coercive force to ordinary coercive force (H_{cr}/H_c) in a so-called Day plot (Figure 7). Following Dunlop (2002), values of 0.5 and 1 for M_{rs}/M_s and 1 and 2 for H_{cr}/H_c are used as single domain (SD) limits. The Day plot confirms pseudo-single-domain (PSD) behavior for all our samples – implying rather large grain sizes for pottery.

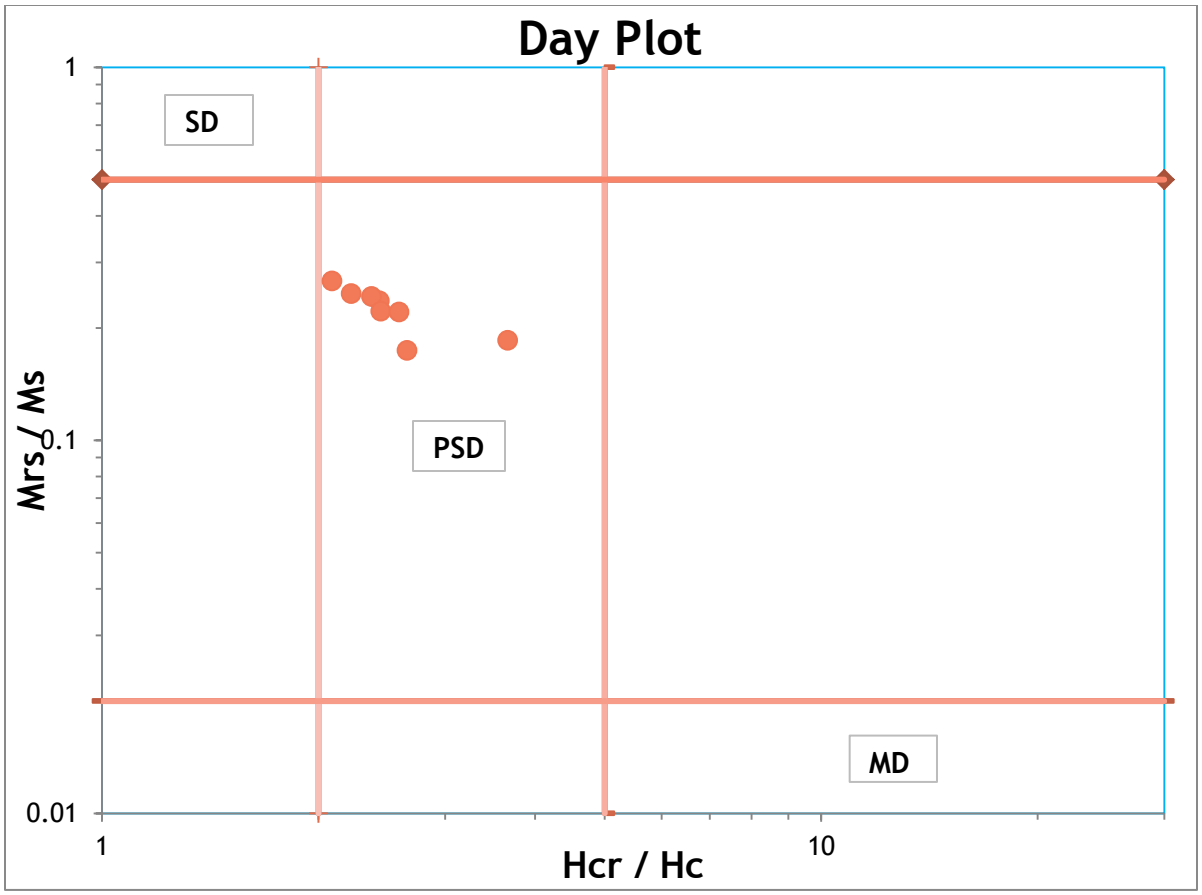

Fig. 7 Hysteresis properties of the Surinamese pottery plotted on a Day Plot; all samples are in the PSD state.

Thermal Demagnetization

The main characteristics of the thermally demagnetized NRM of 2 or 3 specimens per level are in Figure 8. Left, the thermal demagnetization curves are given and on the right the corresponding Zijderveld diagrams of each sample. Sample SUR-1A could not be fully demagnetized, as the measurement had to be terminated prematurely, due disintegration of the sample. Samples SUR-1B, SUR-2A, SUR-2B, SUR-6A and SUR-6B are gradually (i.e. almost linearly) thermally demagnetized between 100 and 580 °C. Samples SUR-3B and SUR-3C, samples SUR-4A and SUR-4B, and samples SUR-5A and SUR-5B loose only ~10 % of their magnetization at respectively 350, 300 and 250 °C; after this temperature, the demagnetization is more or less gradual, but increases rapidly from about 500 °C. The behavior of the latter group of samples implies magnetite as main remanence carrier; the first group of samples might be dominated by titanomagnetites or a mixture of ferromagnetic minerals. Sample SUR-3A, unlike

any other sample, first shows an increase till 300 °C, before demagnetizing; this is explained as a low temperature overprint following its behavior in the Zijderveld diagram. Samples from levels 1 to 3 have a relatively low NRM, as opposed to samples from levels 4 to 6. Samples from another shard of level 2 (SUR-2A, SUR-2B), then previously used for rock magnetism, were also subjected to thermal demagnetization and turned out to have a relatively high NRM too.

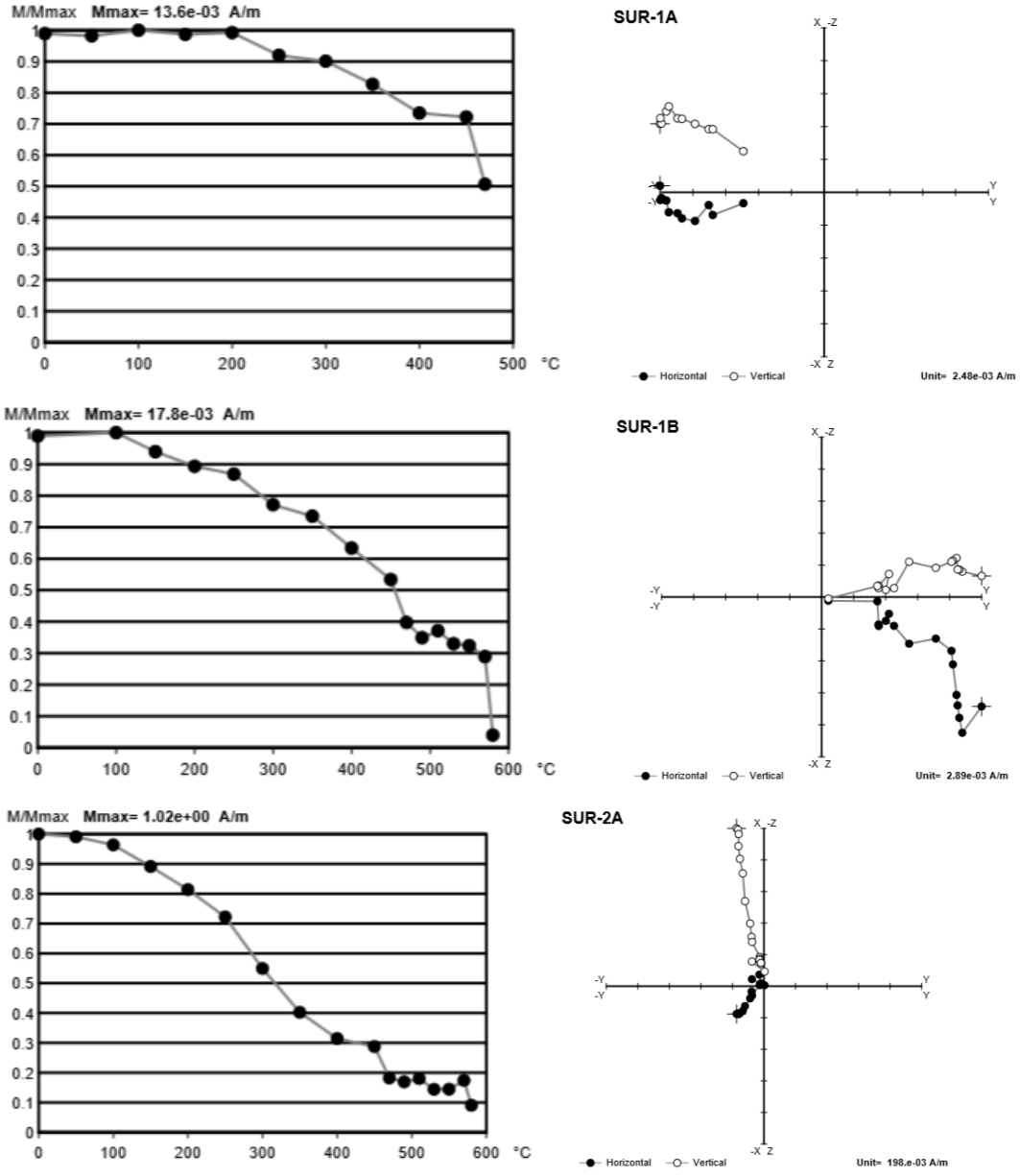

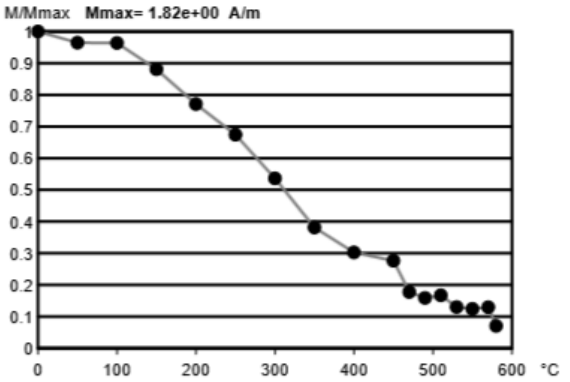
M/Mmax Mmax= 1.82e+00 A/m
0 100 200 300 400 500 600 °C

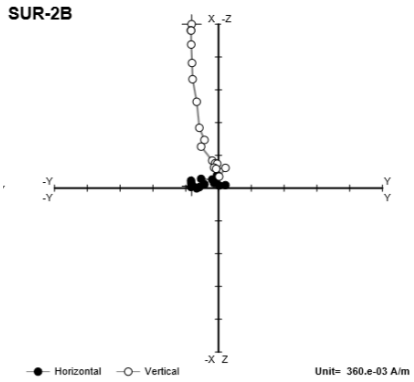
SUR-2B
X -Z
-Y Y
-X Z
Horizontal Vertical
Unit= 360.e-03 A/m

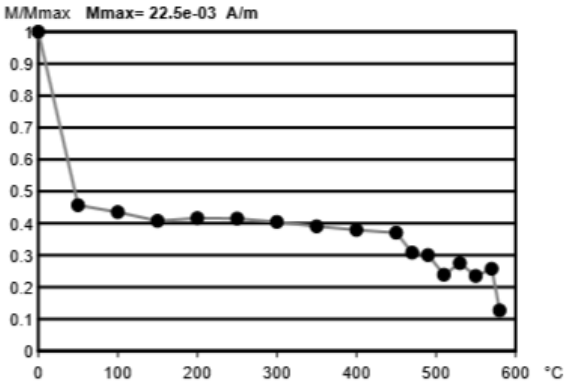
M/Mmax Mmax= 22.5e-03 A/m
0 100 200 300 400 500 600 °C

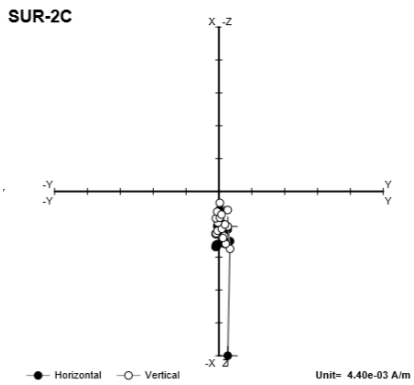
SUR-2C
X -Z
-Y Y
-X Z
Horizontal Vertical
Unit= 4.40e-03 A/m

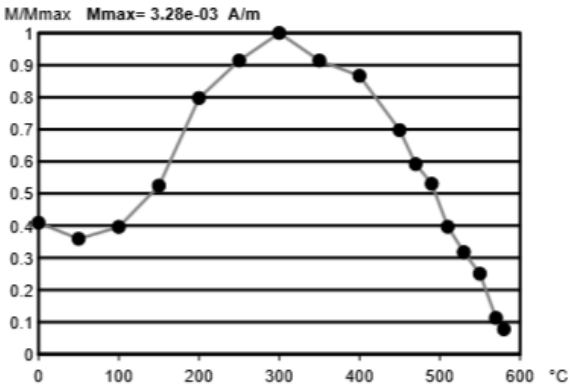
M/Mmax Mmax= 3.28e-03 A/m
0 100 200 300 400 500 600 °C

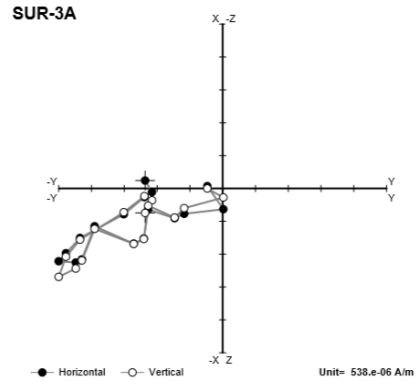
SUR-3A
X -Z
-Y Y
-X Z
Horizontal Vertical
Unit= 538.e-06 A/m

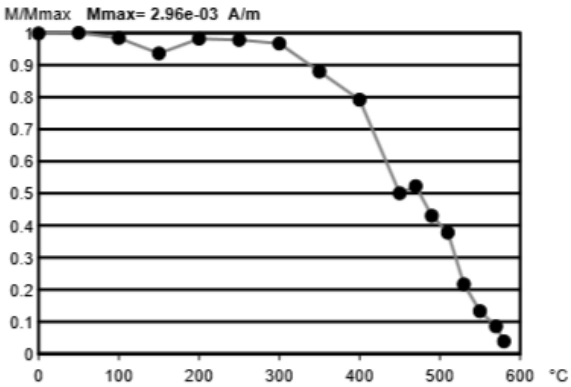
M/Mmax Mmax= 2.96e-03 A/m
0 100 200 300 400 500 600 °C

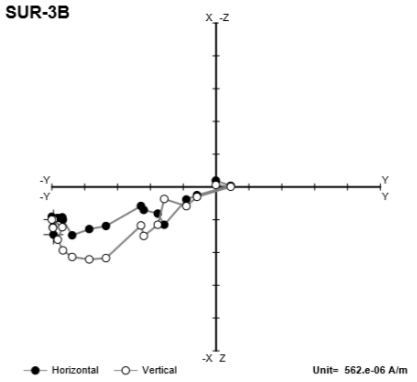
SUR-3B
X -Z
-Y Y
-X Z
Horizontal Vertical
Unit= 562.e-06 A/m

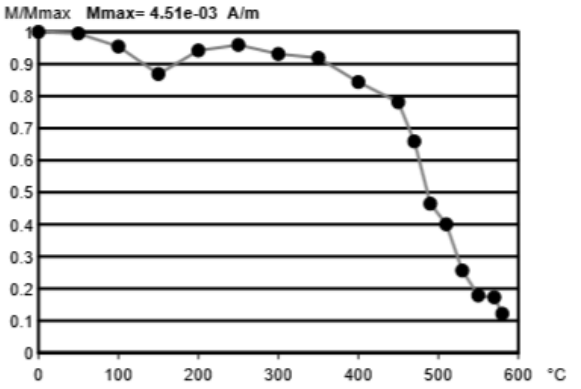
M/Mmax Mmax= 4.51e-03 A/m
1
0.9
0.8
0.7
0.6
0.5
0.4
0.3
0.2
0.1
0
0 100 200 300 400 500 600 °C

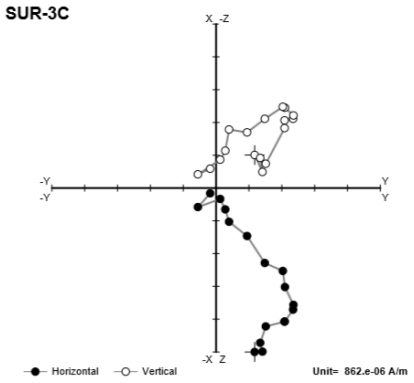
SUR-3C
X -Z
-Y
Y
-X Z
Horizontal
Vertical
Unit= 862.e-06 A/m

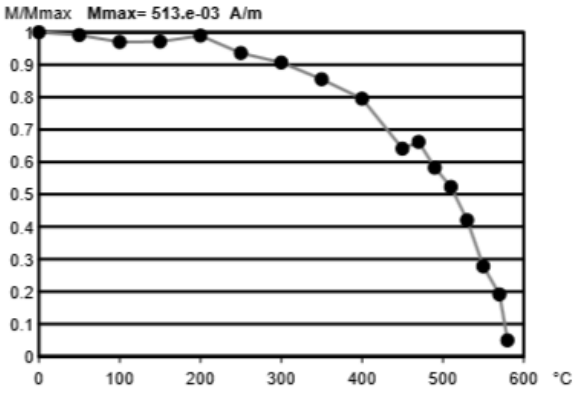
M/Mmax Mmax= 513.e-03 A/m
1
0.9
0.8
0.7
0.6
0.5
0.4
0.3
0.2
0.1
0
0 100 200 300 400 500 600 °C

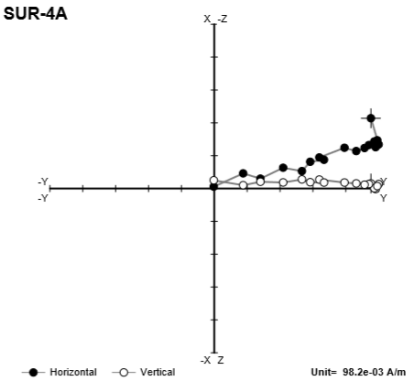
SUR-4A
X -Z
-Y
Y
-X Z
Horizontal
Vertical
Unit= 98.2e-03 A/m

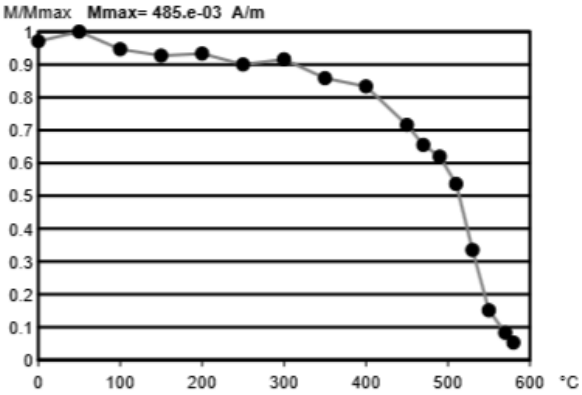
M/Mmax Mmax= 485.e-03 A/m
1
0.9
0.8
0.7
0.6
0.5
0.4
0.3
0.2
0.1
0
0 100 200 300 400 500 600 °C

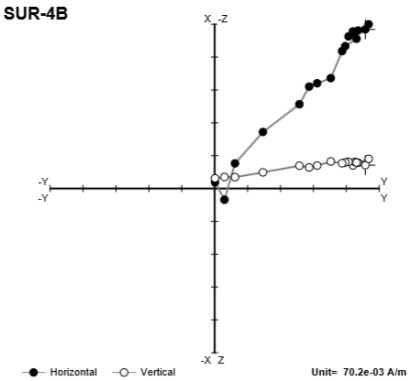
SUR-4B
X -Z
-Y
Y
-X Z
Horizontal
Vertical
Unit= 70.2e-03 A/m

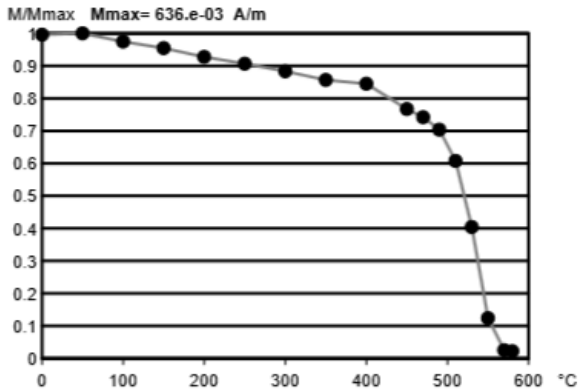
M/Mmax Mmax= 636.e-03 A/m
1
0.9
0.8
0.7
0.6
0.5
0.4
0.3
0.2
0.1
0
0 100 200 300 400 500 600 °C

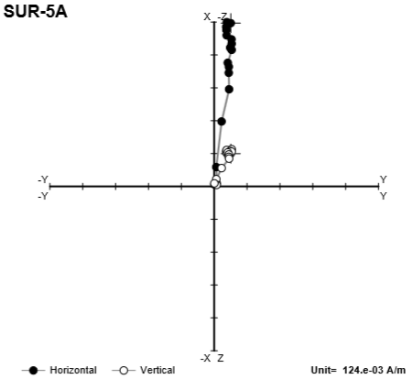
SUR-5A
X -Z
-Y
Y
-X Z
Horizontal
Vertical
Unit= 124.e-03 A/m

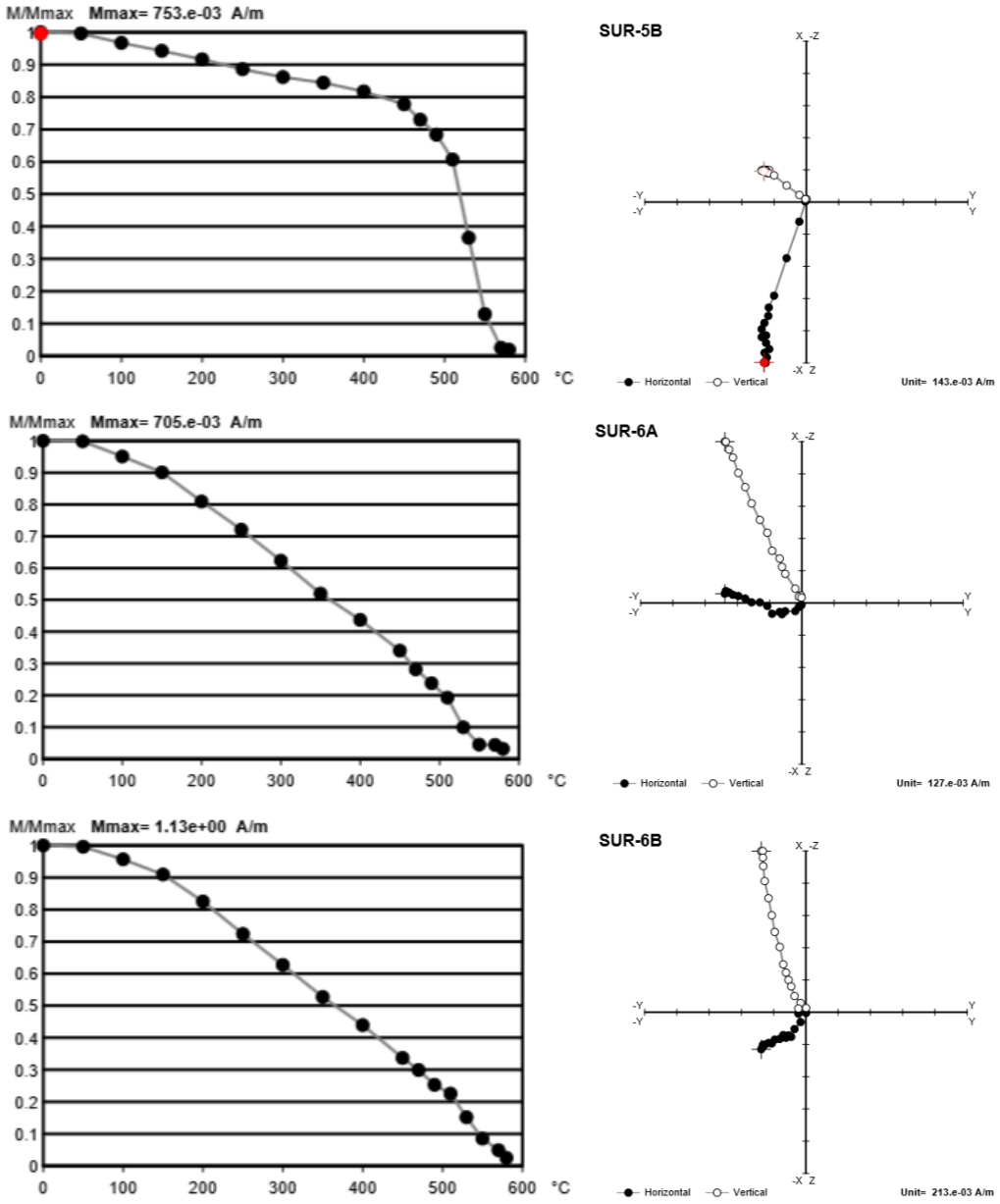

Fig. 8 Thermal demagnetization curves (left) and corresponding Zijderveld diagrams (right) of specimens from representatives shards of each level.

4.2 Archeointensity

Next, the archeointensity results for both methods used in this study will be presented and described.

Microwave-Thellier excitation

As samples from level 4, 5 and 6 turned out to have relatively high NRM's, only specimen from these levels were measured at the microwave using the Microwave-Thellier method. In contrary to other techniques employed in this study, microwave-Thellier analysis was performed using specimen from all shards of levels 4 to 6; samples have been named accordingly. For example, in sample SURIS4-3B, SURI is the code used for the Suriname samples in the Liverpool database (PalaeoDB2012), S4- refers to level 4, 3 to shard 3 and the last letter (B) indicates the nth (second) measurement (in alphabetical order), related to that typical shard. The results are in Table 4, a complete overview of corresponding graphs is given in Appendix 2a. A laboratory field of 30 μT was used for all In-field steps. Unfortunately, many samples tended to physically expand or even explode and/or fall off from the sample holder during the measurements and many archeointensity measurements had to be terminated at an early stage, without obtaining any archeointensity results. In first instance, no pTRM Tail checks were measured, so these are 0 % for specimen from level 4. Out of the 50 initial intensity measurements, only 27 yielded some results, out of which only 3 passed all criteria. The low success rate might also be caused by overlooking a 'z-axis-error' (miscalibration of the field in the z-direction) which occurred in some of the first measurements. Nearing the end of my measuring time the microwave suffered some serious failures (coil problems) and no proper measurement was possible. Some results still produced at that time had to be discarded (i.e. SURIS5B-1F resulted in an Arai plot going backwards). Although results from most identical shards are close, they do not pass the criteria set and thus cannot be relied on. For level 4 an average archeointensity of 26.2 ± 2.3 μT was measured, for level 5A 47.5 ± 4.4 μT, while no measurements of level 5B and 6 passed all criteria.

Table 4 Archeointensity results, obtained using the Microwave-Thellier method for all shards from levels 4 to 6

Sample	Δpower/T (W/s)	*N*	β	*f*	*g*	*q*	*delCK*	*DRAT*	*CDRAT*	*α (°)*	MAD (°)	*DRATtail*	*PI (μT)*	*SD (μT)*	*PI(level)*
SURIS4-2D	35/5	0	---	0.00	---	---	0.0%	0.0%	0.0%	---	---	0.0%	---	---	
SURIS4-3B	**40/12**	**4**	**0.09**	**0.21**	**0.59**	**1.4**	**2.0%**	**7.4%**	**-22.3%**	**13.6**	**1.3**	**0.0%**	**26.2**	**2.3**	26.2 ± 2.3
SURIS4-4C	40/17	5	0.09	0.71	0.67	5.1	31.7%	*29.6%*	68.0%	2.1	1.2	0.0%	33.9	3.2	
SURIS4-4G	22/5	2	---	0.25	---	---	0.0%	0.0%	0.0%	*43.70*	8.10	0.0%	8.9	---	
SURIS5A-1B	40/17	6	0.04	0.42	0.61	8.1	17.4%	*22.0%*	22.0%	17.0	5.8	0.0%	25.7	1.2	
SURIS5A-1C	40/6	4	*0.17*	0.36	0.26	*0.6*	2.6%	6.0%	6.0%	*166.3*	2.8	9.0%	21.7	3.6	
SURIS5A-2B	25/5	3	0.05	0.30	0.40	2.2	56.2%	*127.4%*	127.4%	9.9	1.6	0.0%	33.0	1.8	
SURIS5A-2C	**28/5**	**4**	***0.11***	**0.19**	**0.54**	**1.0**	**0.1%**	**0.4%**	**-0.4%**	**5.7**	**0.4**	**2.8%**	**47.2**	**5.1**	
SURIS5A-2E	**28/5**	**4**	**0.08**	**0.41**	**0.65**	**3.4**	**0.5%**	**0.6%**	**-0.6%**	**3.1**	**0.7**	**3.4%**	**47.9**	**3.7**	
SURIS5A-2F	25/5	3	*0.20*	*0.13*	0.30	*0.2*	0.0%	0.0%	0.0%	9.2	0.6	*49.7%*	37.8	7.4	47.5 ± 4.4
SURIS5A-2G	22/5	3	*0.37*	0.36	0.49	*0.5*	0.0%	0.0%	0.0%	9.9	1.9	0.0%	15.9	5.9	
SURIS5A-2H	26/5	3	*0.25*	0.19	0.43	*0.3*	6.0%	*20.5%*	-20.5%	6.7	0.6	*47.4%*	35.6	8.8	
SURIS5A-2I	26/5	3	0.04	*0.10*	0.23	*0.6*	0.9%	8.5%	-8.5%	*17.5*	1.0	*12.4%*	2.1	0.1	
SURIS5A-2J	24/5	3	0.07	0.32	0.49	2.4	0.0%	0.0%	0.0%	6.7	1.1	0.0%	35.4	2.4	
SURIS5A-3B	27/5	3	0.02	0.16	0.15	1.3	6.5%	*33.3%*	-33.3%	1.0	0.1	0.0%	20.6	0.4	
SURIS5B-1B	40/7	4	*0.24*	0.45	0.46	*0.8*	2.7%	*4.9%*	6.5%	*15.6*	4.3	---	21.4	5.2	
SURIS5B-1C	40/6	3	*0.22*	0.52	0.31	*0.7*	3.1%	4.3%	-4.3%	9.3	3.3	---	29.5	6.6	
SURIS5B-1D	31/5	2	---	0.47	---	---	0.0%	0.0%	0.0%	---	*18.1*	0.0%	3.4	---	---
SURIS5B-1E	40/7	0	---	0.00	---	---	0.0%	0.0%	0.0%	---	---	0.0%	---	---	
SURIS5B-1F	38/5	0	---	0.00	---	---	0.0%	0.0%	0.0%	---	---	0.0%	---	---	
SURIS6B-1C	28/5	2	---	0.49	---	---	0.0%	0.0%	0.0%	28.2	10.8	---	21.2	---	
SURIS6B-2E	21/5	4	*0.16*	0.44	0.51	1.4	0.0%	0.0%	0.0%	28.3	6.5	---	31.0	5.1	
SURIS6B-2F	25/5	6	*0.17*	0.77	0.64	2.8	18.2%	*19.1%*	18.2%	15.0	5.3	---	22.0	3.8	
SURIS6B-3B	25/5	5	0.10	0.82	0.67	5.8	19.3%	*17.4%*	15.9%	1.9	3.5	---	27.0	2.6	---
SURIS6B-3C	30/5	7	0.07	0.80	0.80	9.1	26.5%	*24.9%*	50.6%	7.5	3.8	---	26.1	1.8	
SURIS6B-3D	40/5	4	*0.16*	0.25	0.51	*0.8*	18.3%	*42.5%*	71.8%	4.9	4.9	---	42.1	6.9	
SURIS6B-3E	29/5	6	0.04	0.79	0.76	17.0	20.0%	*18.7%*	19.2%	11.6	8.3	---	27.3	1.0	

Only 11% of the measurements pass all the criteria, given in bold. Red italic text emphasizes the values of the parameters at which the measurements fail. Criteria parameters are as discussed in text. ΔPower is the range of applied Power (W) and T the time of the application (s); PI(level) is the average archeointensity of a level, calculated with passed results.

IZZI-Thellier method

All the archeointensity results obtained using the IZZI Thellier method, as well as their relevant parameters are tabulated and shown in Table 6. (For the corresponding Arai plots, directional plots and Decay of NRM intensity plots see Appendix 2b). For all In-field heating and cooling steps, a laboratory field value of 50 μT was used. Although all samples, except for 6A-4, passed the linear fit criteria (N=3, instead of 5), 27 out of 42 samples from the Surinamese pottery had

to be rejected, as they failed to pass the alteration checks and/or the directional criteria. Either the cumulative check error (dpal) (Leonhardt et al., 2003) or the d(CK) parameter (Leonhardt et al., 2000) or both or the angular difference between anchored and not-anchored criterion (α) were much higher than desired (see italic red text values in Table 5). The rejected measurements were all of class C. For the volcanic samples, 6 out of 10 samples passed all criteria; the 40 % that did not, failed at passing alteration criteria only. Archeointensities for the Surinamese samples range between 10 and 16 μT, whereas the volcanic samples paleointensities range between 60 and 72 μT (standard deviations not taken into account).

Although there is no criterion set for β and g, these parameters are also specified in the table. For each level, an average archeointensity (*PI(sel)*) is determined with those samples that passed all the criteria and also put in the table, with the corresponding standard deviation.

In Table 5 archeointensity results for each level are compared before and after filtering the results through the selection criteria; the measured archeointensity of each level is also compared with its age (Figure 9 and 10). In figure 10, all archeointensity results are plotted (microwave as well as IZZI-Thellier). The age given in Table 5 is determined from the trend line of the age vs depth graph (Figure 5), as mentioned in section 3.1. The sample names in bold (5A and 4) indicate results obtained using the Microwave-Thellier method. The level indications are not placed in order, as an increasing depth range was preferred. In addition, the results of the volcanic samples are also shown (T-3*, T-18*).

Table 5 Obtained archeointensity of each level compared with the corresponding depth and age

Sample (SUR-)	*Depth (cm)*	*Age (calAD)*	*Age error (±)*	*PI (raw)*	*PI (sel)*	*Stddev*
5A	75	921	85	29.40	47.50	4.4
5B	75	921	85	14.72	18.50	1.29
6A	98	906	87	12.76	13.52	0.89
6B	98	906	87	17.45	16.18	2.16
4	145	877	91	15.88	15.88	1.61
4	145	877	91	30.50	26.2	2.3
2	164	865	92	18.81	14.21	0.54
3	292	784	104	16.64	12.75	1.63
1	307	775	105	10.52	10.52	0.75
T-3*				59.67	59.67	2.06
T-18*				49.12	71.83	4.09

Table 6 Archeointensity results, using the IZZI Thellier method; all parameters are as described in the text. Results that passed all criteria are in bold. Values which do not satisfy the criteria set, are in italic red text.

Sample	*N*	*β*	*f*	*g*	*q*	*d(CK)*	*d(pal)*	*Drat*	*α*	*MAD*	*MAD'*	*class*	*PI(ind)*	*Stddev*	*PI(sel)*
1-1	**7**	**0.03**	**0.54**	**0.82**	**14.3**	**2.6**	**0.8**	**4.6**	**5.6**	**2.9**	**6.7**	**A**	**13.64**	**0.42**	
1-2	**11**	**0.06**	**0.62**	**0.87**	**9.5**	**2.6**	**7.3**	**4.2**	**13.9**	**6.5**	**17.4**	**B**	**9.02**	**0.51**	
1-3	**14**	**0.04**	**0.61**	**0.88**	**12.1**	**2.7**	**4.1**	**4.3**	**1.1**	**4.6**	**18**	**A**	**9.63**	**0.43**	
1-4	**13**	**0.04**	**0.56**	**0.89**	**11.8**	**2.8**	**2.9**	**4.9**	**12.7**	**5.3**	**17.7**	**A**	**10.80**	**0.46**	
1-5	**14**	**0.06**	**0.57**	**0.88**	**8**	**3**	**2.7**	**5.2**	**10.5**	**5.8**	**21.6**	**A**	**8.97**	**0.56**	**10.52 ± 0.75**
1-6	**6**	**0.13**	**0.39**	**0.74**	**2.2**	**4.1**	**1.9**	**10.3**	**9.7**	**9.1**	**27.3**	**B**	**12.21**	**1.60**	
1-7	**13**	**0.11**	**0.68**	**0.86**	**5.2**	**3.4**	**7.2**	**5**	**11.7**	**8.7**	**24.2**	**B**	**8.09**	**0.91**	
1-8	**6**	**0.09**	**0.38**	**0.74**	**3.1**	**3.4**	**6.1**	**8.7**	**9.7**	**10.2**	**30.1**	**B**	**11.83**	**1.08**	
2-1	12	0.08	0.96	0.87	10.8	5.7	*18*	5.4	4.6	5.2	9.2	C	22.10	1.73	
2-2	12	0.06	0.87	0.85	11.6	5	*25.8*	5.3	4.5	3.1	5.5	C	20.03	1.29	
2-3	12	0.07	0.95	0.88	12.3	7.2	*37.8*	6.8	2.3	3.8	7	C	25.75	1.75	
2-4	11	0.09	0.91	0.87	9.1	6.6	*36.2*	6.6	3.9	4.6	9.1	C	20.67	1.80	
2-5	**10**	**0.04**	**0.73**	**0.83**	**15.8**	**6.1**	**9.3**	**8.1**	**3.6**	**6.2**	**17.2**	**B**	**14.21**	**0.54**	**14.21 ± 0.54**
2-6	14	0.04	0.84	0.86	18.9	6.2	*29.5*	7.1	2.9	6.4	19.3	C	12.81	0.49	
2-7	14	0.05	0.92	0.85	16	5.2	*22.1*	5.3	2.3	4.1	11.4	C	20.02	0.98	
2-8	14	0.04	0.9	0.85	20.8	6.5	*28*	7	5.8	6.9	19.1	C	14.89	0.54	
3-1	8	0.08	0.68	0.67	5.9	*19*	*30.1*	25.9	1.9	5.4	9.2	C	20.51	1.59	
3-2	8	0.07	0.65	0.64	6.3	*20.1*	*35.6*	28.9	6.7	10.1	15.7	C	20.03	1.32	
3-3	8	0.07	0.72	0.73	7.4	*14*	*36.7*	18.3	2	6.4	10.9	C	18.03	1.28	
3-4	8	0.06	0.72	0.77	9.1	6	*21.1*	7.9	4.1	9	14.5	C	16.71	1.02	
3-5	**14**	**0.11**	**0.91**	**0.85**	**6.8**	**9.9**	**6.3**	**10.6**	**2.5**	**5.8**	**12.7**	**C**	**11.26**	**1.28**	**12.75 ± 1.63**
3-6	**14**	**0.14**	**0.83**	**0.81**	**4.9**	**6.5**	**8.8**	**7.5**	**6.1**	**7.5**	**17.2**	**B**	**14.24**	**1.98**	
3-7	8	0.2	0.54	0.78	2.1	*14.9*	3.3	26.8	14.3	18	30	C	14.44	2.91	
3-8	8	0.14	0.61	0.77	3.4	*23.3*	11.8	36.1	1.2	17.9	31.8	C	17.89	2.47	
4-1.1	**7**	**0.1**	**0.54**	**0.73**	**3.8**	**6.2**	**9.4**	**10.9**	**2**	**5.7**	**17.2**	**B**	**17.63**	**1.82**	
4-1.2	**8**	**0.07**	**0.54**	**0.81**	**6.4**	**5.5**	**8.7**	**9.7**	**6.7**	**7.2**	**22.7**	**B**	**15.18**	**1.04**	**15.88 ± 1.61**
4-2.1	**11**	**0.14**	**0.53**	**0.86**	**3.3**	**6.8**	**9.7**	**12.3**	**2.8**	**6.5**	**23.8**	**B**	**15.90**	**2.19**	
4-2.2	**7**	**0.09**	**0.43**	**0.8**	**3.7**	**6.3**	**8.1**	**14**	**8.3**	**3.1**	**8.4**	**B**	**14.82**	**1.40**	
5B-1	14	0.14	0.68	0.62	3.1	8.2	4.7	11.8	*27.4*	10.1	25.5	C	11.53	1.57	
5B-2	14	0.11	0.69	0.67	4	8.2	11.3	11.6	*29.1*	10.5	24.7	C	12.91	1.46	**18.50 ± 1.29**
5B-3	**7**	**0.07**	**0.43**	**0.71**	**4.3**	**3.8**	**5.4**	**8.3**	**5.9**	**5.7**	**21.1**	**B**	**18.50**	**1.29**	
5B-4	7	0.05	0.73	0.66	9.4	9.2	*21.7*	12.1	13.3	9.4	19.6	C	15.92	0.81	
6A-1	**8**	**0.07**	**0.47**	**0.79**	**5.7**	**5.3**	**8.5**	**10.7**	**4**	**4.4**	**16**	**B**	**13.52**	**0.89**	
6A-2	8	0.03	0.75	0.8	19.4	6.2	*19.1*	7.9	3.9	4.8	10.9	C	14.07	0.44	**13.52 ± 0.89**
6A-3	9	0.05	0.78	0.79	12.8	6.1	*18.2*	7.5	1.6	3.2	7.9	C	16.50	0.80	
6A-4	*3*	0.01	0.47	0.45	15.5	5.7	*14.8*	12	2.4	3.6	5	C	6.95	0.10	
6B-1.1	8	0.04	0.8	0.78	16.8	6.8	*23.9*	7.9	3	3	6	C	19.88	0.74	
6B-1.2	7	0.04	0.67	0.74	12.7	5.6	*20.4*	8	4.8	7.5	16.6	C	14.96	0.58	
6B-2.1	8	0.05	0.74	0.75	10.3	4.6	*21.4*	6	5.1	6.9	16.3	C	12.58	0.68	**16.18 ± 2.16**
6B-2.2	10	0.06	0.83	0.78	11.1	9.7	*42.3*	10.5	10.8	7.8	16.3	C	24.02	1.39	
6B-3.1	**8**	**0.13**	**0.69**	**0.66**	**3.4**	**4.9**	**7.8**	**6.8**	**6.8**	**4.8**	**11.7**	**B**	**16.18**	**2.16**	
6B-3.2	14	0.08	0.79	0.84	8.3	*12.8*	*29.3*	15.2	*26.9*	12.2	21	C	17.05	1.37	
T3-A	**14**	**0.02**	**0.92**	**0.9**	**34.6**	**9.5**	**2.4**	**6.5**	**1.7**	**3.4**	**6.4**	**C**	**62.05**	**1.48**	
T3-B	**14**	**0.02**	**0.92**	**0.9**	**36.6**	**5.8**	**3.1**	**4.2**	**1.6**	**2.8**	**5.6**	**B**	**57.77**	**1.30**	
T3-C	**7**	**0.08**	**0.49**	**0.81**	**5**	**6.8**	**7.3**	**9**	**3.6**	**5.7**	**10.4**	**B**	**58.18**	**4.63**	**59.67 ± 2.06**
T3-D	**14**	**0.02**	**0.89**	**0.9**	**38.3**	**4.1**	**3.3**	**2.9**	**2.5**	**3.6**	**6.8**	**A**	**60.90**	**1.28**	
T3-E	**14**	**0.03**	**0.96**	**0.9**	**31.8**	**8.9**	**9.5**	**6**	**1**	**2.4**	**5**	**C**	**59.46**	**1.61**	
T18-A	14	0.08	1	0.87	10.3	*18.6*	*30.8*	13.7	1.1	2.3	4.1	C	46.45	3.94	
T18-B	14	0.08	1	0.88	10.4	*19.9*	*31*	14.5	0.8	1.6	2.6	C	46.95	3.97	
T18-C	14	0.12	1	0.88	7.3	*31.6*	*33.2*	25.3	0.7	1.3	2.2	C	37.20	4.49	**71.83 ± 4.09**
T18-D	**9**	**0.06**	**0.5**	**0.75**	**6.6**	**4.4**	**4.3**	**5**	**2.2**	**1.8**	**7.5**	**A**	**71.83**	**4.09**	
T18-E	13	0.09	1	0.88	10.1	*10.6*	*32.7*	8.1	1.2	1.7	2.9	C	43.16	3.80	

Fig. 9 Measured archeointensity and standard deviation of each level of the Wageningen-1 mound against calibrated age of the samples. Horizontal and vertical error bars are errors corresponding to respectively the age estimates and calculated archeointensities.

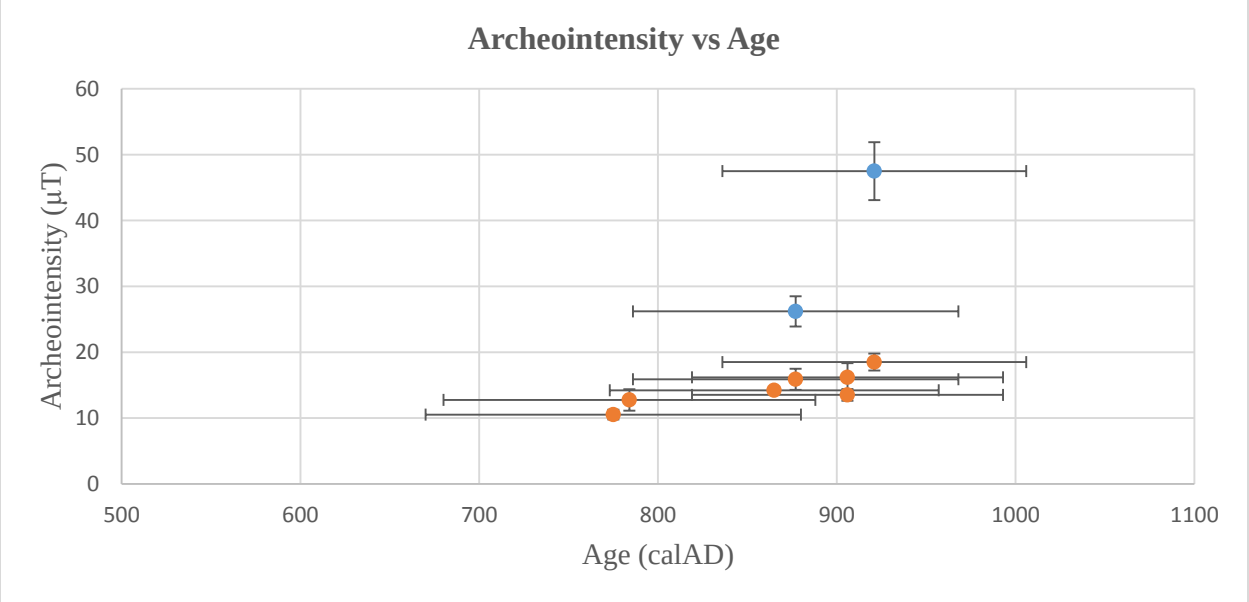

Fig. 10 A comparison of all archeointensity results and corresponding age. Microwave-Thellier results (2) given by blue dots; the remaining (orange dots) are results from conventional IZZI Thellier experiments. Horizontal and vertical error bars are errors related to respectively the age estimates and calculated archeointensities.

5 Discussion

This study was an attempt to narrow the existing gap of scarce data from the Southern hemisphere and around the equator, which is especially reflected in the different geomagnetic models (e.g. SHA.DIF.14K, pfm9k.1, CALS10K). After rock magnetic experiments, absolute archeointensities of the geomagnetic field in Suriname were measured on unoriented and undecorated archaeological potsherds from the Wageningen-1 mound, Hertenrits Culture, dated between 1145 ± 25 and 1310 ± 30 BP (655 to 975 AD), using the IZZI-Thellier method (Tauxe and Staudigel, 2004) and the Microwave-Thellier method.

The potsherds come from six different levels of the mound. Although it is not certain that all shards from the same level come from the same pottery, their ages may be assumed to be the same, because the stratigraphy of the mound is not found to be interrupted and thus the layers were not displaced. Using ^{14}C datings, the levels (from 0.75 to 3 m) have been dated quite precisely between 1145 ± 25 and 1310 ± 30 BP (655 to 975 AD). When the levels from which the samples come from are compared with the dated levels, their ages fall within acceptable limits, allowing us to estimate their dates.

Prior the archeointensity analysis, rock magnetic experiments were carried out to explore the magnetic character of the minerals present in the different potsherds. The high-field (magnetization versus temperature) and the low-field (susceptibility vs temperature) thermomagnetic runs indicate magnetite being the main carrier of the magnetic remanence. This was also suggested for levels 1, 2 and 6 from the thermal demagnetization, but thermal demagnetization of samples from levels 3 to 5 indicated a titanomagnetite or a mixture of ferromagnetic mineralogy. Only one sample from level 3 (SUR-3A) exhibited a low temperature overprint; this is interpreted as this pottery was used for cooking. However, this is just an assumption, as we are not certain what the potteries were used for, due lack of data. The hysteresis loops suggested a pseudo-single domain behavior, which was confirmed by our Day plot. The associated grain sizes are thus larger than of typical pottery. This could be expected from their composition, as the pottery temper is made up of either crushed pottery or of atypical materials such as quartz, charcoal/cariapé, shell and mica (Versteeg, 2003, p. 104, 106).

After the production of the first reliable paleointensity determinations, many modifications and additions have been suggested to the basic experimental method. In this study we used the IZZI-Thellier method (Tauxe and Staudigel, 2004) and an alternative Microwave-Thellier method.

On the microwave, archeointensities were measured on all shards of levels 4 to 6. Many of these measurements had to be terminated early, as the samples tended to physically expand, explode and/or fall off from the sample holder during the measurements. From the 50 initial intensity measurements, 27 measurements only yielded some results, of which 24 were rejected. The few measurements that passed (almost) all criteria, yielded an average intensity of 26.2 ± 2.3 μT for level 4 and 47.5 ± 4.4 μT for level 5A, which corresponds respectively to the period 877 ± 91 AD and 921 ± 85 AD. These values, however, are fortuitous rather than reliable, as these were obtained by choosing the first (and usually only) low temperature points on the Arai plot, which may produce too high an archeointensity (Dunlop, 2011).

The low success rate might also be caused by a 'z-axis-error' (miscalibration of the field in the z-direction).Therefore all 27 measurements were re-calculated, taking only the contribution of the x- and y-axis into account. To do this, the actual laboratory magnetic field had to be determined, as the intensity $|B| = (B_x^2 + B_y^2 + B_z^2)^{1/2}$, where B_x, B_y and B_z are the vector components of the magnetic field expressed in a local geographic coordinate system at any given location. The inclination (I) measured was based on: $I = \tan^{-1} (B_z/(B_x^2 + B_y^2)^{1/2})$, and was thus set on zero. The parameters obtained after the correction have also been tabulated and given in Table 7 below. By applying the correction, clear improvements in data could be observed in some cases (i.e. SURIS4-2D, SURIS5B-1F, SURIS6B-1C and SURIS6B-2F). See appendix 2a for Arai plots, obtained before and after correcting for the z-axis failure. However, still no reliable intensity value was obtained.

Table 7 Archeointensity results obtained from Microwave-Thellier, after correcting for the z-axis failure

Sample	*Hlab.c*	*N*	β	*f*	*g*	*q*	*delCK*	*DRAT*	*CDRAT*	MAD	*DRATtail*	*PI (μT)*	*SD (μT)*	*PI(level)*
SURIS4-2D	24.3	4	*0.24*	0.41	0.5	*0.8*	56.4%	*128.9%*	261.5%	2.7	0.0%	9.2	2.2	
SURIS4-3B	29.5	6	*0.14*	0.26	0.7	1.4	3.8%	8.9%	-43.0%	1.1	0.0%	37.9	5.1	---
SURIS4-4C	27.4	12	0.04	0.82	0.7	14.6	30.6%	*25.8%*	59.5%	0.5	0.0%	29.0	1.2	
SURIS4-4G	24.3	*2*	---	0.29	---	---	0.0%	0.0%	0.0%	9.2	0.0%	10.5	---	
SURIS5A-1B	29.9	6	0.04	0.60	0.6	8.2	17.4%	*22.0%*	22.0%	5.8	0.0%	25.6	1.1	
SURIS5A-1C	29.6	4	*0.16*	0.37	0.3	*0.6*	2.6%	5.7%	5.7%	1.9	9.0%	22.0	3.6	
SURIS5A-2B	30.0	*3*	0.05	0.30	0.4	2.2	56.1%	*127.7%*	127.7%	1.3	0.0%	32.8	1.8	
SURIS5A-2C	**29.7**	**4**	**0.10**	**0.19**	**0.5**	**1.0**	**0.1%**	**0.2%**	**-0.2%**	**0.3**	**2.8%**	**47.7**	**4.8**	
SURIS5A-2E	**29.9**	**4**	**0.08**	**0.41**	**0.6**	**3.4**	**0.5%**	**0.6%**	**-0.6%**	**0.5**	**3.4%**	**47.9**	**3.7**	
SURIS5A-2F	30.0	*3*	*0.19*	*0.13*	0.3	*0.2*	0.0%	0.0%	0.0%	0.4	49.7%	37.9	7.3	47.8 ± 4.3
SURIS5A-2G	29.8	*3*	*0.37*	0.37	0.5	*0.5*	0.0%	0.0%	0.0%	1.8	0.0%	15.9	5.9	
SURIS5A-2H	30.0	*3*	*0.25*	0.19	0.4	*0.3*	-6.0%	*20.5%*	-20.5%	0.6	*47.4%*	35.7	8.8	
SURIS5A-2I	29.8	*3*	0.03	*0.10*	0.2	*0.9*	-0.5%	-4.4%	-4.4%	0.9	*12.4%*	17.8	0.5	
SURIS5A-2J	29.6	*3*	0.07	0.32	0.5	2.2	0.0%	0.0%	0.0%	1.0	0.0%	35.1	2.5	
SURIS5A-3B	25.7	*3*	0.02	0.16	0.2	1.3	6.6%	*33.7%*	-33.7%	0.1	0.0%	17.4	0.3	
SURIS5B-1B	29.8	4	*0.25*	0.44	0.5	*0.8*	2.7%	5.0%	6.7%	3.6	---	20.9	5.2	
SURIS5B-1C	29.8	*3*	*0.22*	0.52	0.3	*0.7*	3.1%	4.2%	-4.2%	3.4	---	29.4	6.5	
SURIS5B-1D	29.9	*2*	---	0.59	---	---	0.0%	0.0%	0.0%	2.6	---	35.2	---	---
SURIS5B-1E	30.0	0	---	0.00	---	---	0.0%	0.0%	0.0%	---	0.0%	---		
SURIS5B-1F	29.1	*3*	*0.29*	*0.06*	0.4	*0.1*	38.7%	*440.7%*	392.3%	0.70	---	35.3	10.2	
SURIS6B-1C	28.4	*3*	0.05	0.33	-0.03	*-0.2*	0.0%	0.0%	0.0%	*12.7*	---	10.3	0.6	
SURIS6B-2E	29.0	*4*	*0.16*	0.42	0.5	1.3	0.0%	0.0%	0.0%	3.7	0.0%	34.7	5.7	
SURIS6B-2F	27.8	6	*0.17*	0.81	0.6	3.0	18.9%	*18.5%*	18.1%	5.0	---	21.3	3.7	
SURIS6B-3B	29.9	5	0.09	0.82	0.7	5.9	19.2%	*17.3%*	15.8%	2.6	---	26.9	2.5	---
SURIS6B-3C	29.9	7	0.07	0.80	0.8	9.1	26.5%	*24.8%*	50.6%	3.3	---	26.1	1.8	
SURIS6B-3D	26.0	4	*0.17*	0.24	0.5	*0.7*	18.0%	*43.2%*	72.5%	4.9	---	36.0	6.2	
SURIS6B-3E	29.5	6	0.05	0.80	0.7	12.8	21.2%	*19.7%*	20.1%	6.4	---	26.3	1.2	

Hlab.c is the measured laboratory value, due the z-axis failure; parameters that failed the criteria, are given in red italic text and the results that passed all criteria are in bold.

As the 2 DC SQUID system is relatively more sensitive compared to the microwave system, even the samples with the weakest magnetic moments (levels 1-3) were measured and average archeointensities between 10.52 ± 0.75 μT and 16.18 ± 2.16 μT were obtained for the period 655 to 975 AD. From the 6 levels, 42 subsamples from representative potsherds were subjected to the IZZI-Thellier method, out of which 27 were rejected, when analyzed by the ThellierTool 4.2 software (Leonhardt et al., 2004). The measurements that were rejected, failed in general to pass the alteration checks or the directional criteria or both (except for 6A-4, 5B-1 and 5B-2). To estimate alteration, three parameters were calculated by the program, from which d(CK) and d(pal) were used as criteria. Small archeointensities lead to relatively higher experimental errors, in particular regarding small variations of the applied field (Leonhardt et al., 2004). Thus

experimental variations and errors may have led to an exceeding of the 5% (class A) or 10% (B) limit of d(pal) in our intensity determinations, causing us to reject more samples. d(CK) is preferred over DRAT, because it does not overemphasize low temperature steps, where the pTRM acquired is rather small and the amount of data points often is very high, nor does it tolerate large check errors if the selected segment is long, which could occur when only few data points at high temperature steps are used. d(CK) generally shows smaller values than DRAT (Leonhardt et al., 2004).

Although the microwave method has its advantages over conventional methods (i.e. reducing experimental time and eliminating the need to heat the bulk sample), it has not been successful in this study. When we compare the archeointensities obtained by both methods, we see that the intensity obtained from the Microwave-Thellier method is two to three times higher than the IZZI-Thellier results, although the latter indicates a slight increase over time. As noted above, the results from the Microwave-Thellier method which passed all criteria, were obtained by choosing the first (and only) low temperature points on the Arai plot, producing most likely an overestimate. We also need to keep in mind that the results obtained by the Microwave-Thellier method for level 4 and 5A differ significantly (respectively 26.2 ± 2.3 μT versus 47.5 ± 4.4 μT), while for level 5B and 6 no measurement passed all criteria. As the microwave results seem fortuitous, underlying results from the microwave differ much and samples from level 5A and from two shards of level 4 (4-3 and 4-4) were not measured using the IZZI-Thellier method, further comparison between both methods is not justified.

However, the intensity obtained by the IZZI-Thellier method compared to the SHA.DIF.14K and pfm9k.1 model is three to four times lower than predicted and about half the present day field value (~29 μT). For the period 500 to 1000 AD archeointensities ranging from 37.01 ± 0.89 to 45.79 ± 0.93 and 37.6 ± 3.68 to 40.7 ± 3.21 are predicted from the SHA.DIF.14K and pfm9k.1 model respectively. In the next figures (Figure 11 and 12) the intensities measured in this study and those predicted by the models (respectively SHA.DIF.14K and pfm9k.1) are illustrated.

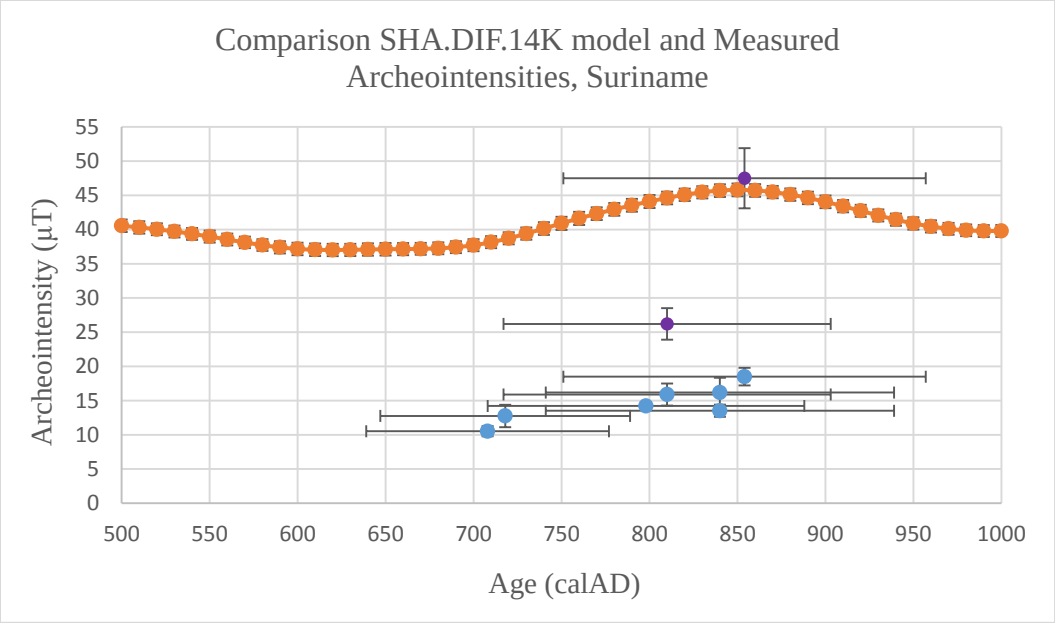

Fig. 11 Plot showing the predicted intensities calculated from SHA.DIF.14K for the Wageningen-1 mound, Suriname for 500 to 1000 AD (orange circles), as well as the intensities measured in this study (blue and purple circles as obtained from respectively the IZZI-Thellier and Microwave-Thellier method). Horizontal and vertical error bars are errors corresponding to respectively the age estimates and the determined archeointensities.

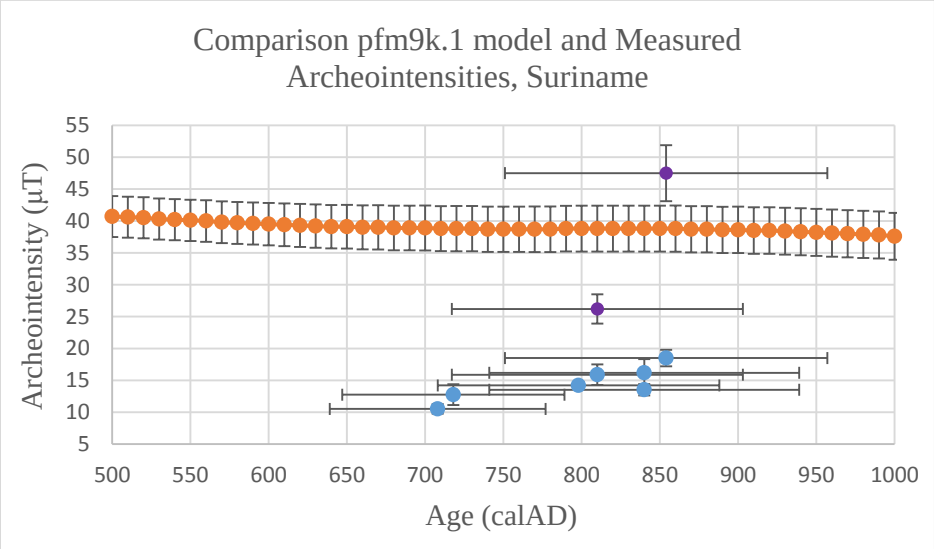

Fig. 12 Plot showing the predicted intensities (orange circles) calculated from pfm9k.1 for the Wageningen-1 mound, Suriname (500 to 1000 AD), as well the intensities measured in this study (blue and purple circles as obtained from respectively the IZZI-Thellier and Microwave-Thellier method)). Horizontal and vertical error bars are errors corresponding to respectively the age estimates and the determined archeointensities.

Choosing only high temperature points on the Arai plots due viscous effects at low temperatures can account for a too low intensity determination (Dunlop, 2011), but this has not been applied in the current study. Archeointensity results may further be biased by alteration during the experiments (e.g. Coe, 1967b), the presence of multidomain grains (McClelland et al., 1996), the cooling rate dependence of TRM acquisition (Dodson and McClelland-Brown, 1980; McClelland, 1984) and/or remanence anisotropy (Selkin et al., 2000).

As noted previously, the law of additivity is not valid for multidomain grains; they do not have a single T_B as with SD grains, but a wide span of unblocking temperatures that can extend up to the Curie temperature (T_c). Consequently, a tail will lead to an increased pTRM in the following heating-cooling step and will thus result in an underestimate of the field intensity (McClelland et al., 1996). However, our Day plot demonstrated that all our samples have pseudo-single domain particles.

The cooling rate dependence of TRM acquisition is based on Néel's theory (1949). Dodson and McClelland Brown (1980) have predicted and experimentally proved (e.g. McClelland, 1984) that the magnitude of a TRM acquired by single domain (SD) grains not only depends on the field magnitude, but also on the rate at which they cooled. The calculated ancient field magnitude will thus be incorrect (McClelland, 1984), since samples were cooled down much more rapidly in our archeointensity experiments than during the original cooling of the studied pottery. This is especially true for the Microwave method, where the duration of heating is only of the orders of seconds, opposed to the IZZI-Thellier experiments, where the samples were cooled in ~35 min from 590 °C to 25 °C. Although a correction may be necessary for both methods, Hammond et al. (*in press*) showed that this is more crucial for intensity determinations using the Microwave method and that the IZZI-Thellier determinations are affected to a lesser extent. So even though the obtained Microwave results seem to be consistent with the models, if they were reliable, applying a cooling rate correction would only lower the measured intensities.

Remanent anisotropy (preferred alignment of the magnetic grains) is also one of the mechanisms than can cause a bias of the recorded magnetic field (Tema, 2009); it can lead to errors in the intensity estimation of up to 40% (Rogers et al., 1979) and requires to be tested and eventually to be corrected for our archeointensity results, obtained from pottery from Suriname. Selkin et al. (2000) showed that anisotropy of magnetic susceptibility (AMS) may be a very poor proxy for

either the magnitude or orientation of remanence anisotropy and suggested that anisotropy of anhysteretic remanent magnetization (ARM) provides a more suitable measure of the remanence anisotropy. A possible way to minimize the effects of remanence anisotropy is to apply the laboratory field such that samples acquire a thermal remanence (TRM) parallel to the natural remanent magnetization (NRM), but this technique requires the use of a specialized oven and orientation device and is only suitable for samples with a univectorial magnetization, where the NRM direction can reliably be used to align the laboratory field (Selkin et al., 2000).

On the other hand, the data the geomagnetic models rely on for the Southern hemisphere is very scarce, contributing to a lack of structure in the Southern hemisphere. Models using sedimentary records (e.g. CALS10K) have to deal with additional setbacks; intensity variations obtained from sediments are relative, and need to be calibrated somehow for use in global geomagnetic modelling. In addition, sediments have greater experimental uncertainties opposed to archeomagnetic data, and their dating is often less precise. Although they have a better geographic distribution, they are intrinsically noisier and rapid field variations may be smoothed out by depositional and post-depositional processes (Korte & Constable, 2011).

6 Conclusion

For Suriname, which is located on the northeastern coast of South-America, average absolute archeointensities between 10.52 ± 0.75 μT and 16.18 ± 2.16 μT have been determined for the time period 655 to 975 AD, using the IZZI-Thellier method. Although a slight increase in intensity during this period could be observed, these determinations are three to four times lower than expected from the global geomagnetic models (i.e. SHA.DIF.14K, pfm9k.1) and about half of the present day field. Archeointensity results can be biased by a number of factors, e.g. alteration during the experiments, the presence of an MD component (McClelland, 1996), cooling rate differences between laboratory and nature (Dodson and McClelland-Brown, 1980) and or magnetic anisotropy (Selkin et al., 2000). However, none of these can adequately account for the low archeointensities obtained by the IZZI-Thellier method. On the other hand, due to the scarce number of data from the Southern hemisphere, the geomagnetic models are not well constrained in the Southern hemisphere yet (Pavón-Carrasco et al., 2014).

Although the microwave method has its advantages over conventional methods (i.e. reducing experimental time and eliminating the need to heat the bulk sample, thus discouraging alteration), it did not turn out successful for this study. Only 3 out of 27 measurements passed all criteria, yielding an average of 40.4 ± 3.7 μT. This value seems to be consistent with the intensities predicted by the SHA.DIF.14K and pfm9k.1 model for the corresponding period, but would be lowered significantly when corrected for cooling rate and remanence anisotropy effects. However, since the results seem to be incidental, a comparison with the geomagnetic models and with the results obtained using the IZZI-Thellier method is meaningless.

This study is certainly not sufficient to fill in the gap and to enhance the reliability of the geomagnetic models. Definitely more paleomagnetic research over a larger time period and in others regions around the equator and especially on the Southern hemisphere is required to support our lower than expected, but high-quality IZZI-Thellier data and to improve the resolution of the geomagnetic models, preferably incorporating full vector analysis.

Without more experiments it is not possible to draw any further conclusions.

References

Agico, Inc. (2004) Spinner magnetometer JR6/JR6A user's manual. Brno, Czech Republic. http://www.agico.com

Aitken, M., J., Allsop, A., L., Busell, G., D., Winter, M., B., (1988), Determination of the intensity of the Earth's magnetic field during archeological times: reliability of the Thellier technique. *Reviews of Geophysics*, 26, 3-12.

Barton, C., E., and McElhiny, M., W., (1981), A 10000 yr geomagnetic secular variation record from three Australian maars. *Geophysical Journal International, on behalf of the Royal Astronomical Society*, 67, 465-485.

Barton, C., E., and Torgerson, T., (1988), Palaeomagnetic and 210PB estimates of sedimentation in Lake Turkana, East Africa. *Palaeogeography, Palaeoclimatology, Palaeoecology*, 68, 53-59.

Biggin, A., J., (2006), First-order symmetry of weak-field partial thermoremanence in multi-domain (MD) ferromagnetic grains: 2. Implications for Thellier-type palaeointensity determination. *Earth and Planetary Science Letters*, 245 (1-2), 454-470.

Biggin, A., J., and Böhnel, H., N., (2003), A method to reduce the curvature of Arai plots produced during Thellier palaeointensity experiments performed on multidomain grains. Geophysical Journal International. 155, F13-F19.

Biggin, A., J., and Perrin, M., (2007), The behaviour and detection of partial thermoremanent magnetisation (PTRM) tails in Thellier palaeointensity experiments. *Earth, Planets and Space*, 59, 717-725.

Biggin, A. J., Perrin, M., Shaw, J., (2007), A comparison of a quasi-perpendicular method of absolute palaeointensity determination with other thermal and microwave techniques. *Earth and Planetary Science Letters* 257, 564-581.

Brachfeld, S., Acton, G., D., Guyodo, Y., Banerjee, S., K., (2000), High resolution Paleomagnetic records from Holocene sediments from the Palmer Deep, Western Antarctic Peninsula. *Earth and Planetary Science Letters*, 181, 429-441.

Calvo, M., Prévot, M., Perrin, M., Riisager, J., (2002), Investigating the reasons for the failure of palaeointensity experiments: a study on historical lava flows from Mt. Etna (Italy). *Geophysical Journal International*, 149, 44-63.

Chadima, M., Pokorný, J., Dušek, M., (2011), Rema6W - MS Windows Software for Controlling JR-6 Series Spinner Magnetometers. In: E. Petrovský et al. (eds.).The Earth's Magnetic Interior, IAGA Special Sopron Book Series 1, 303-309, doi:10.1007/978-94-007-0323-0_21

Coe, R., S., (1967a), Paleo-Intensities of the Earth's magnetic field determined from Tertiary and Quaternary rocks. *Journal of Geophysical Research*, 72, 3247-3262.

Coe, R., S., (1967b), The determination of paleointensities of the Earth's magnetic field with emphasis on mechanisms which could cause non-ideal behavior in Thellier's method. *Journal of Geomagnetism and Geoelectricity*, 19, 157-179.

Coe, R., S., Grommé, C., S., Mankinen, E., A., (1978), Geomagnetic paleointensities from radiocarbon dated lava flows on Hawaii and the question of the Pacific non-dipole low. *Journal of Geophysical Research – Solid Earth*, 83, 1740-1756.

Constable, C., G., and McElhinny, M., W., (1985), Holocene geomagnetic secular variation records from north-eastern Australian lake sediments. *Geophysical Journal International, on behalf of the Royal Astronomical Society*, 81, 103-120.

Creer, K., M., Valencio, D., A., Sinito, A., M., Tucholka, P., Vilas, J., F., (1983), Geomagnetic secular variation 0-14000 yr BP as recorded by lake sediments from Argentina. *Geophysical Journal International, on behalf of the Royal Astronomical Society*, 74, 199-221.

Daly, L., and Le Goff, M., (1996), An updated and homogeneous world secular variation data base. 1. Smoothing of the archaeomagnetic results. *Physics of the Earth and Planetary Interiors*, 93, 159-190.

Day, R., Fuller, M., Schmidt, V., A., (1977), Hysteresis properties of titanomagnetites: grain size and composition dependence. *Physics of the Earth and Planetary Interiors*, 13, 260-267.

Dekkers, M., J., and Böhnel, H., N., (2006), Reliable palaeointensities independent of magnetic domain state. *Earth and Planetary Science Letters*, 248 (1-2), 508-517.

Dodson, M., and McClelland-Brown, E., (1980), Magnetic blocking temperatures of single domain grains during slow cooling. *Journal of Geophysical Research*, 85, 2625– 2637.

Donadini, F., Korte, M., Constable, C., (2009), Geomagnetic field for 0-3 ka: 1. New data sets for global modeling. *Geochemistry, Geophysics, Geosystems*, 10, Q06007. Doi:10.1029/2008GC002295.

Draeger, U., Prévot, M., Poidras, T., Riisager, J., (2006), Single-domain chemical, thermochemical and thermal remanences in a basaltic rock. *Geophysical Journal International*, 166, 12-32.

Dunlop, D., J., (2002), Theory and application of the Day plot (M_{rs}/M_s versus H_{cr}/H_c) 1. Theoretical curves and tests using titanomagnetite data. *Journal of Geophysical Research*, 107 (B3), 10.1029/2001JB000486.

Dunlop, D. J., (2011), Physical basis of the Thellier-Thellier and related paleointensity methods. *Physics of the Earth and Planetary Interiors*, doi:10.1016/j.pepi.2011.03.006.

Dunlop, D., J., Zhang, B., Özdemir, Ö., (2005), Linear and nonlinear Thellier paleointensity behavior of natural minerals. *Journal of Geophysical Research*, 110, B0103, doi:10.1029/2004JB003095.

Genevey, A., and Gallet, Y., (2002), Intensity of the geomagnetic field in western Europe over the past 2000 years: New data from ancient French pottery. *Journal of Geophysical Research*, 107 (B11), 2285, doi:10.1029/2001JB000701.

Gogorza, C., S. G., Irurzun, M., A., Chaparro, M., A., E., Lirio, J., M., Nuñez, H., Becoff, P., G., Sinito, A., M., (2006), Relative paleointensity of the geomagnetic field over the last 21,000 years BP from sediment cores, Lake El Trébol (Patagonia, Argentina). *Earth, Planets and Space*, 58, 1323-1332.

Gogorza, C., S. G., Lirio, J., M., Nuñez, H., Chaparro, M., Bertorello, H., R., Sinito, A., M., (2004), Paleointensity studies on Holocene-Pleistocene sediments from Lake Escondido, Argentina. *Physics of the Earth and Planetary Interiors*, 145, 219-238.

Gogorza, C., S., G., Sinito, A., M., Lirio, J., M., Nuñez, H., Chaparro, M., Vilas, J., F., (2002), Paleosecular variations 0-19,000 years recorded by sediments from Escondido Lake (Argentina). *Physics of the Earth and Planetary Interiors*, 133, 35-55.

Gogorza, C., S., G., Sinito, A., M., Tomasso, I., D., Vilas, J., F., Creer, K., M., Nuñez, H., (2000), Geomagnetic secular variations 0–12 kyr as recorded by sediments from Lake Moreno (southern Argentina). *Journal of South American Earth Sciences*, 13, 627–645.

Hammond, M., L., Hill, M., J., Biggin, A., J., Greaves, A., M., Langereis, C., G., Ertepinar, P., Yenner, K., A., (2015), Increasing the duration of the 1000 BC geomagnetic intensity high: the first continuous archaeointensity dataset from Turkish potsherds, *Earth and Planetary Science Letters*, in press.

Hill, M. J., and Shaw, J., (1999), Palaeointensity results for historic lavas from Mt Etna using microwave demagnetization/remagnetization in a modified Thellier-type experiment. *Geophysical Journal International,* 139, 583-590.

Hill, M. J., and Shaw, J., (2000), Magnetic field intensity study of the 1960 Kilauea lava flow, Hawaii, using the microwave palaeointensity technique. *Geophysical Journal International*, 142, 487-504.

Hillenbrand, C., D., Smith, J., Kuhn, G., Esper, O., Gersonde, R., Larter, R., Maher, B., Moreton, S., Shimmield, T., Korte, M., (2009), Age assignment of a diatomaceous ooze deposited in the western Amundsen Sea Embayment after the last glacial maximum. *Journal of Quaternary Science*, 25, 280-295.

Hongre, L., Hulot. G., Khokhlov, A., (1998), An analysis of the geomagnetic field over the past 2000 years. *Physics of the Earth and Planetary Interiors*, 106, 311-335.

Irurzun, M., A., Gogorza, C., S., G., Chaparro, M., A., E., Lirio, J., M., Nuñez, H., Vilas, J., F., Sinito, A., M., (2006), Paleosecular variations recorded by Holocene-Pleistocene sediments from Lake El Trébol (Patagonia, Argentina). *Physics of the Earth and Planetary Interiors*, 154, 1-17.

Kirschvink, J., L., (1980), The least-squares line and plane and the analysis of palaeomagnetic data. *Geophysical Journal International*, 62, 699-718.

Koenigsberger, J., G., (1938), Natural residual magnetism of eruptive rocks. *Terrestrial Magnetism and Atmospheric Electricity*, 43, 299-320.

Korte, M., and Constable, C., (2011), Improving geomagnetic field reconstructions for 0-3 ka. *Physics of the Earth and Planetary Interiors*, 188, 247-259.

Korte, M., Constable, C., Donadini, F., Holme, R., (2011), Reconstructing the Holocene geomagnetic field. *Earth and Planetary Science Letters*, 312, 497-505.

Lawrence, K., P., Tauxe, L., Staudigel, H., Constable, C., G., Koppers, A., McIntosh, W., Johnson, C., L., (2009), Paleomagnetic field properties at high southern latitude. *Geochemistry, Geophysics, Geosystems*, 10, doi:10.1029/2008GC002072.

Leonhardt, R., Heunemann, C., Krása D., (2004), Analyzing absolute paleointensity determinations: Acceptance criteria and the software ThellierTool4.0. *Geochemistry, Geophysics, Geosystems*, 5, Q12016, doi:10.1029/2004GC000807.

Leonhardt, R., Hufenbecher, F., Heider, F., Soffel, H., (2000), High absolute paleointensity during a mid Miocene excursion of the Earth's magnetic field. *Earth and Planetary Science Letters*, 184, 141-154.

Leonhardt, R., J., Matzka, J., Menor, E., A., (2003), Absolute paleointensities and paleodirections of miocene and pliocene lavas from Fernando de Noronha, Brazil. *Physics of the Earth and Planetary Interiors*, 139, 285-303.

Levi, S., (1977), The effect of magnetite particle size on paleointensity determination of the geomagnetic field. *Physics of the Earth and Planetary Interiors*, 13, 245-259.

McClelland-Brown, E., (1984), Experiments on TRM intensity dependence on cooling rate. *Geophysical Research Letters*, 11, 205-208.

McClelland, E., and Briden, J., C., (1996), An improved methodology for Thellier-type paleointensity determination in igneous rocks and its usefulness for verifying primary thermoremanence. *Journal of Geophysical Research*, 101, 21995-22013.

McClelland, E., Muxworthy, A., R., Thomas, R., M., (1996), Magnetic properties of the stable fraction of remanence in large multidomain (MD) magnetite grains: single or MD? *Geophysical Research Letters*, 23, 2831-2834.

Mothersill, J., S., (1996), Paleomagnetic results from lakes Victoria and Albert, Uganda. *Studia Geophysica et Geodaetica*, 40, 25-35.

Nagata, T., Arai, Y., and Momose K., (1963), Secular variation of the geomagnetic total force during the last 5000 years. *Journal of Geophysical Research*, 68, 5277–5281.

Néel, L., (1949).Théorie du traînage magnétique des ferromagnétiques en grains fins avec applications aux terres cuites. *Ann. Géophys*., 5, 99-136.

Nilsson, A., Holme, R., Korte, M., Suttie, N., Hill, M., (2014), Reconstructing Holocene geomagnetic field variation: new methods, models and implications. *Geophysical Journal International*, 198 (1), 229-248.

Pavón-Carrasco, F., J., Osete, M., L., Torta, J., M., De Santis, A., (2014), A geomagnetic field model for the Holocene based on archaeomagnetic and lava flow data. *Earth and Planetary Science Letters*, 388, 98-109.

Prévot, M., Mankinen, E., A., Coe, R., S., Grommé, S., (1985), The Steens Mountain (Oregon) geomagnetic polarity transition: 2. Field intensity variations and discussion of reversal models. *Journal of Geophysical Research*, 90, 10417-10448.

Ramsey, C., B., (2009), Bayesian analysis of radiocarbon dates. *Radiocarbon*, 51 (1), 337-360.

Reimer, P., J., Bard, E.,Bayliss, A., Beck, J., W., Blackwell, P., G., Bronk Ramsey, C., Grootes, P., M., Guilderson, T., P., Haflidason, H., Hajdas, I., Hatt, C., Heaton, T., J., Hoffmann, D., L., Hogg, A., G., Hughen, K., A., Kaiser, K., F., Kromer, B., Manning, S., W., Niu, M., Reimer, R., W., Richards, D., A., Scott, E., M., Southon, J., R., Staff, R., A., Turney, C., S., M., van der Plicht, J., (2013), IntCal13 and Marine13 Radiocarbon Age Calibration Curves 0-50,000 Years cal BP. *Radiocarbon*, 55 (4), 1869-1887.

Riisager, P., and Riisager, J., (2001), Detecting multidomain magnetic grains in Thellier palaeointensity experiments. *Physics of the Earth and Planetary Interiors*, 125, 111-117.

Rogers, J., Fox, J., M., W., Aitken, M., J., (1979), Magnetic-anisotropy in ancient pottery. *Nature*, 277, 644-646.

Schmidt, P., W., (1993), Palaeomagnetic cleaning strategies. *Physics of the Earth and Planetary Interiors*, 76, 169-178.

Selkin, P., A., Gee, J., S., Tauxe, L., Meurer, W., P., Newell, A., J., (2000), The effect of remanence anisotropy on paleointensity estimates: a case study from the Archean Stillwater Complex. *Earth and Planetary Science Letters*, 183, 403-416.

Selkin, P., A., and Tauxe, L., (2000), Long-term variations in palaeointensity, Philosophical Transactions of the Royal Society A: Mathematical Physical and Engineering Sciences, 358, 1065-1088.

Shaw, J., Walton, D., Yang, S., Rolph, T., C., Share, J., A., (1996), Microwave archaeointensities from Peruvian ceramics. *Geophysical Journal International*, 124, 241-244.

Tauxe, L., and Staudigel, H. (2004). Strength of the geomagnetic field in the Cretaceous Normal Superchron: New data from submarine basaltic glass of the Troodos Ophiolite. *Geochemistry, Geophysics, Geosystems*, 5, Q02H06, doi:10.1029/2003GC000635.

Tema, E., (2009), Estimate of the magnetic anisotropy effect on the archaeomagnetic inclination of ancient bricks. *Physics of the Earth and Planetary Interiors*, 176, 213-223.

Thouveny, N., and Williamson, D., (1988), Palaeomagnetic study of the Holocene and upper Pleistocene sediments from lake Barombi Mbo, Cameroun; first results. *Physics of the Earth and Planetary Interiors*, 52, 193-206.

Turner, G., M., and Lillis, D., A., (1994), A Paleomagnetic secular variation record for New Zealand during the past 2500 years. *Physics of the Earth and Planetary Interiors*, 83, 265-282.

Valet, J., P., Brassart, J., Le Meur, I., Soler, V., Quidelleur, X., Tric, E., Gillot, P., Y., (1996), Absolute paleointensity and magnetomineralogical changes. *Journal of Geophysical Research*, 101, 25029-25044.

Versteeg, A. H., (2003). Suriname voor Columbus, Suriname. Paramaribo: Stichting Surinaams Museum, 270 p.

Walton, D., (1988), The lack of reproducibility in experimentally determined intensities of the Earth's magnetic field. *Reviews of Geophysics*, 26, 15-22.

Walton, D., (1991), A New Technique for Determining Palaeomagnetic Intensities. *Journal of Geomagnetism and Geoelectricity*, 43, 333-339.

Walton, D., Share, J., Rolph, T., C., Shaw, J., (1993), Microwave magnetisation. *Geophysical Research Letters*, 20, 109-111.

Walton, D., Snape, S., Rolph, T., C., Shaw, J., Share, J., (1996), Application of ferrimagnetic resonance heating to palaeointensity determinations. *Physics of the Earth and Planetary Interiors*, 94, 183-186.

Wong, Th. E., de Vletter, D. R., Krook, K., Zonneveld, J. I. S., van Loon, A. J., (1998). The history of earth sciences in Suriname. Amsterdam: Netherlands Institute ofApplied Geoscience TNO/ Royal Netherlands Academy of Arts and Sciences, 479 p.

Xu, S., and Dunlop., (2004), Thellier paleointensity theory and experiments for multidomain grains. *Journal of Geophysical Research*, 109, B07103, doi:10.1029/2004JB003024.

Yu, Y., and Dunlop, D., J., (2003), On partial thermoremanent magnetization tail checks in Thellier paleointensity determination. *Journal of Geophysical Research*, 108 (B11), 2523, doi:10.1029/2003JB002420.

Yu, Y., Tauxe, L.,Genevey, A., (2004), Toward an optimal geomagnetic field intensity determination technique. *Geochemistry, Geophysics, Geosystems*, 5, Q02H07. Doi: 10.1029/2003GC000630.

Zijderveld, J., D., A., (1967), AC demagnetisation of rocks: analysis of results, in D.W. Collinson, K.M. Creer, S.K. Runcorn (Eds.), Methods in Palaeomagnetism, Elsevier, 254-286.

Appendices

On the next pages, a complete overview of all hysteresis loops and back-field curves (Appendix 1) is given, as well as the Arai plots obtained using the Microwave-Thellier method (Appendix 2a) and the Arai plots, directional plots and Decay of NRM intensity plots obtained using the IZZI-Thellier method (Appendix 2b).

Appendix 1

Hysteresis parameters (left) and back field curves (right) of one specimen per level; the red curves in the hysteresis diagrams are raw hysteresis loops; green ones are the corrected loops.

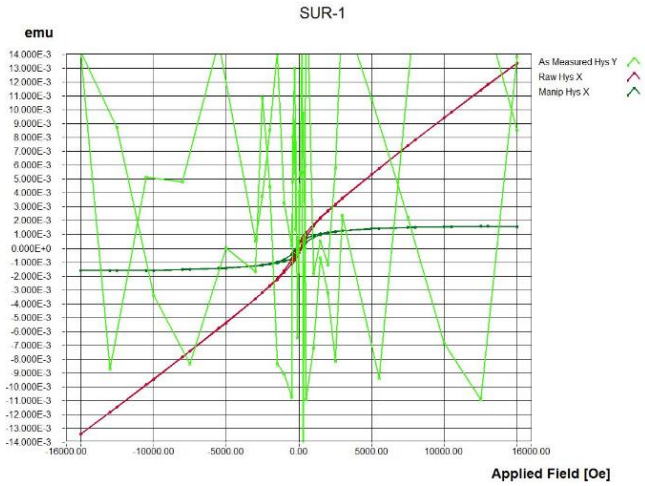

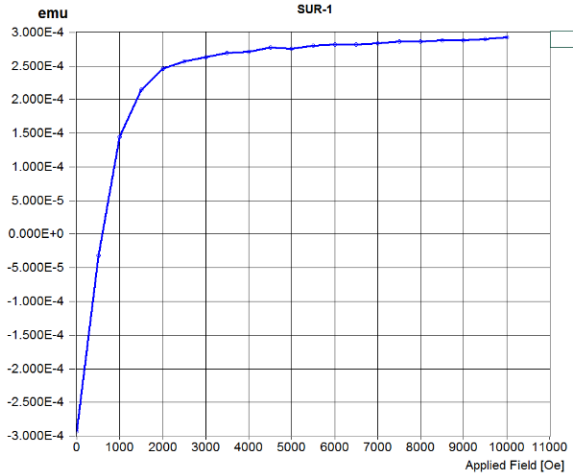

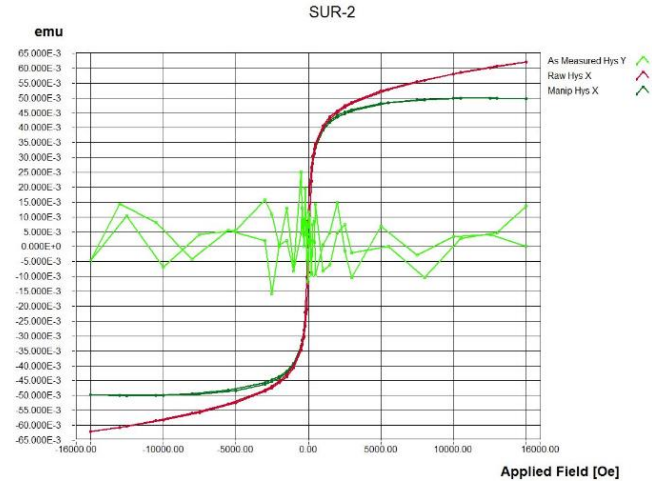

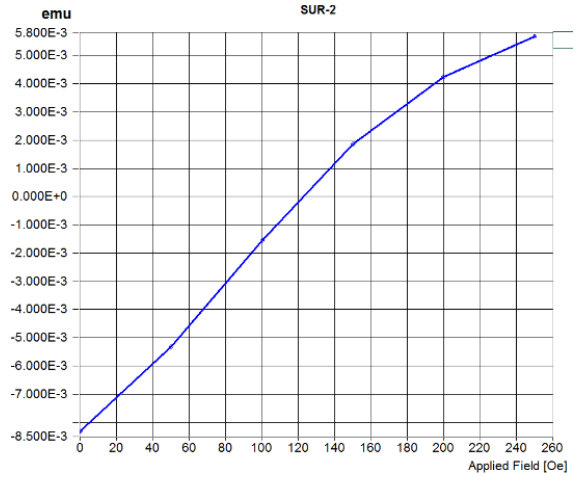

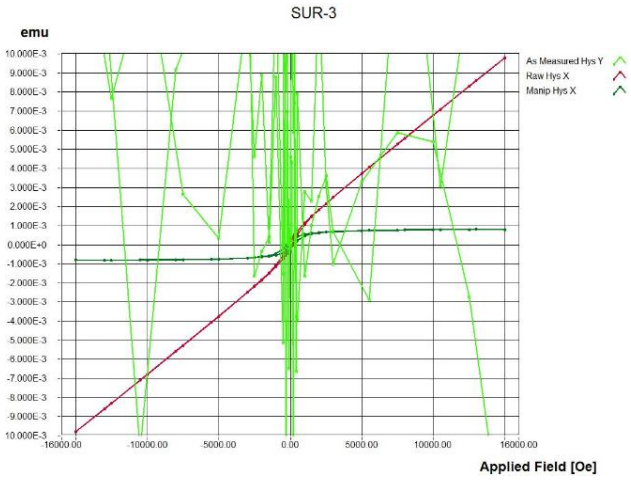

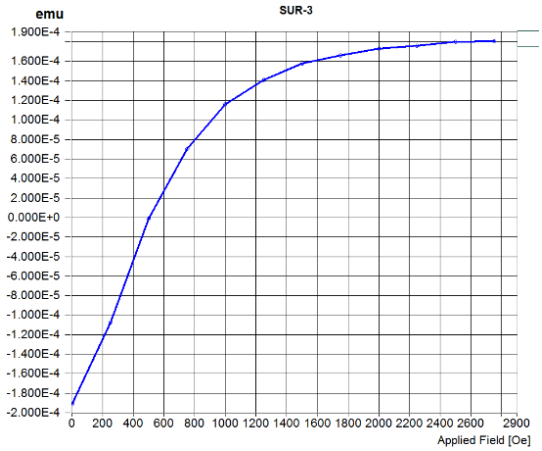

SUR-4

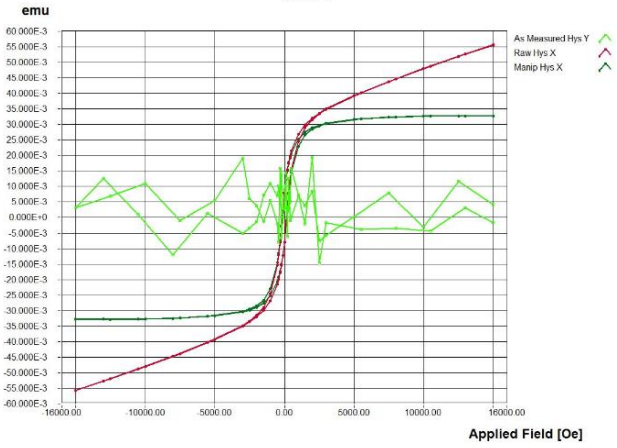

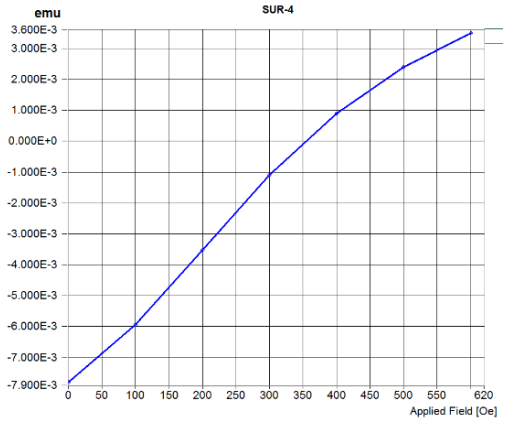

SUR-5A

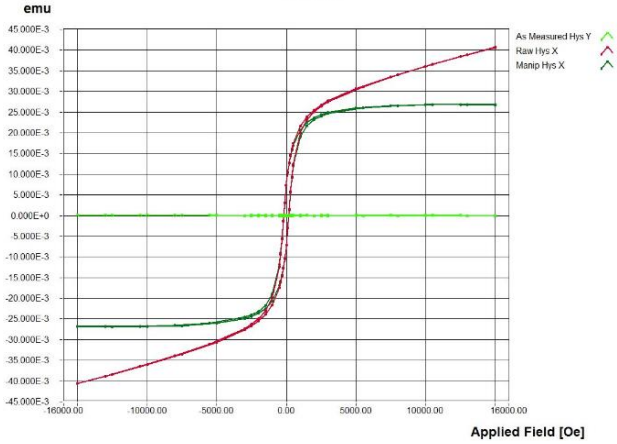

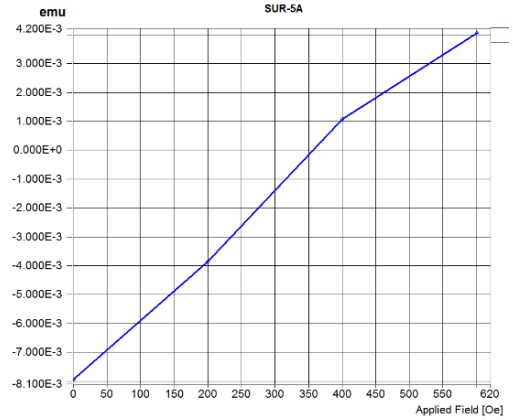

SUR-5B

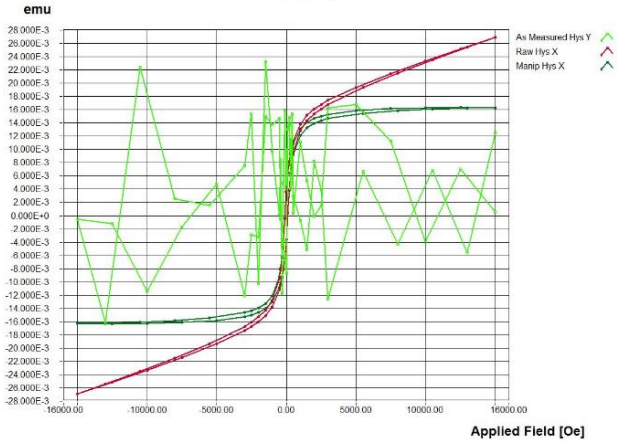

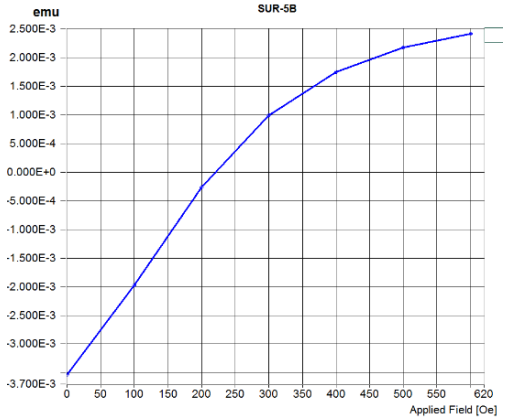

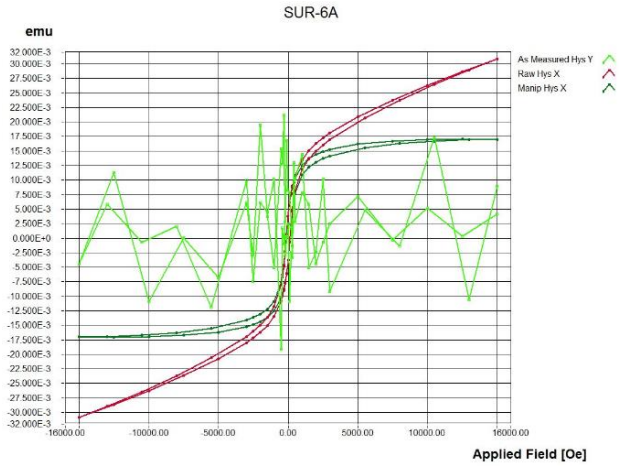
SUR-6A
emu
As Measured Hys Y
Raw Hys X
Manip Hys X
Applied Field [Oe]

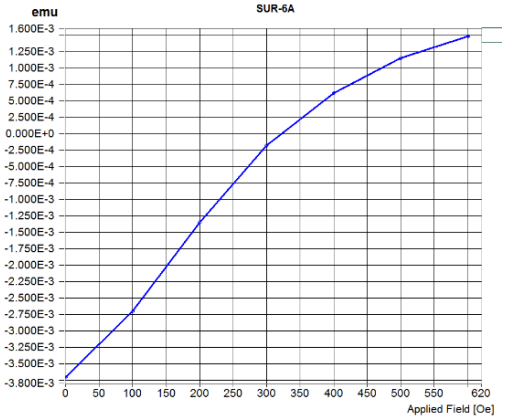
SUR-6A
emu
Applied Field [Oe]

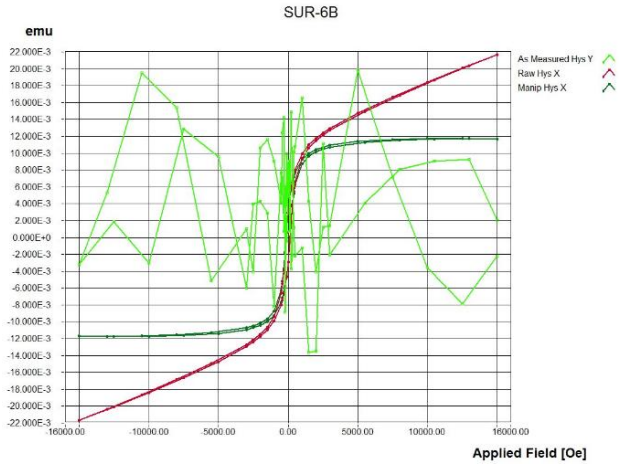
SUR-6B
emu
As Measured Hys Y
Raw Hys X
Manip Hys X
Applied Field [Oe]

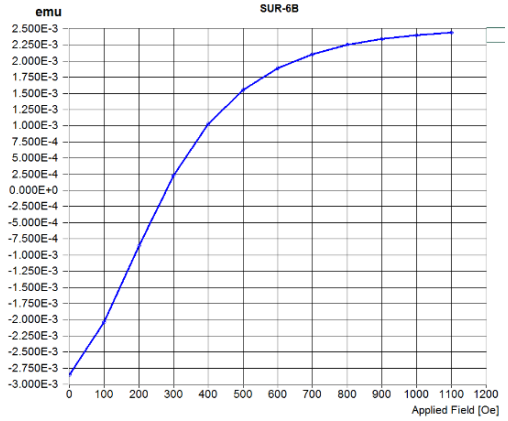
SUR-6B
emu
Applied Field [Oe]

Appendix 2a

Archeointensity results (Microwave-Thellier method)

Arai plots of each sample. Left: without z-axis correction; Right: after z-axis correction

SURIS4-2D

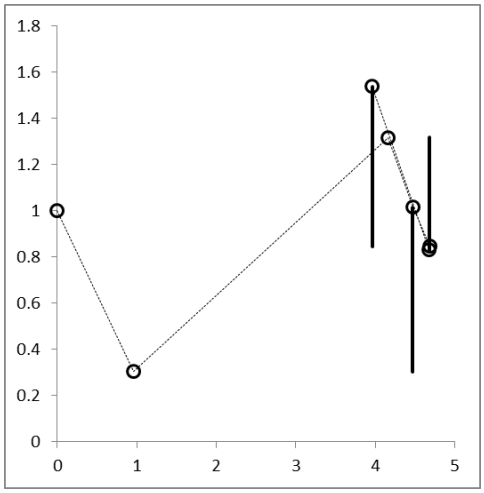

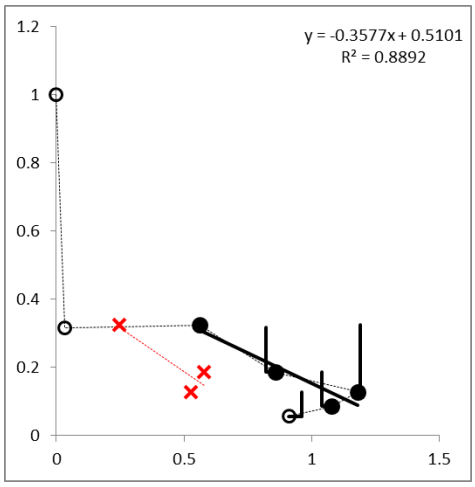

SURIS4-3B

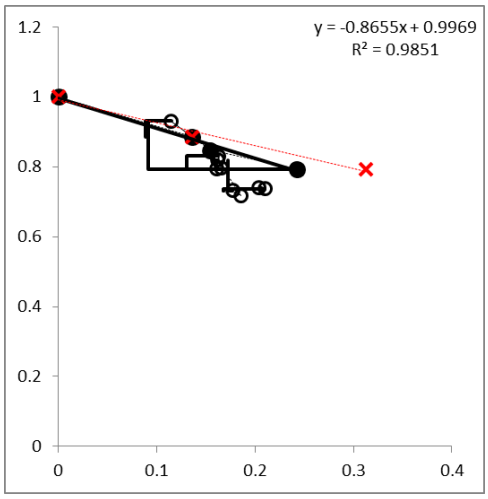

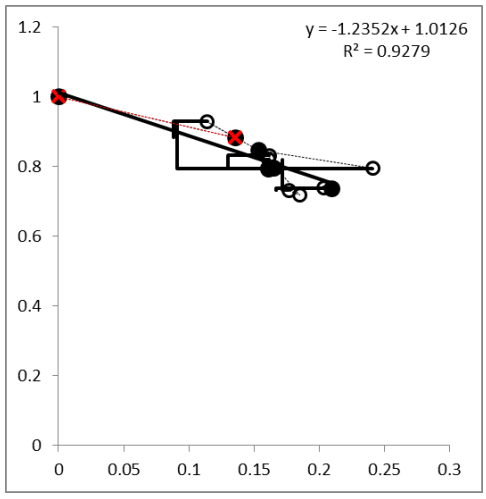

SURIS4-4C

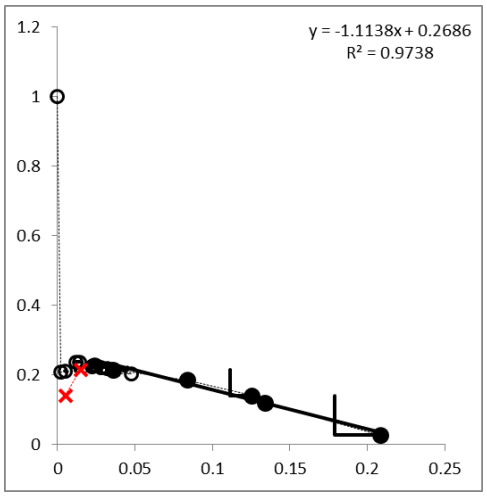

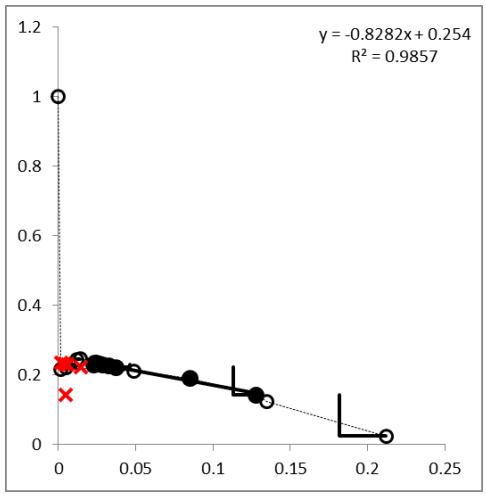

SURIS4-4G

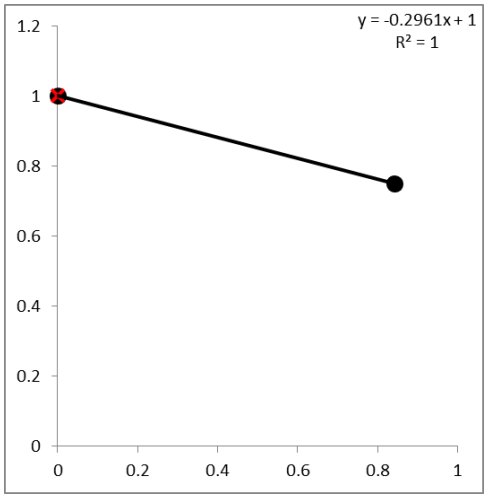

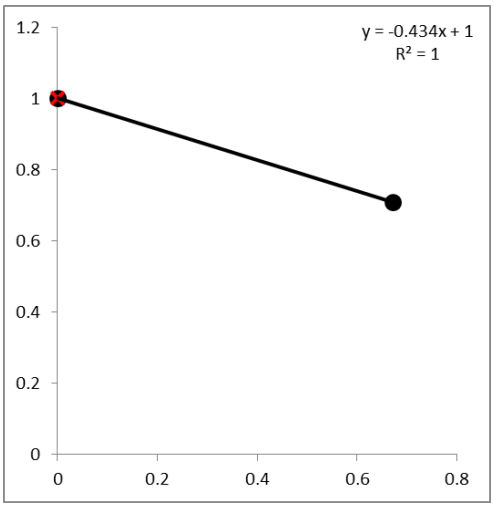

SURIS5A-1B

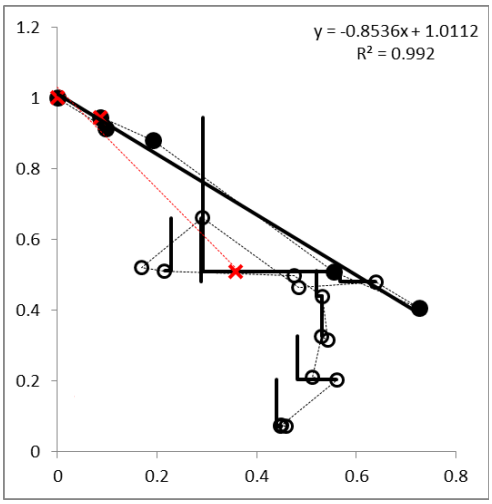

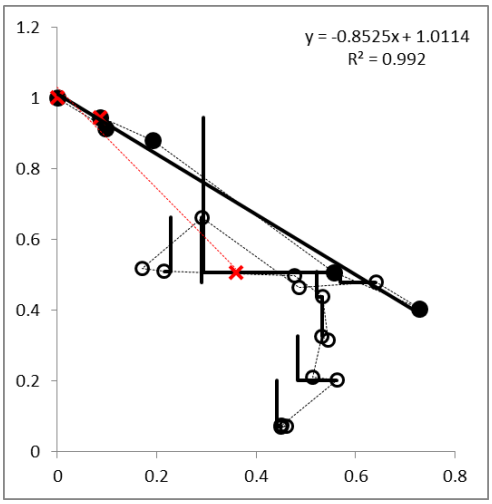

SURIS5A-1C

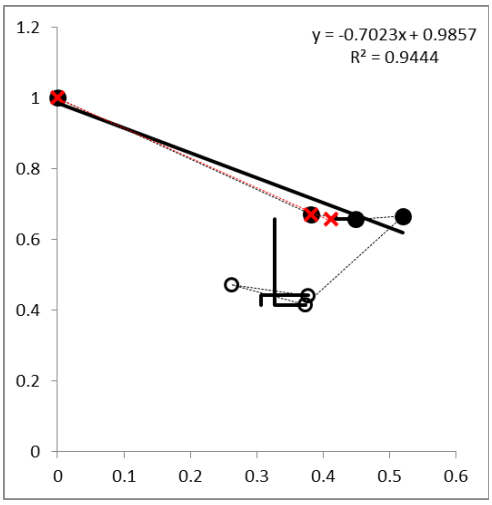

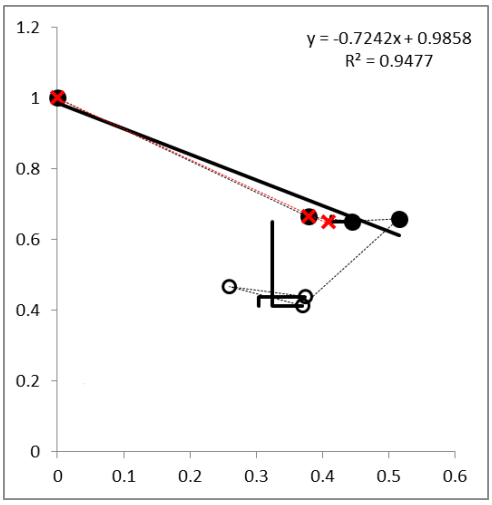

SURIS5A-2B

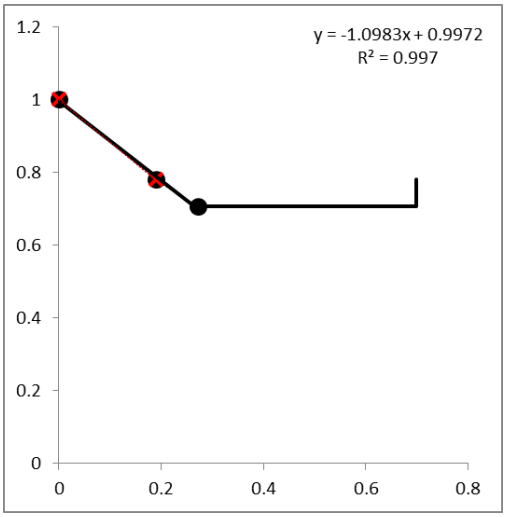

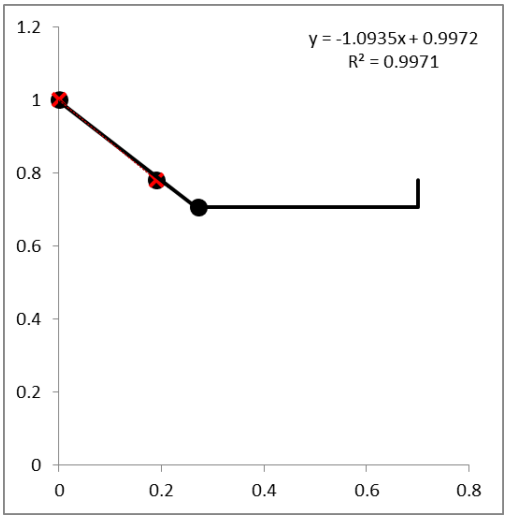

SURIS5A-2C

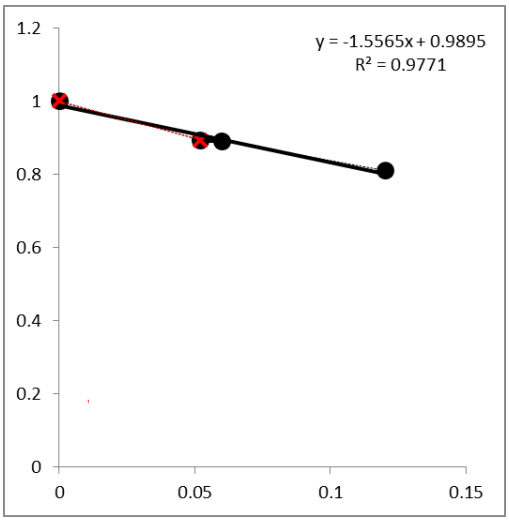

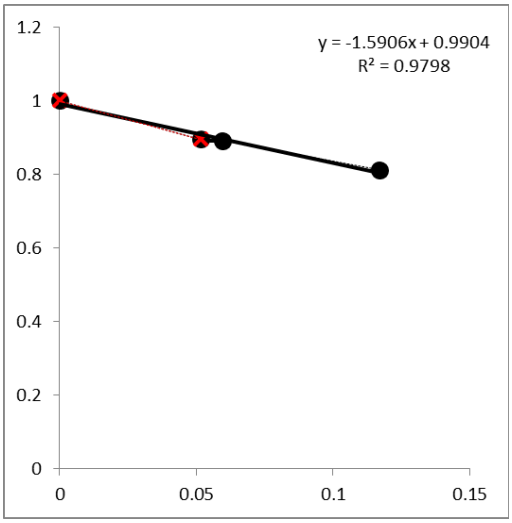

SURIS5A-2E

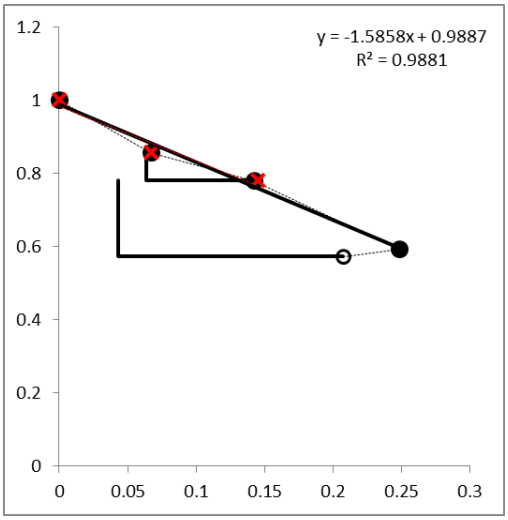

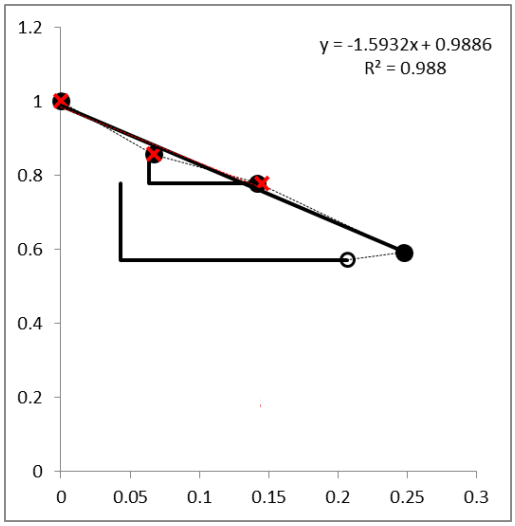

SURIS5A-2F

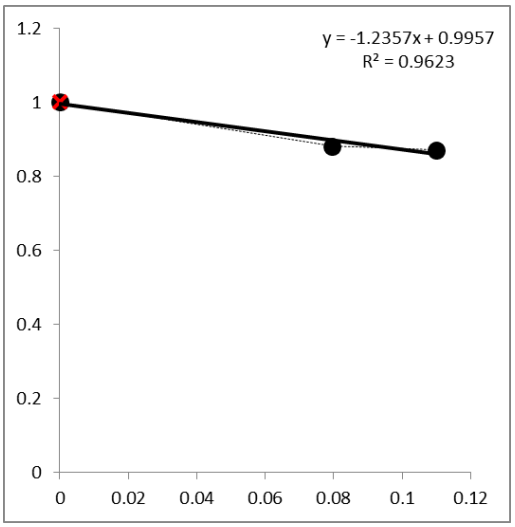

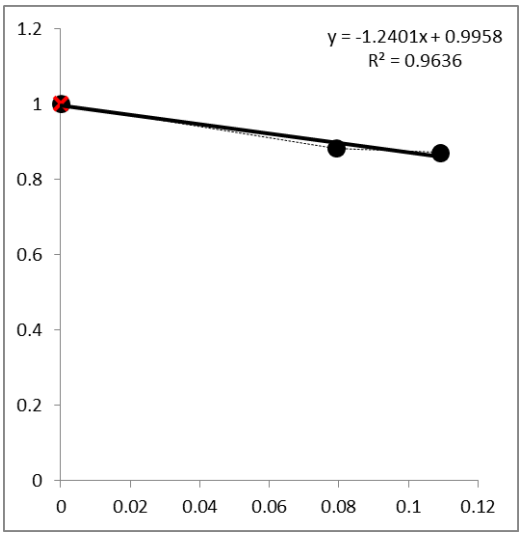

SURIS5A-2G

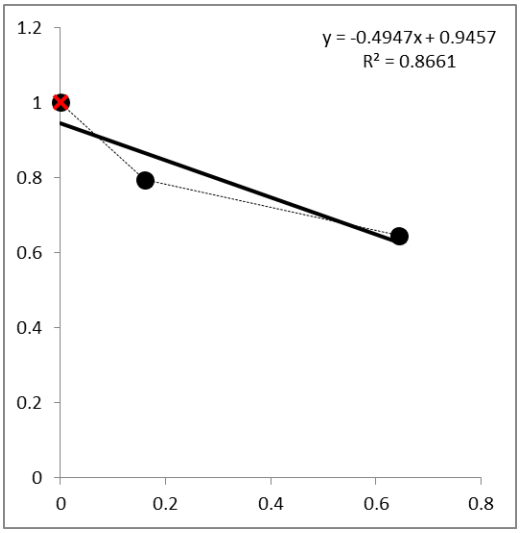

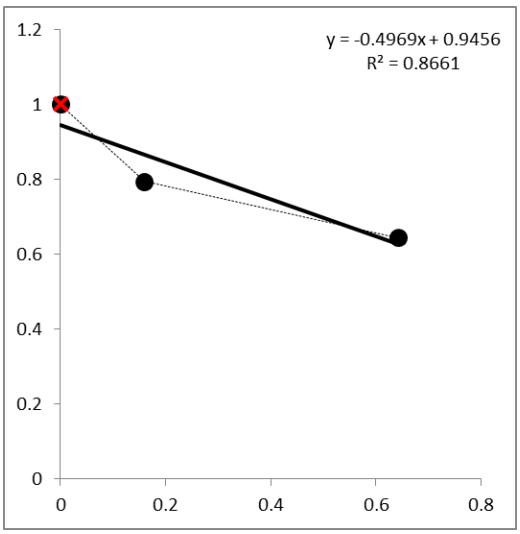

SURIS5A-2H

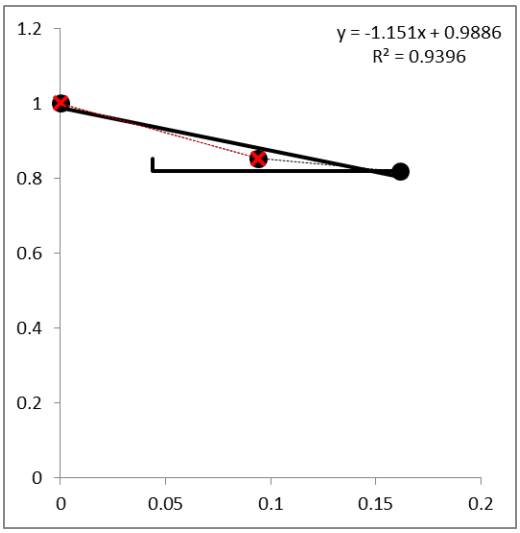

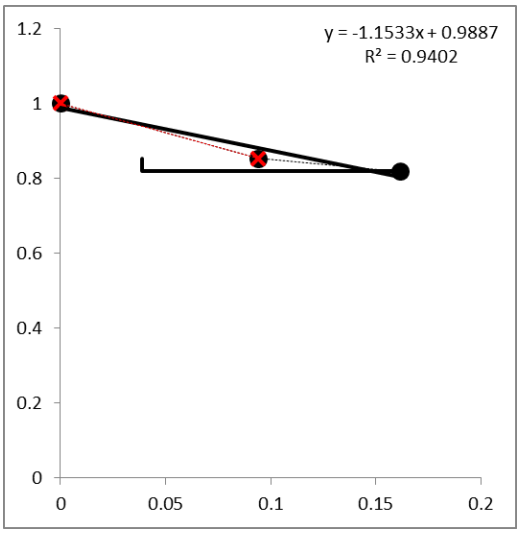

SURIS5A-2I

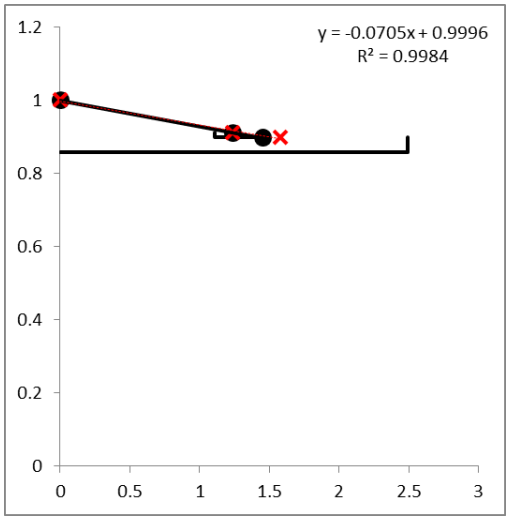

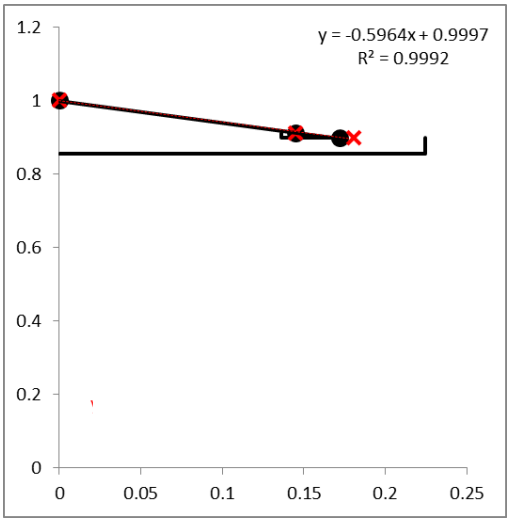

SURIS5A-2J

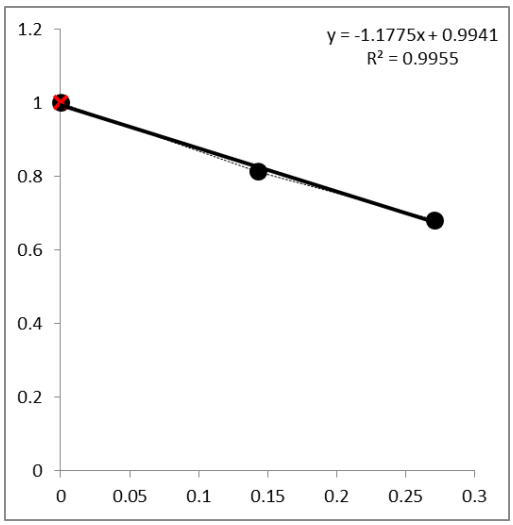

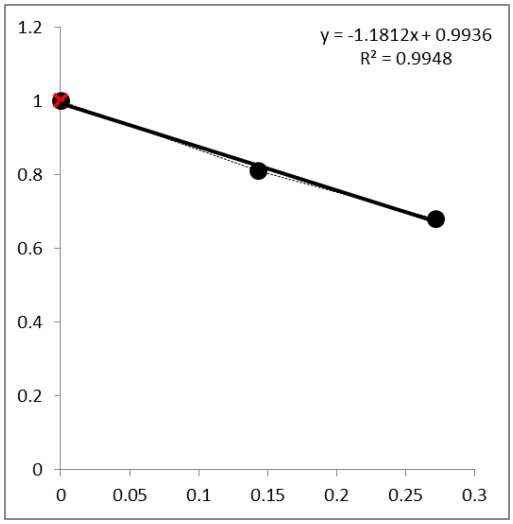

SURIS5A-3B

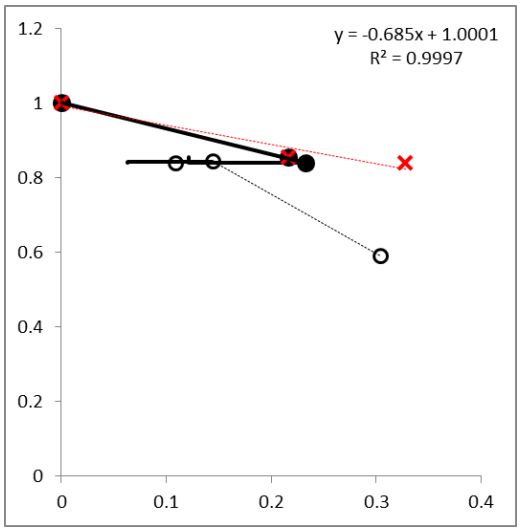

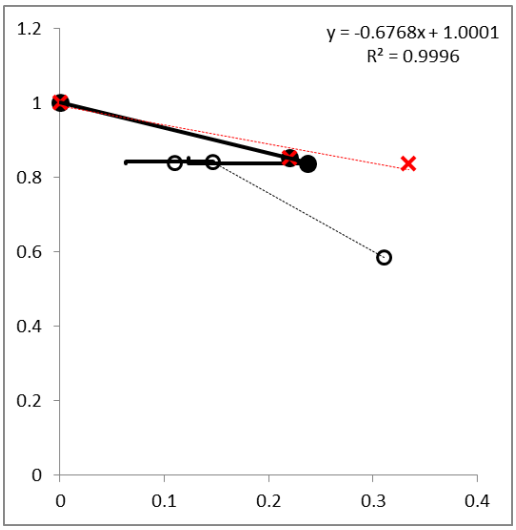

SURIS5B-1B

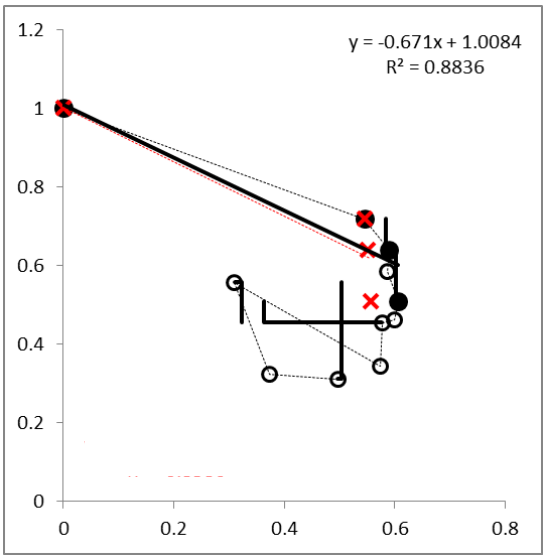

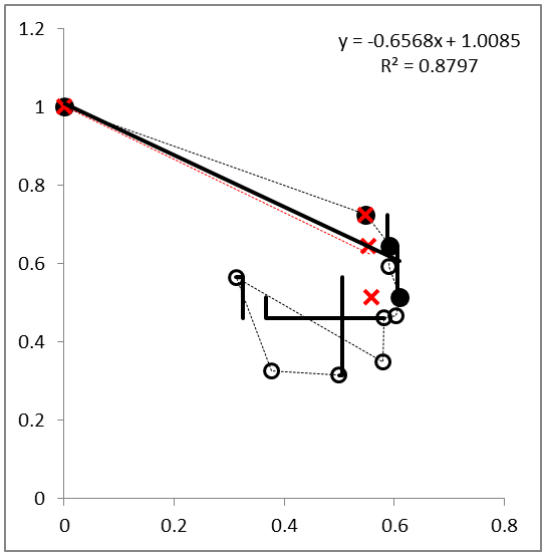

SURIS5B-1C

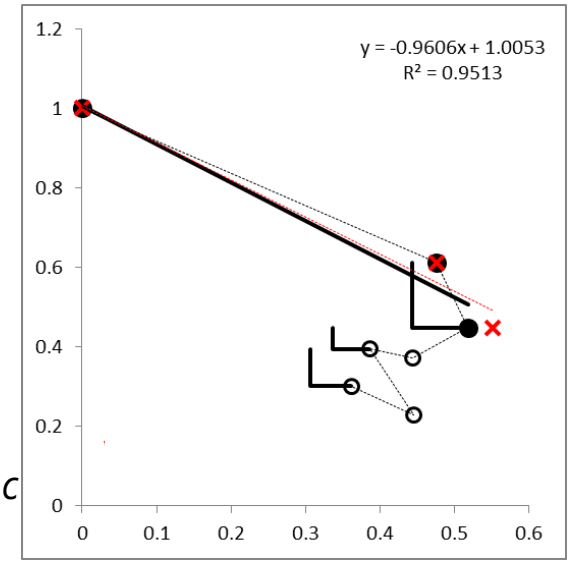

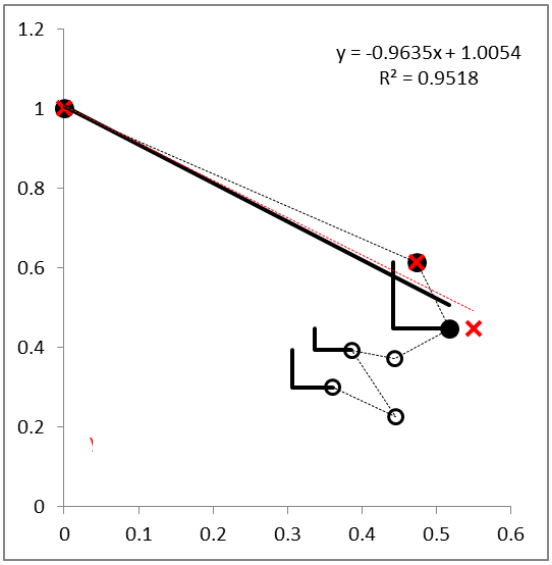

SURIS5B-1D

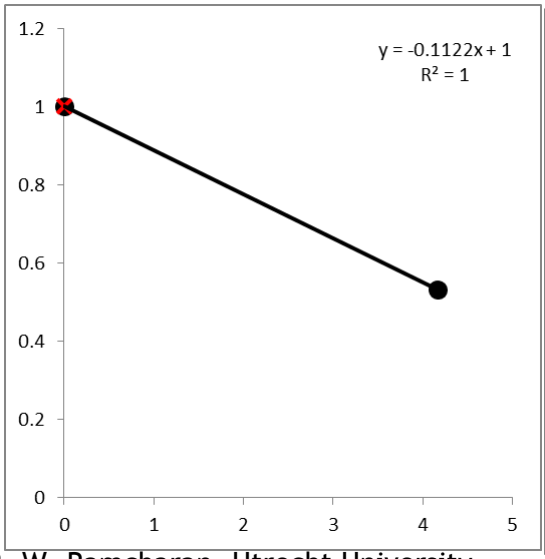

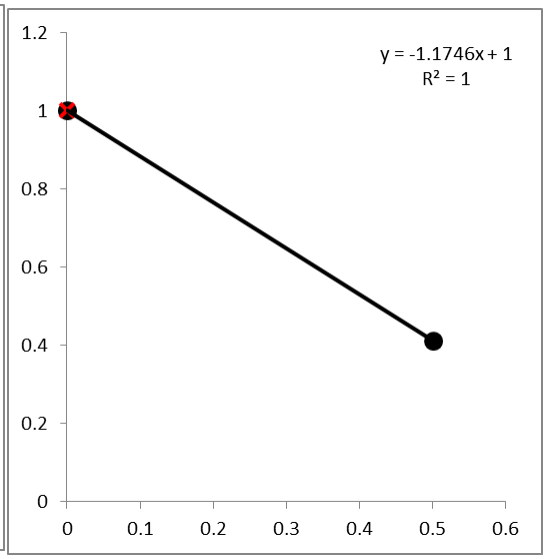

SURIS5B-1E

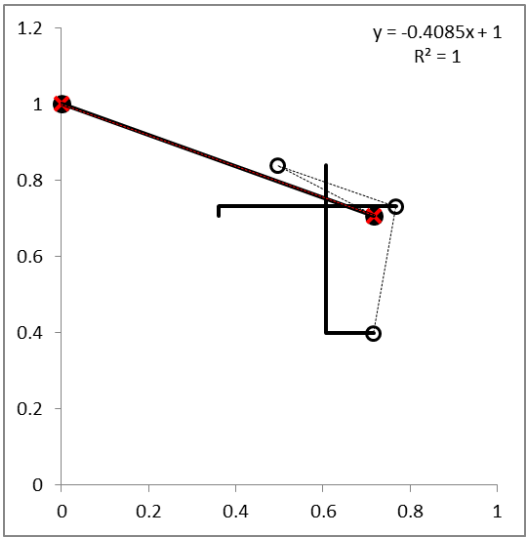

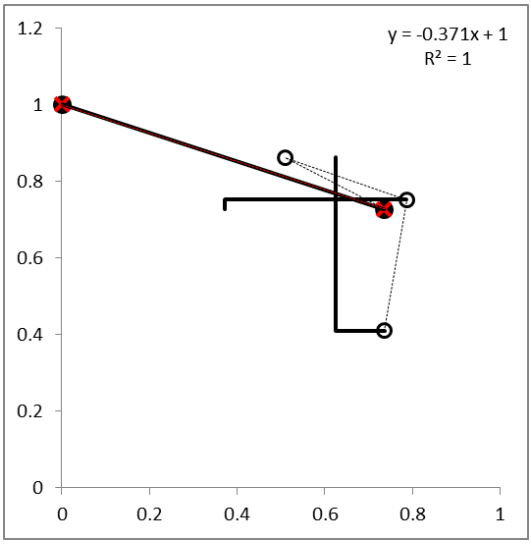

SURIS5B-1F

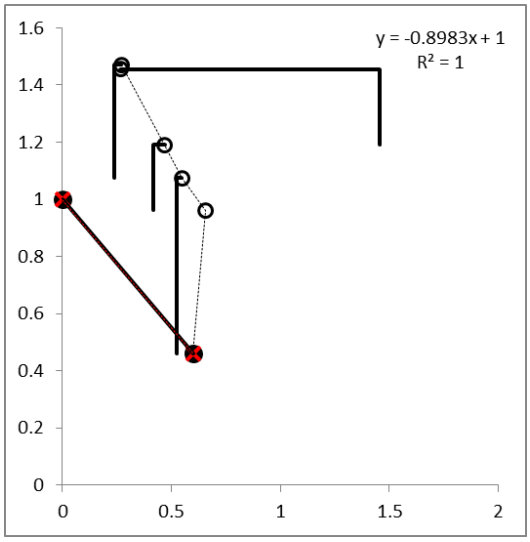

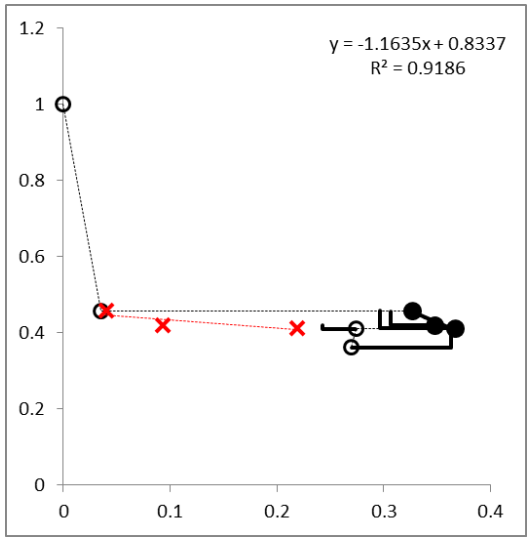

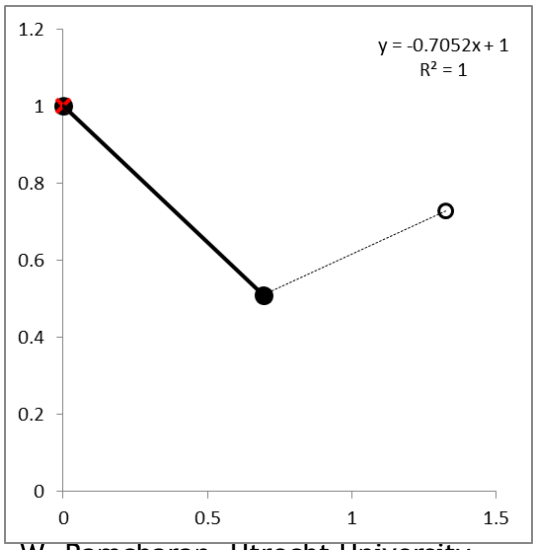

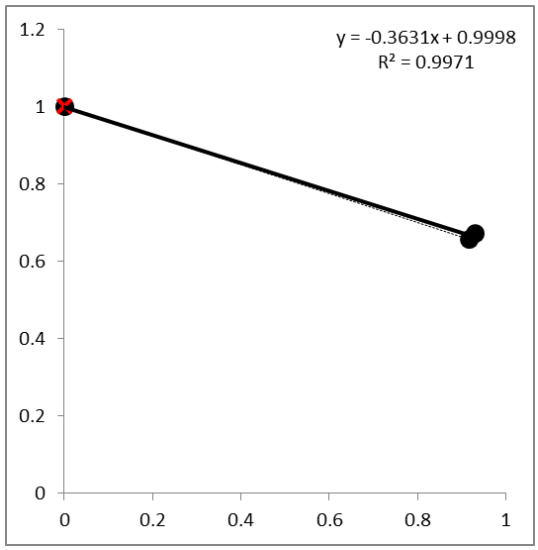

SURIS6B-1C

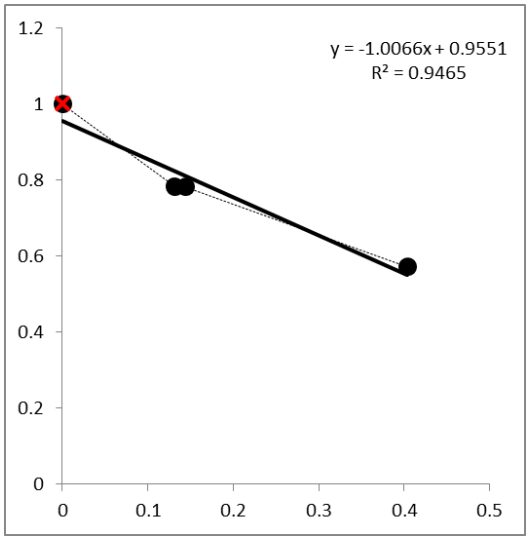

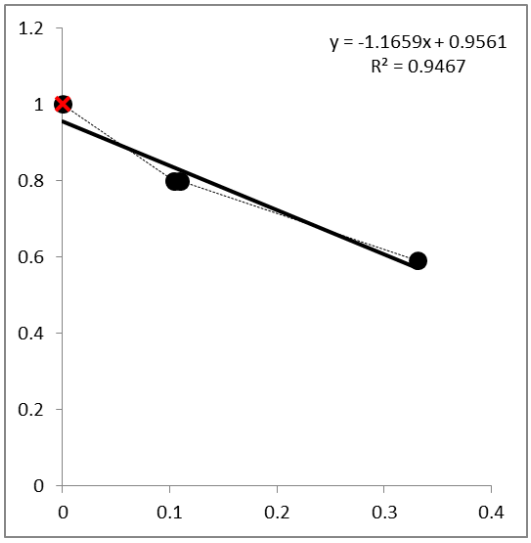

SURIS6B-2E

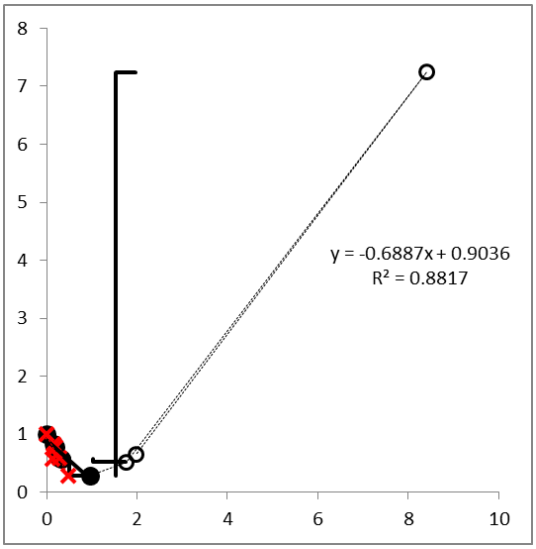

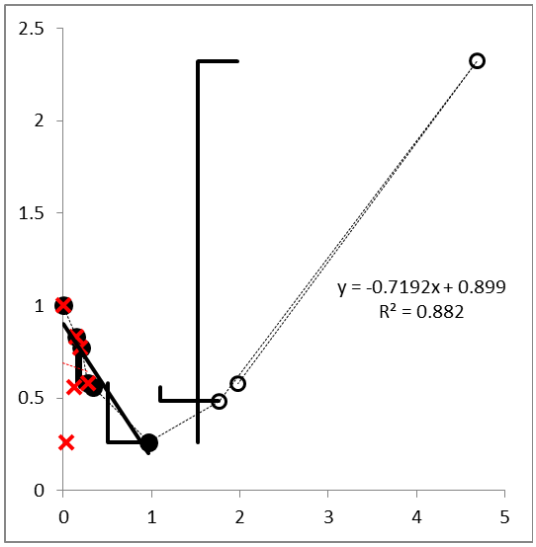

SURIS6B-2F

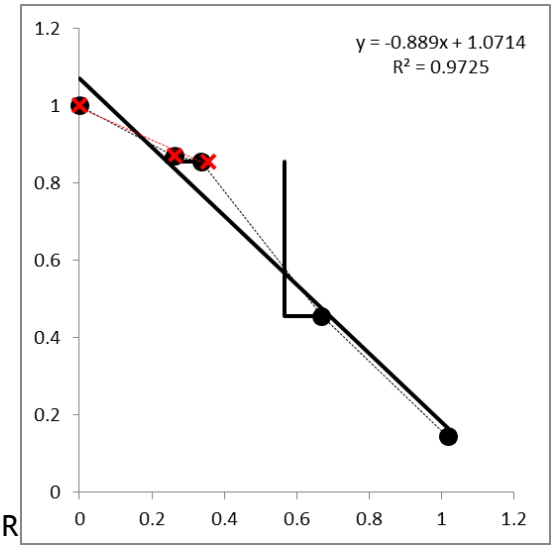

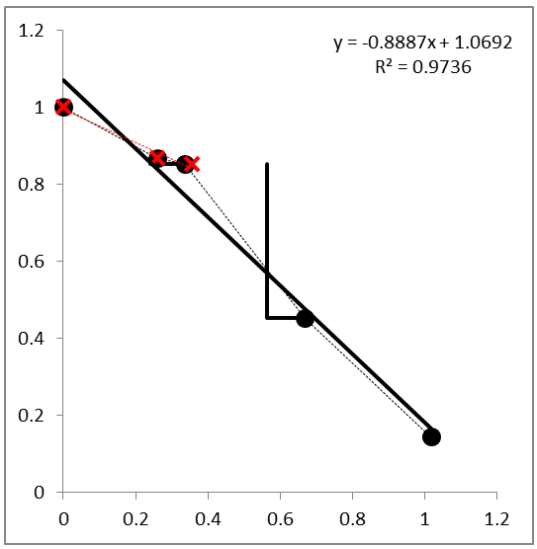

SURIS6B-3B

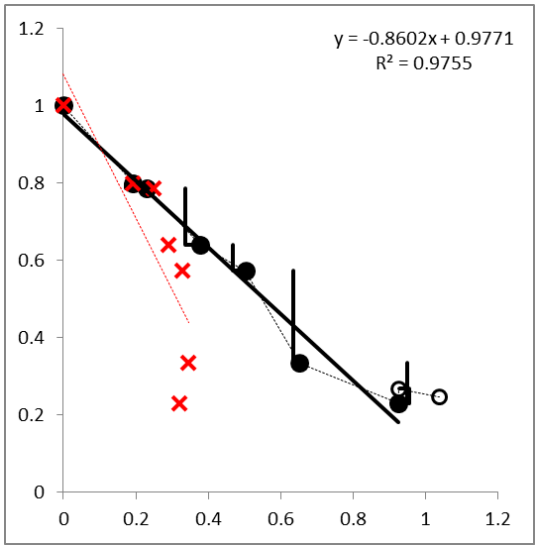

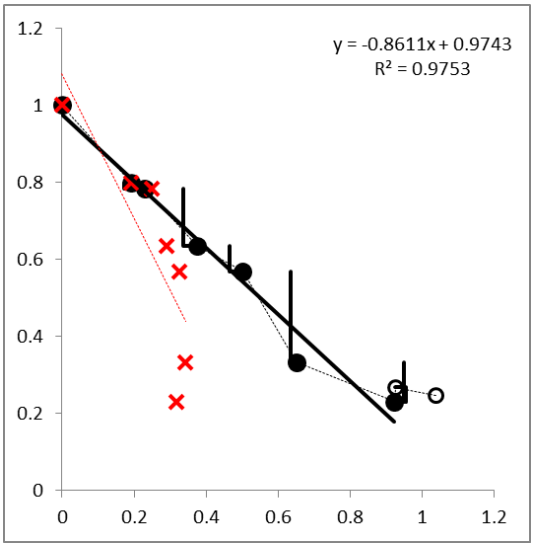

SURIS6B-3C

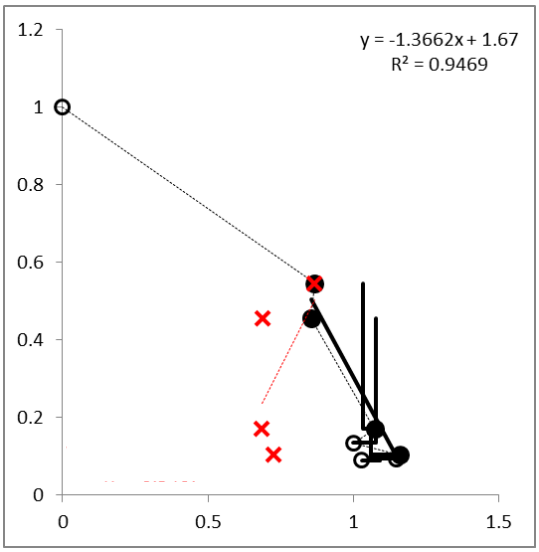

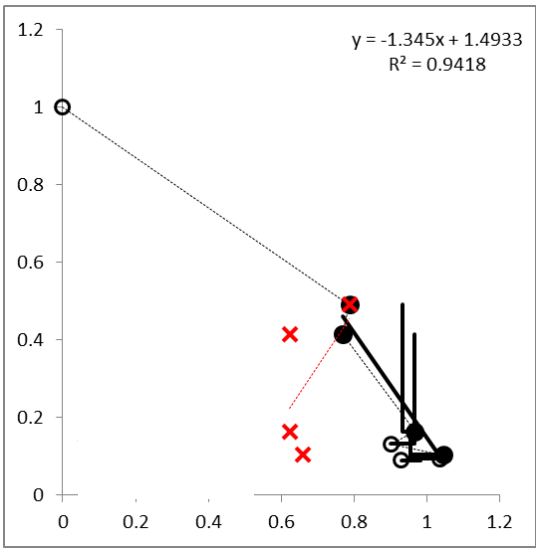

SURIS6B-3D

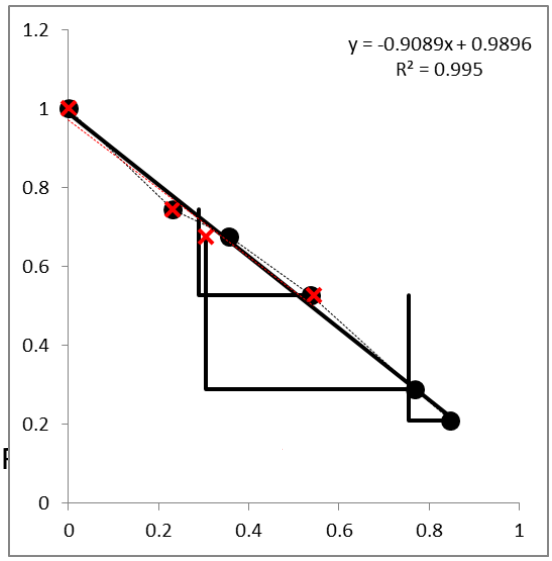

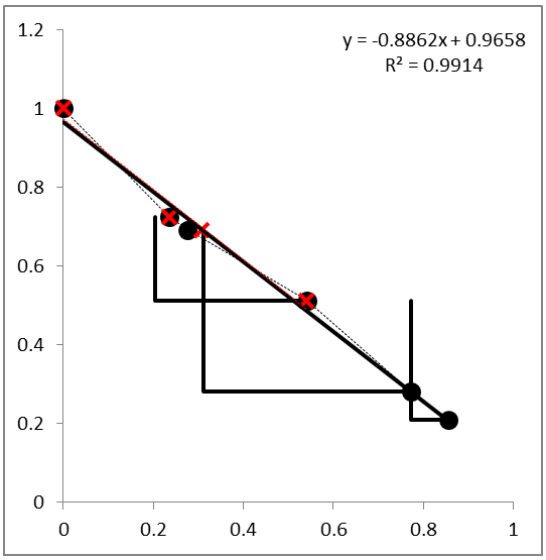

MSc thesis- F

Appendix 2b

Archeointensity results (IZZI-Thellier method)

From left to right, respectively Arai plot, directional plot and Decay of NRM intensity plot of each sample.

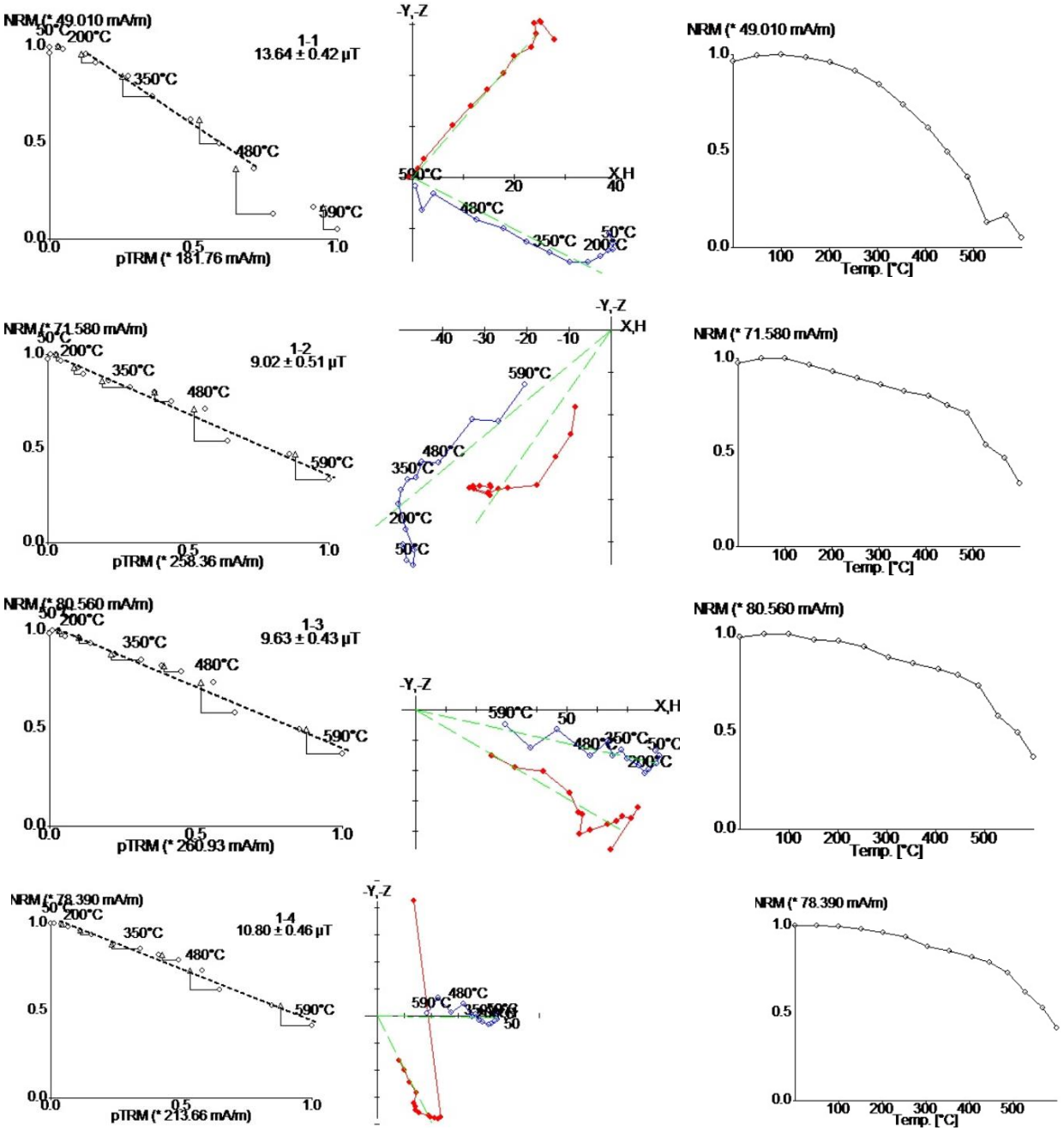

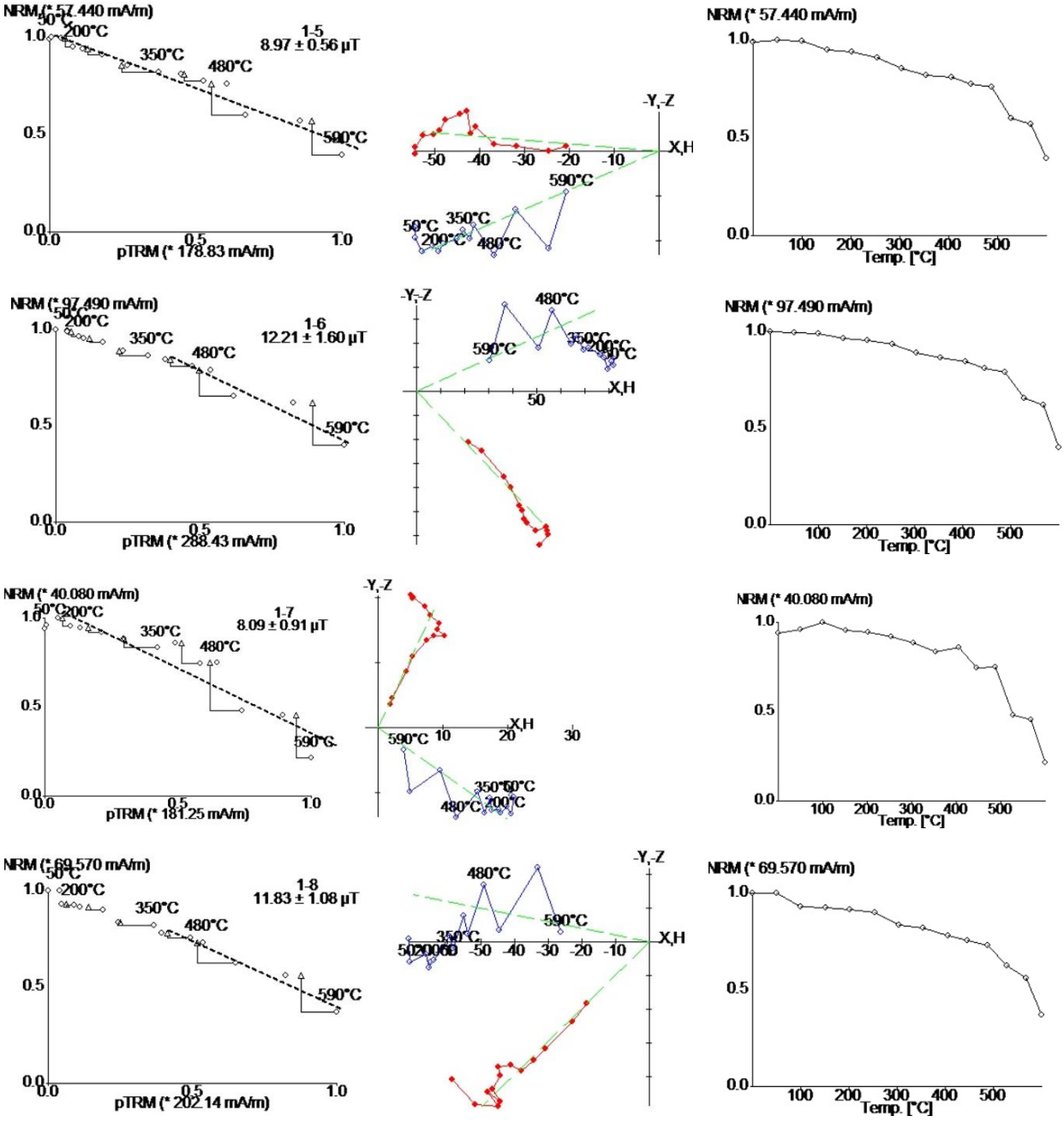

Plots (above) belonging to specimen of level 1 (307 cm depth)

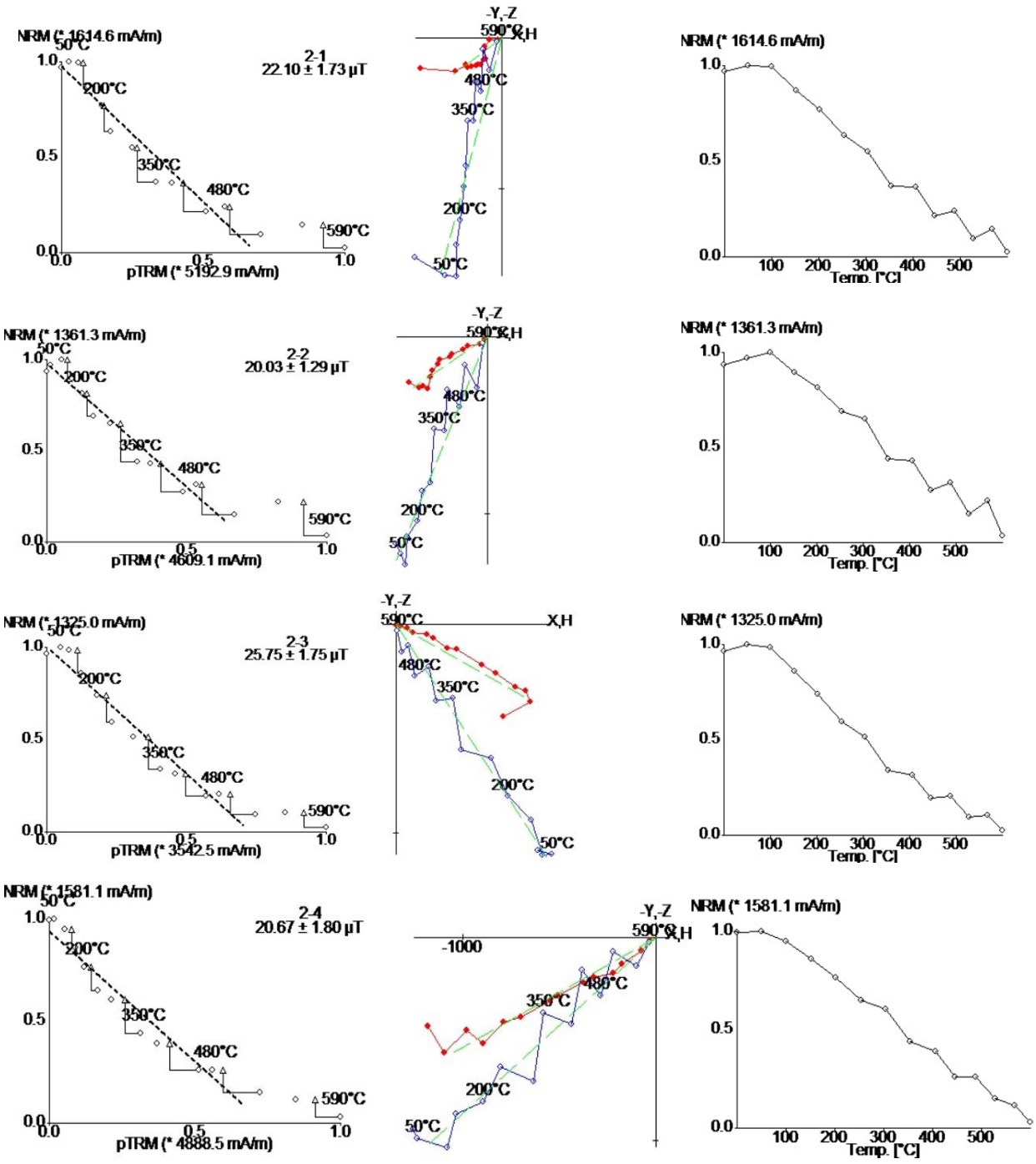
NRM (* 1614.6 mA/m)
50°C
200°C
350°C
480°C
590°C
2-1
22.10 ± 1.73 µT
pTRM (* 5192.9 mA/m)
-Y,-Z
590°C
X,H
480°C
350°C
200°C
50°C
NRM (* 1614.6 mA/m)
Temp. [°C]
NRM (* 1361.3 mA/m)
2-2
20.03 ± 1.29 µT
pTRM (* 4609.1 mA/m)
NRM (* 1325.0 mA/m)
2-3
25.75 ± 1.75 µT
pTRM (* 3542.5 mA/m)
NRM (* 1581.1 mA/m)
2-4
20.67 ± 1.80 µT
pTRM (* 4888.5 mA/m)
-1000

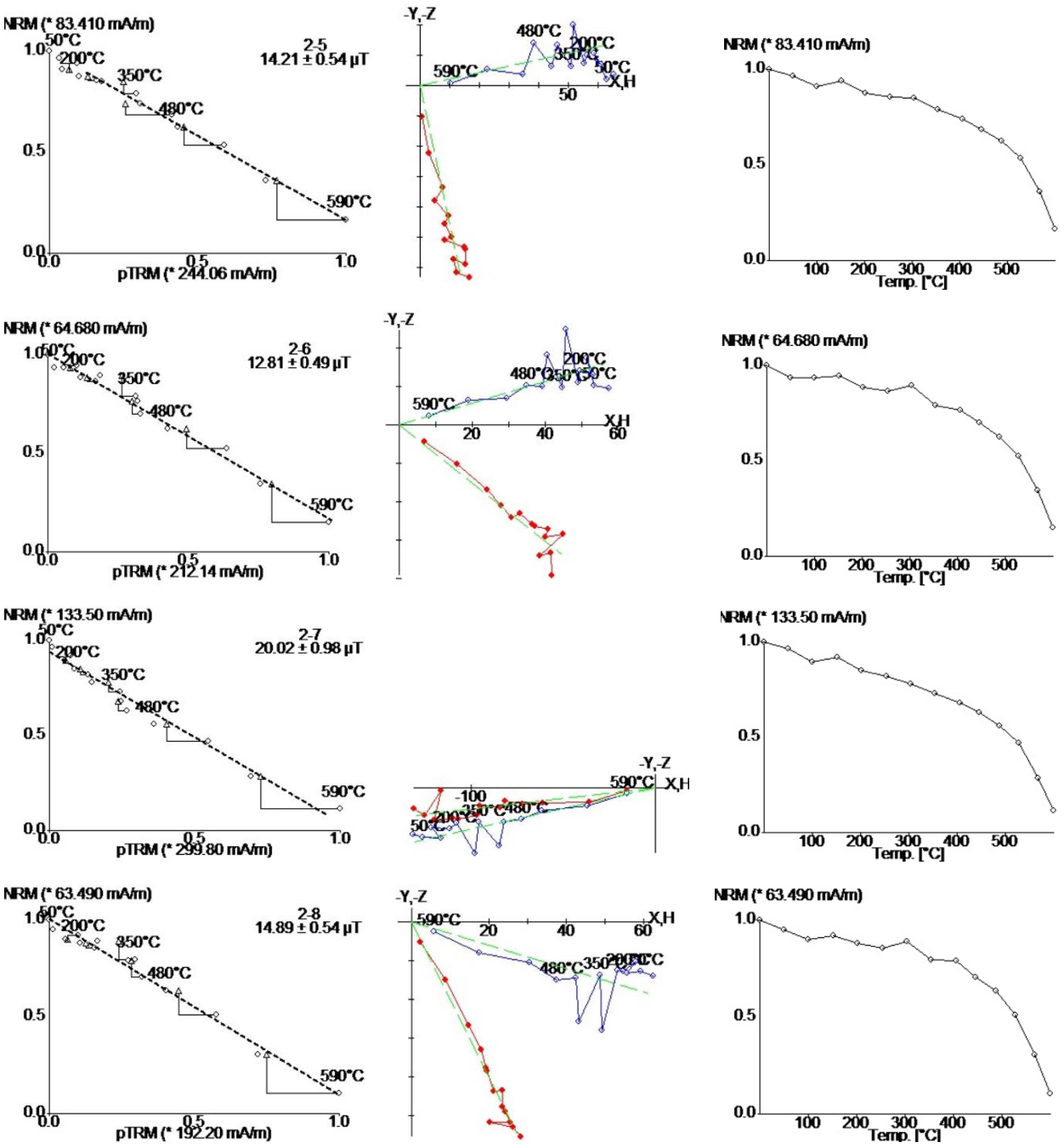

Plots (above) belonging to specimen of level 2 (164 cm depth)

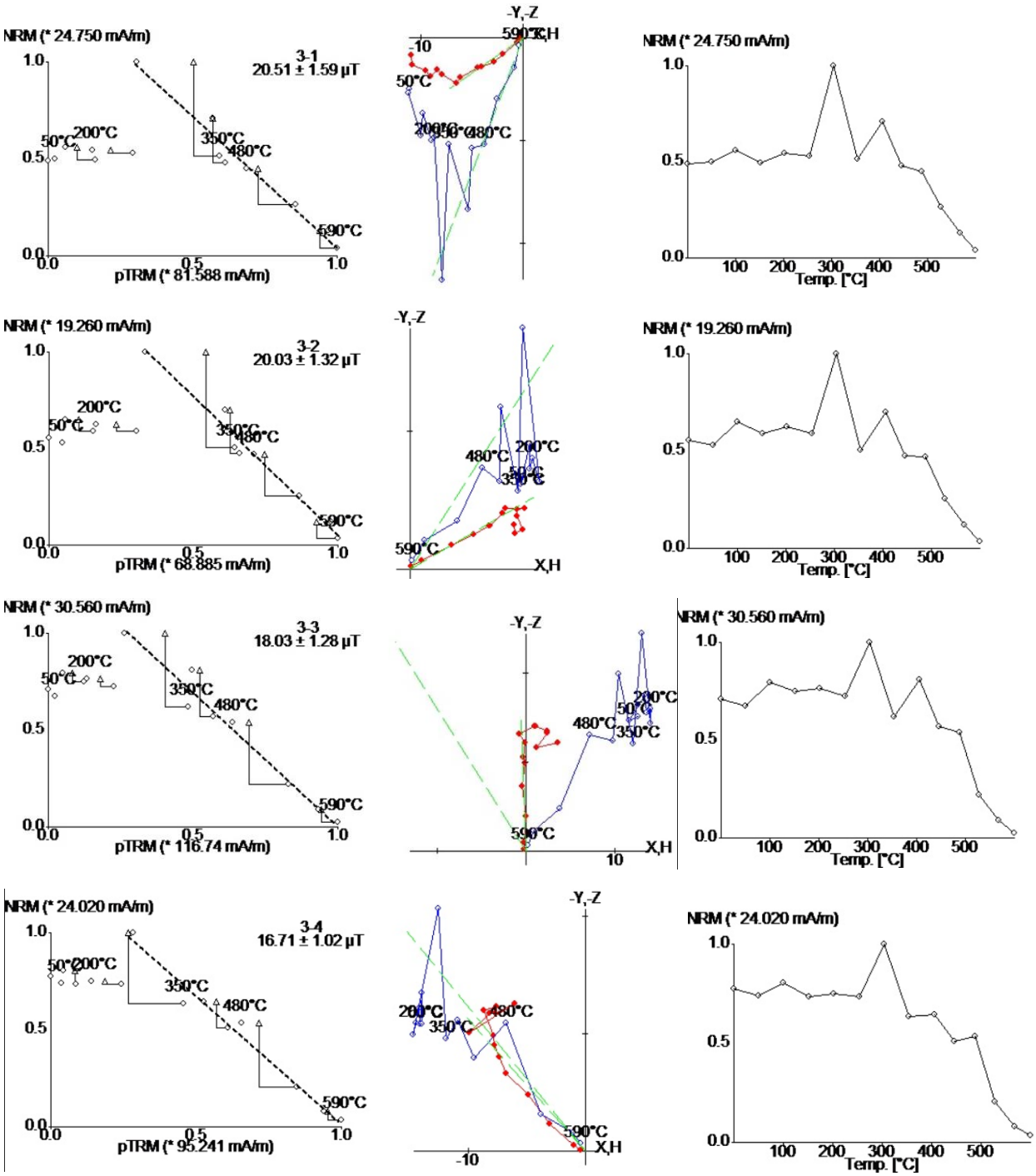
NRM (* 24.750 mA/m)
3-1
20.51 ± 1.59 µT
50°C
200°C
350°C
480°C
590°C
pTRM (* 81.588 mA/m)
-Y,-Z
X,H
NRM (* 24.750 mA/m)
Temp. [°C]
NRM (* 19.260 mA/m)
3-2
20.03 ± 1.32 µT
pTRM (* 68.885 mA/m)
NRM (* 19.260 mA/m)
Temp. [°C]
NRM (* 30.560 mA/m)
3-3
18.03 ± 1.28 µT
pTRM (* 116.74 mA/m)
NRM (* 30.560 mA/m)
Temp. [°C]
NRM (* 24.020 mA/m)
3-4
16.71 ± 1.02 µT
pTRM (* 95.241 mA/m)
NRM (* 24.020 mA/m)
Temp. [°C]

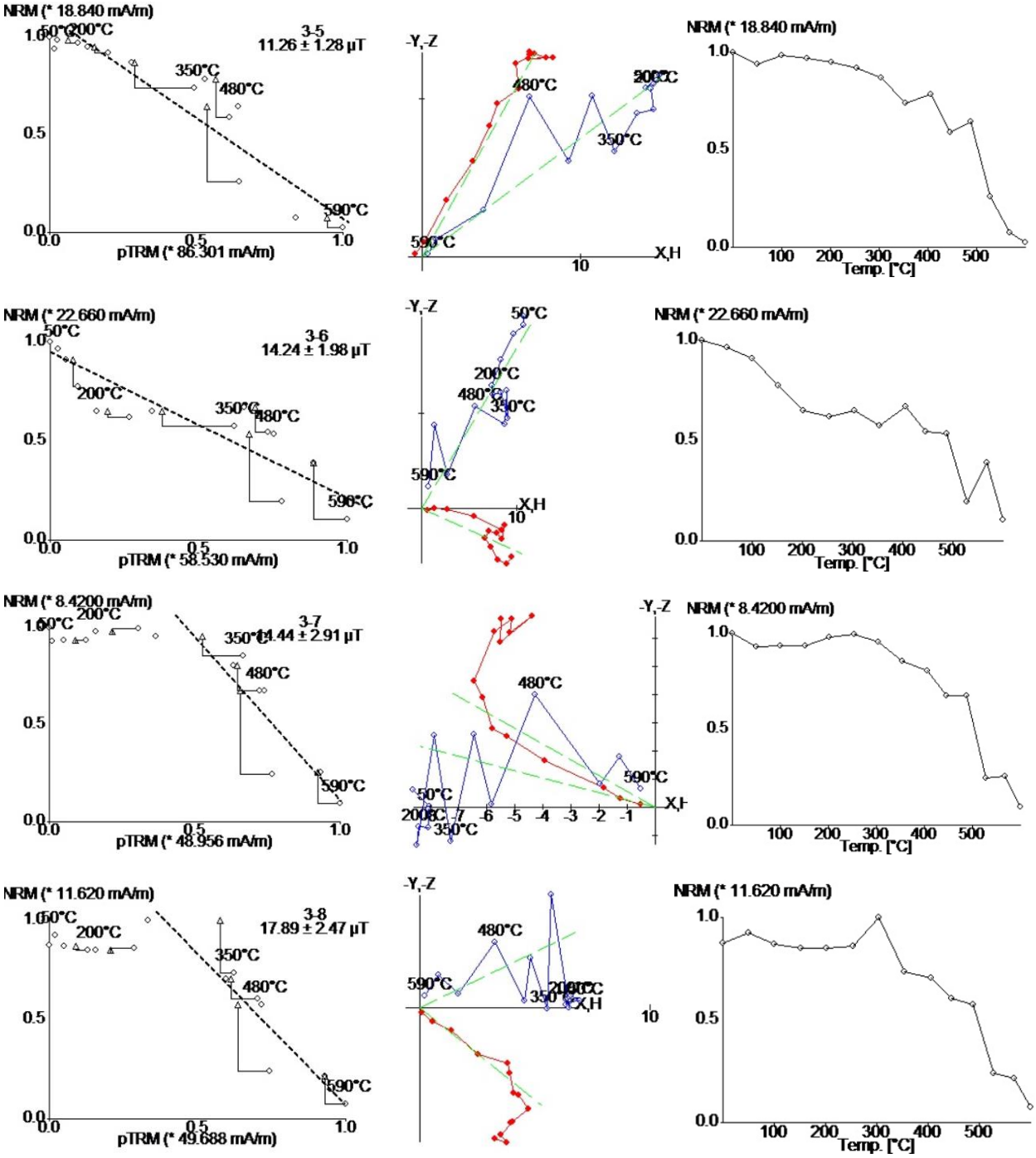

Plots (above) belonging to specimen of level 3 (292 cm depth)

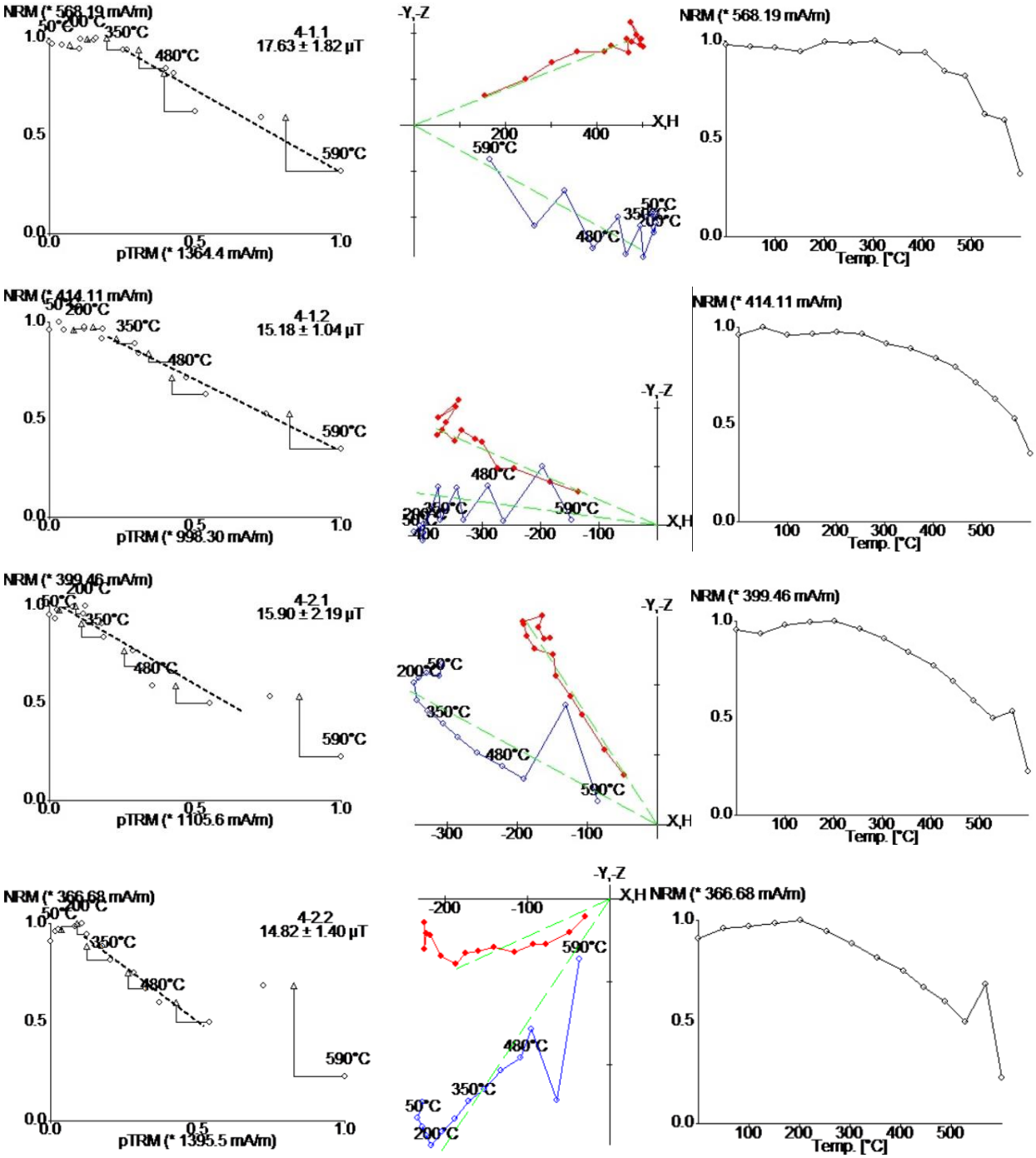

Plots (above) belonging to specimen of level 4 (145 cm depth)

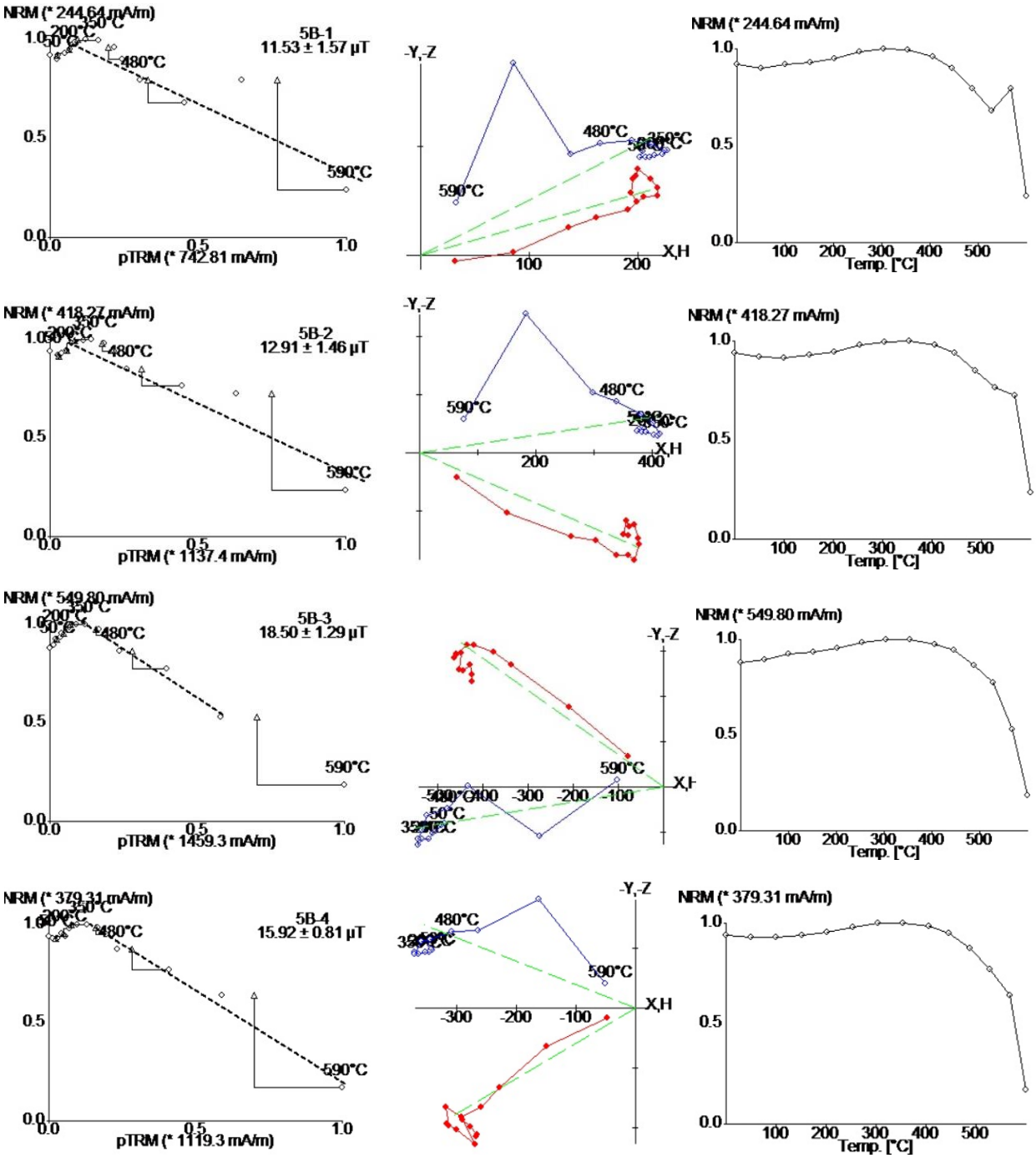

Plots (above) belonging to specimen of level 5B (75 cm depth)

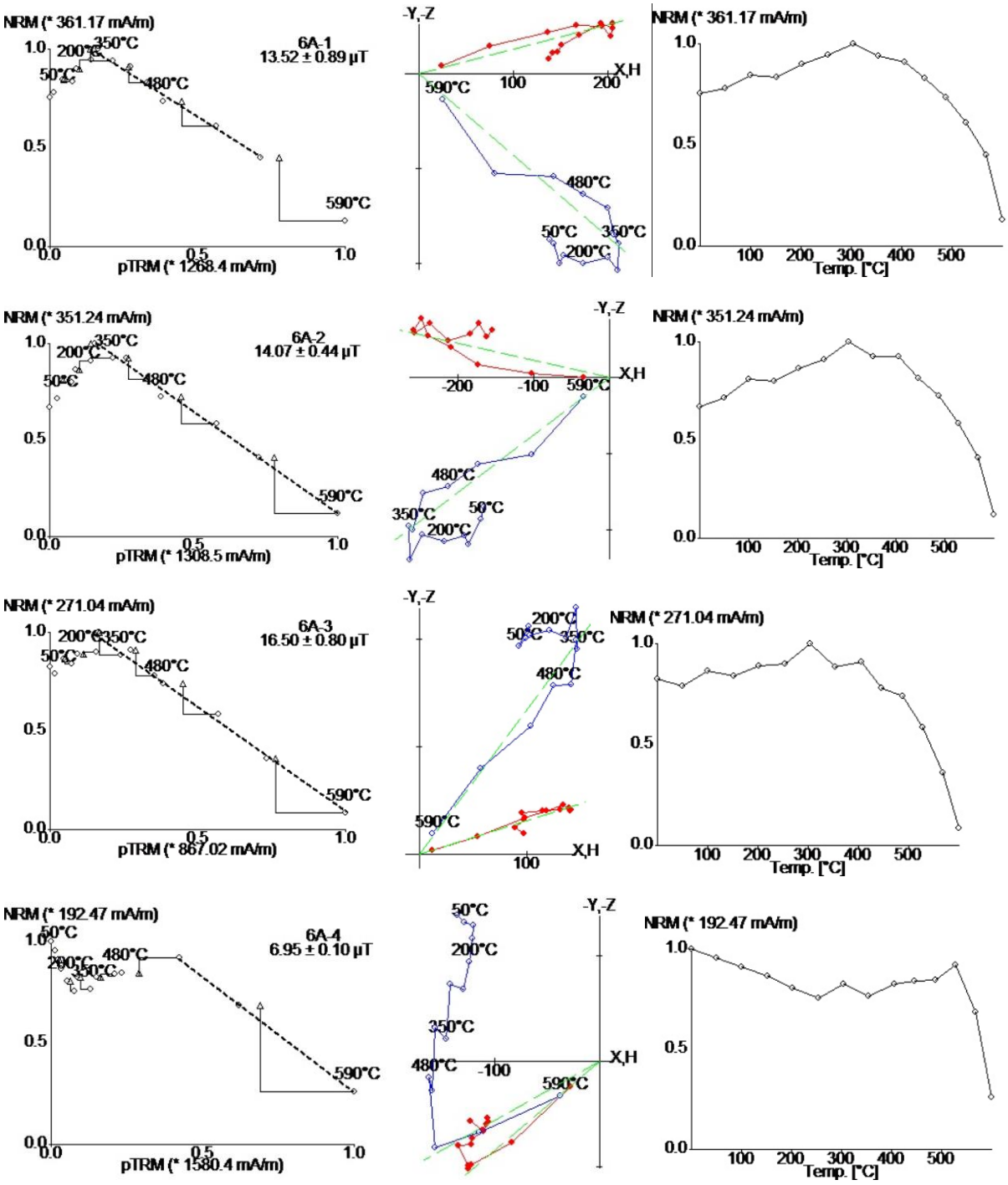

Plots (above) belonging to specimen of level 6A (98 cm depth)

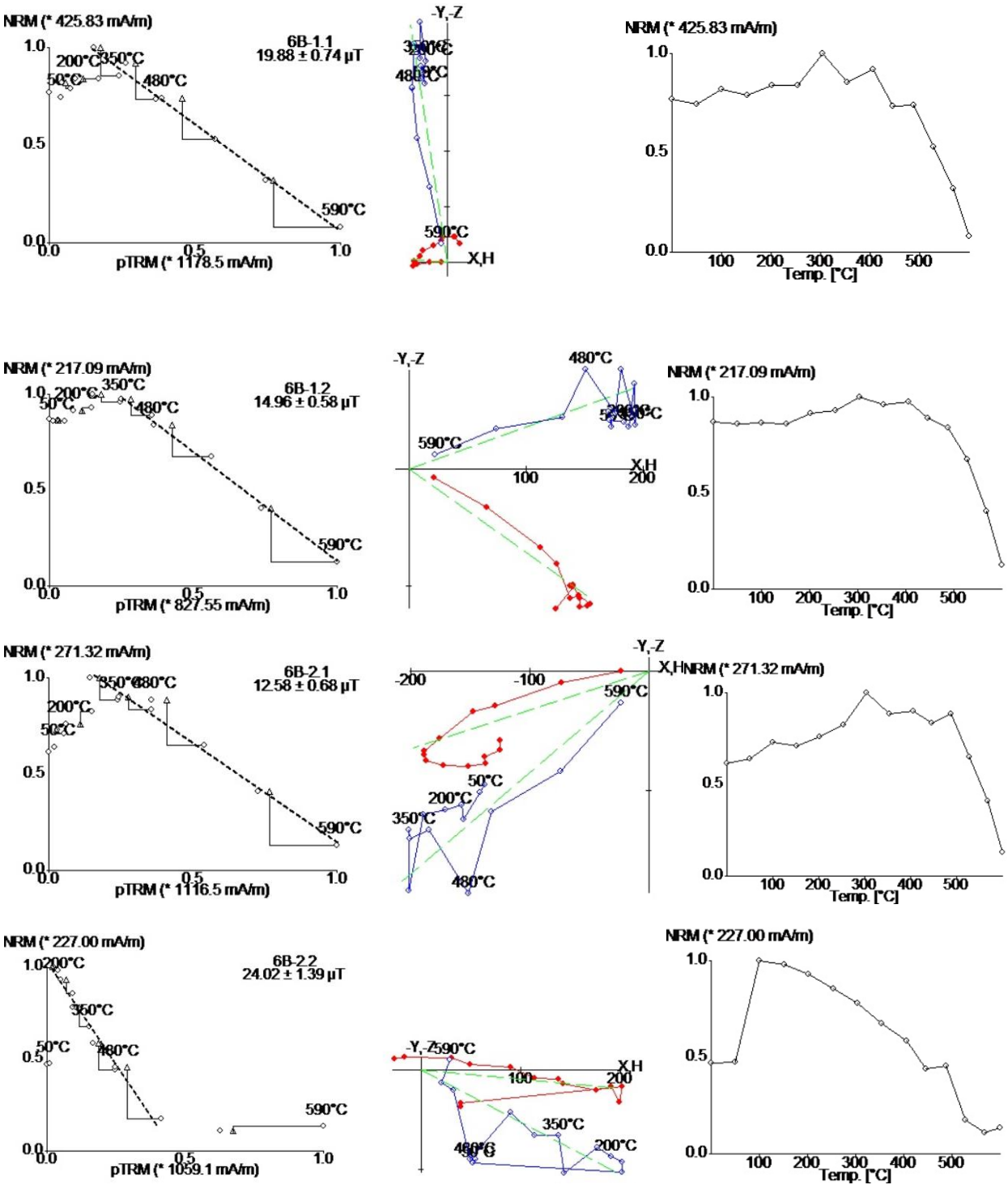
NRM (* 425.83 mA/m)
6B-1.1
19.88 ± 0.74 µT
200°C
350°C
50°C
480°C
590°C
pTRM (* 1178.5 mA/m)
-Y,-Z
X,H
NRM (* 425.83 mA/m)
Temp. [°C]
NRM (* 217.09 mA/m)
6B-1.2
14.96 ± 0.58 µT
pTRM (* 827.55 mA/m)
NRM (* 271.32 mA/m)
6B-2.1
12.58 ± 0.68 µT
pTRM (* 1116.5 mA/m)
NRM (* 227.00 mA/m)
6B-2.2
24.02 ± 1.39 µT
pTRM (* 1059.1 mA/m)

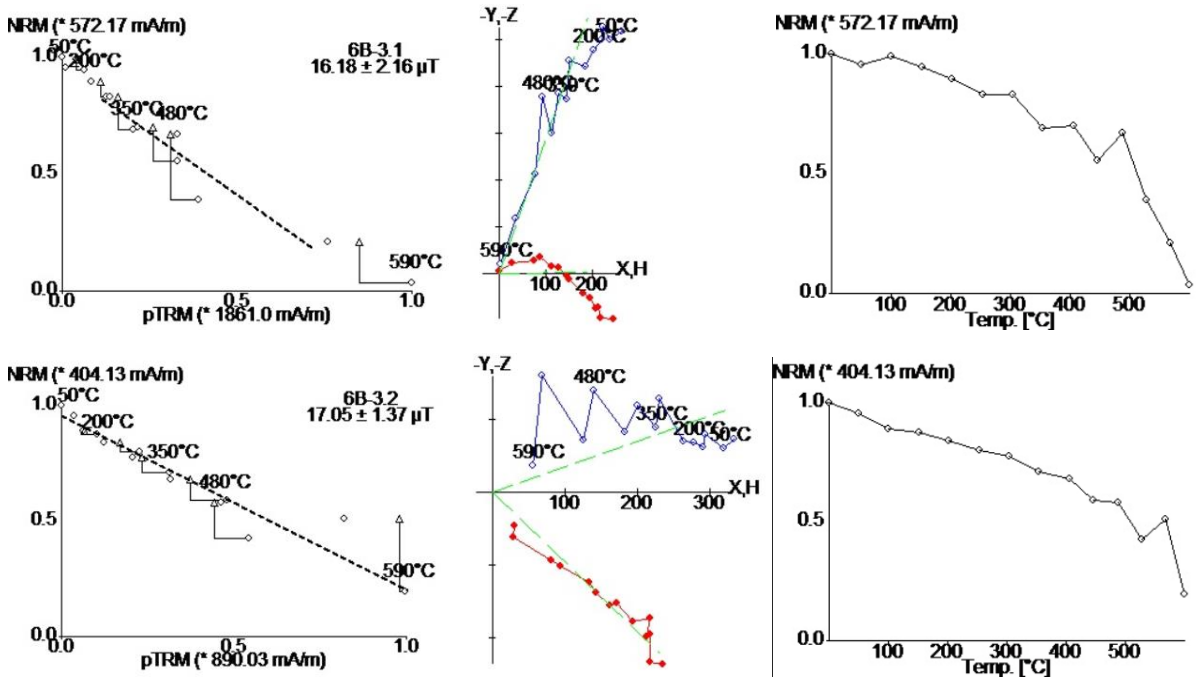

Plots (above) belonging to specimen of level 6B (98 cm depth)

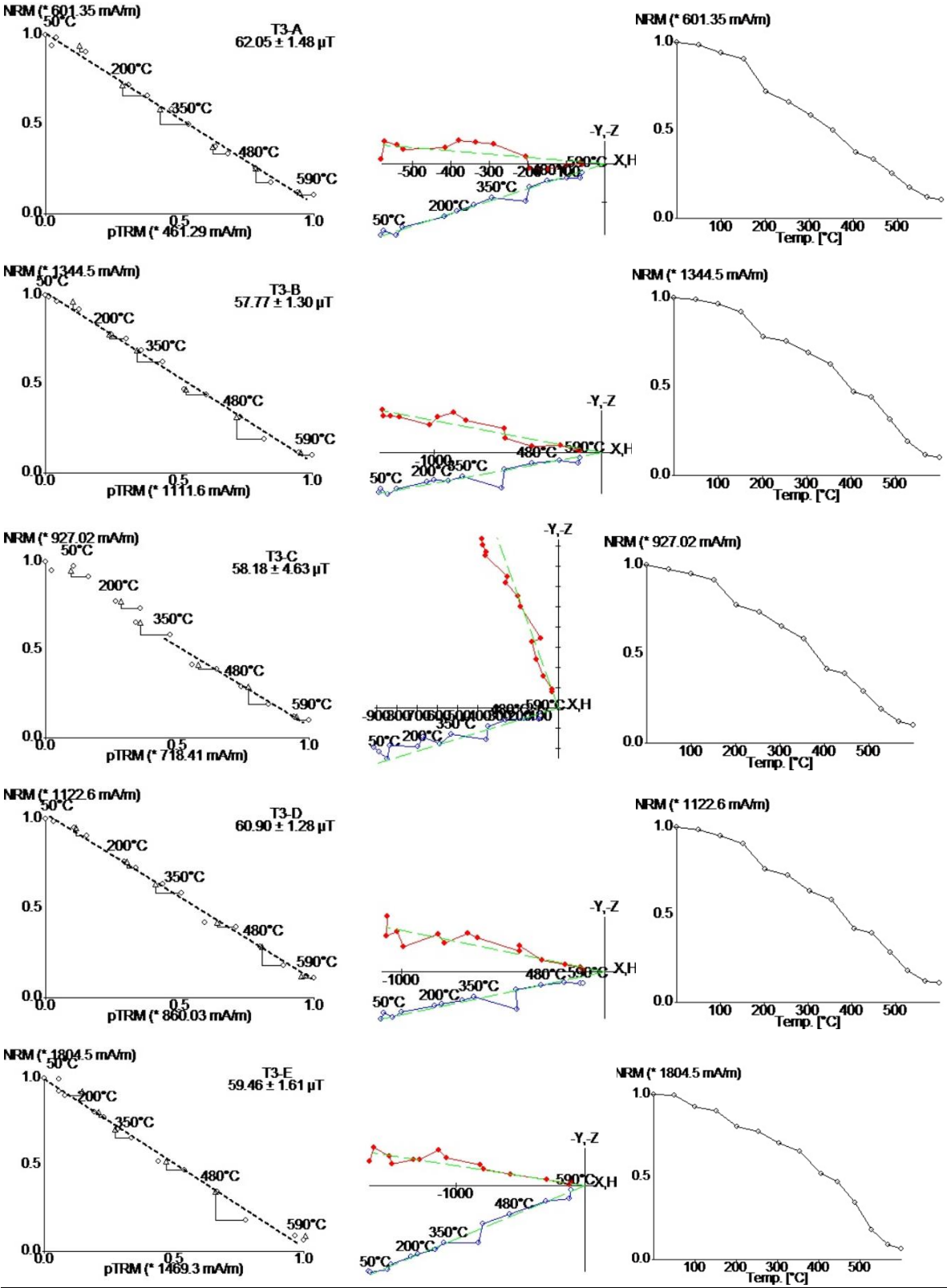

Plots (above) belonging to volcanic specimen of section T-3

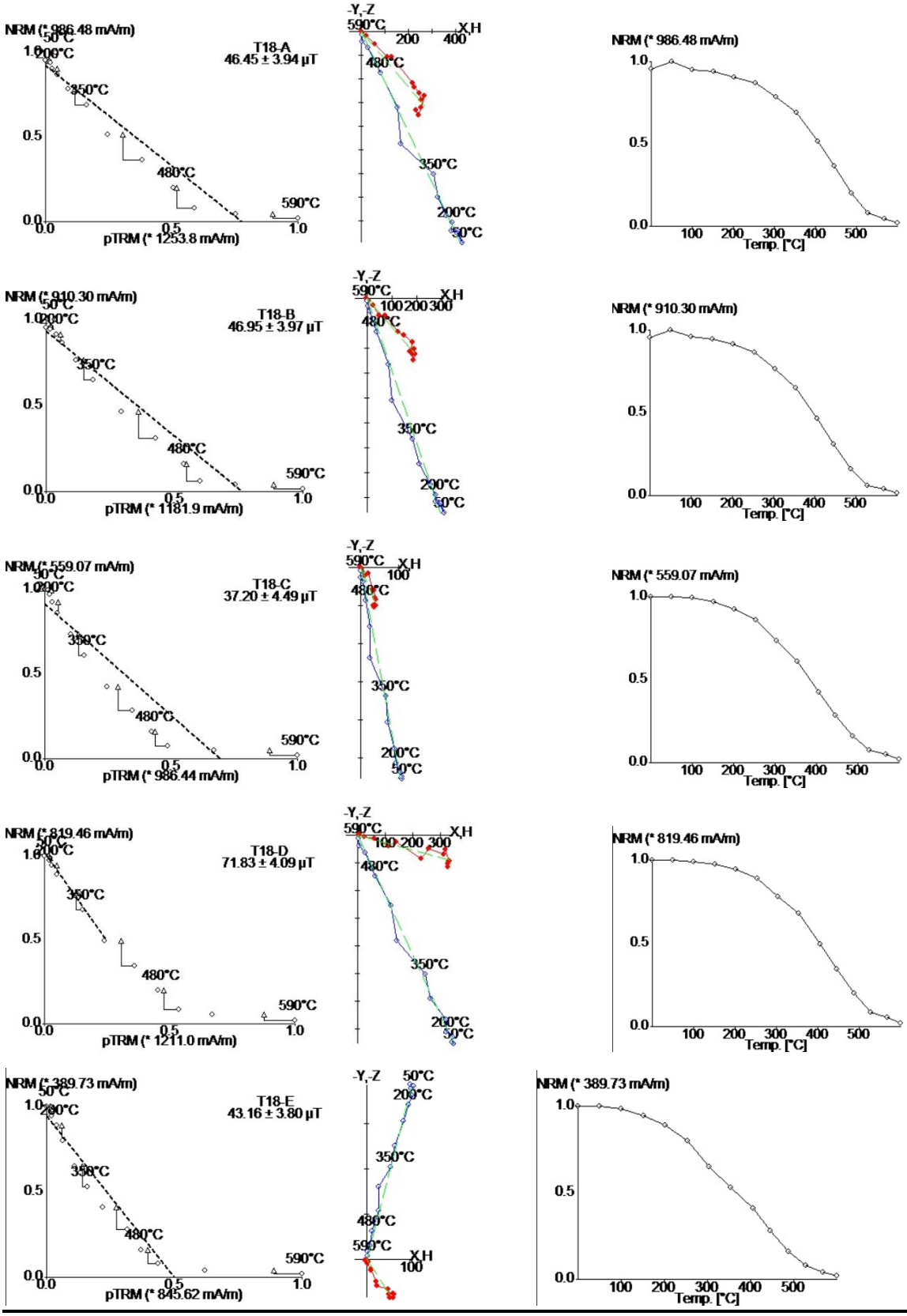

Plots (above) belonging to volcanic specimen of section T-18